KUOPION YLIOPISTON JULKAISUJA G. - A.I. VIRTANEN -INSTITUUTTI 20
KUOPIO UNIVERSITY PUBLICATIONS G.
A.I. VIRTANEN INSTITUTE FOR MOLECULAR SCIENCES 20

MARTIN KAVEC

Magnetic resonance imaging of misery perfusion, chronic cerebrovascular disease and acute stroke

A study using transverse relaxation contrast

Doctoral dissertation

To be presented by permission of the Faculty of Natural and Environmental Sciences of the University of Kuopio for public examination in Auditorium L21, Snellmania building, University of Kuopio, on Monday 28th June 2004 at 12 noon

Department of Biomedical NMR and Bio-NMR Facility
A.I. Virtanen Institute for Molecular Sciences
University of Kuopio

KUOPION YLIOPISTO
KUOPIO 2004

Distributor:
Kuopio University Library
P.O. Box 1627
FIN-70211 KUOPIO
FINLAND
Tel. +358 17 163 430
Fax +358 17 163 410
http://www.uku.fi/kirjasto/julkaisutoiminta/julkmyyn.html

Series Editors:
Professor Karl Åkerman
Department of Neurobiology
A.I. Virtanen Institute for Molecular Sciences

Research Director Jarmo Wahlfors
Department of Biotechnology and Molecular Medicine
A.I. Virtanen Institute for Molecular Sciences

Author's address:
Department of Biomedical NMR and National Bio-NMR Facility
A.I. Virtanen Institute for Molecular Sciences
University of Kuopio
P.O. Box 1627
FIN-70211 KUOPIO
FINLAND
Tel. +358 17 163 299
Fax +358 17 163 030

Supervisors:
Professor Risto Kauppinen, M.D. Ph.D.
School of Biological Sciences
University of Manchester, UK

Docent Olli Gröhn, Ph.D.
Department of Biomedical NMR
A.I. Virtanen Institute for Molecular Sciences
University of Kuopio

Reviewers:
Mark Lythgoe, Ph.D.
RCS Unit of Biophysics
Institute of Child Health
London, UK

James J. Pekar, Ph.D.
F. M. Kirby Research Center for Functional Brain Imaging
Johns Hopkins University
Baltimore, MD, USA

Opponent:
Professor Steve Williams, Ph.D.
Department of Clinical Neurosciences, Institute of Psychiatry
King's College
London, UK

ISBN 951-781-979-X
ISBN 951-27-0084-0 (PDF)
ISSN 1458-7335

Kopijyvä
Kuopio 2004
Finland

Kavec, Martin. Magnetic resonance imaging of misery perfusion, chronic cerebrovascular disease and acute stroke. A study using transverse relaxation contrast. Kuopio University Publications G. - A.I. Virtanen Institute for Molecular Sciences 20. 2004. 75 p.
ISBN 951-781-979-X
ISBN 951-27-0084-0 (PDF)
ISSN 1458-7335

Abstract

Over the last three decades magnetic resonance imaging (MRI) has developed into a versatile diagnostic imaging modality, being able to provide high quality anatomical images from the human body as well as accurately revealing pathology, function and chemical structure of tissues. In particular, MRI techniques have substantially expanded the knowledge about the pathophysiology of cerebral ischaemia. Despite strong interest within scientific community and efforts in this field, several clinically interesting aspects of acutely ischaemic brain, including assessment of tissue at risk and tissue viability by MRI are still only partially understood. The present study was aimed at sheding light on these issues by scrutinising the value of blood oxygen level dependent (BOLD) contrast effect, using transverse relaxation time based MRI, to provide information from acute vascular insults and ischaemic stoke both in experimental and clinical settings. The negative BOLD effect associated with the early moments of cerebral ischaemia has been explained by elevated oxygen extraction ratio (OER) in recent high field animal T_2 MRI studies. Interestingly, a haemodynamic condition, caused by a mismatch between oxygen delivery and consumption leading to elevated OER, has also been associated with a higher risk of ischaemic stroke in man.

By using T_2 MRI, the present study shows that a drop in the cerebral blood flow (CBF) which resembles a misery perfusion, without signs of ischaemia in rat brain, causes a negative BOLD effect. This contrast can be readily detected at 1.5 T magnetic field and importantly, the magnitude of T_2 changes in a CBF compromised brain can be precisely predicted by the intravascular BOLD model. Using T_2 MRI, cerebral haemodynamic adaptations were studied in carotid stenosis patients. A method employing T_2 BOLD, together with quantification of cerebral blood volume by bolus tracking MRI, was proposed and applied, to estimate parenchymal OER. Using this approach, average OER of 0.40 ± 0.05 and 0.55 ± 0.21 were determined in control subjects and patients with occlusion of internal carotid artery, respectively. Both OER values are in an excelent agreement with previously published data suggesting novel applications for T_2 MRI in the assessment of cerebral haemodynamics in cerebrovascular disease.

The relaxation mechanisms contributing to parenchymal T_2 in acute cerebral ischaemia were explored in rat at 4.7 T. It was shown that the primary contributions generated in blood or tissue can be modulated by interpulse interval (τ_{CP}) in a Carr-Purcell spin echo experiment. While long τ_{CP} T_2 depends greatly on the dephasing taking place in the extravascular compartment due to a BOLD effect, the short τ_{CP} T_2 shows reduced sensitivity to BOLD and approaches that achieved by spin-lock MRI.

The latter observation is explained in terms of a suppressed effect of dynamic dephasing in short τ_{CP} T_2. Interestingly, in developing infarction, Carr-Purcell T_2 MRI reveals dynamic dephasing contrast coinciding with water accumulation and cell loss in the brain tissue. This observation may provide a novel way in which to monitor the evolution of an ischaemic infarction by T_2 MRI.

In conclusion, the present study provides novel mechanistic information about acute ischaemic stroke and developing infarctions by using Hahn and Carr-Purcell spin echo T_2 contrast. It also provides a new means to quantify OER by T_2 MRI to be used for the assessment of cerebrovascular disease patients.

National Library of Medicine Classification: WN 180, WN 185, WL 355
Medical Subject Headings: diagnostic imaging; magnetic resonance imaging; brain ischemia / diagnosis; cerebrovascular circulation; hemodynamics; cerebrovascular disorders / diagnosis; carotid stenosis

…to my dearest wife Mária and my parents.

Acknowledgments

These studies were carried out at the A.I. Virtanen Institute for Molecular Sciences, University of Kuopio, during the years 1999-2004.

First and foremost I would like to offer my sincerest gratitude to my principal supervisor, Professor Risto Kauppinen, M.D. Ph.D. for his invaluable and continuous guidance as well as sharing his insight into the world of MR. His enthusiasm and endless devotion towards science resulted in the successful completion of this project.

My second supervisor, Docent Olli Gröhn, Ph.D., had the greatest influence over my day-to-day research during the last two years of my studies. For his unfaltering input, many fruitful discussions and friendship I am also truly grateful.

Furthermore, I wish to thank James J. Pekar, Ph.D., and Mark Lythgoe, Ph.D., the official reviewers of this thesis, for their invaluable comments and constructive criticism. I would also like to thank Tom Dunlop, Ph.D. for revising the language of this manuscript.

My sincerest thanks go out to all my co-authors: Mikko Kettunen, Ph.D., whom I always admire for his broad MR knowledge, Johanna Närväinen, Ph.D., our "blood" and physics expert, Professor Michael Garwood, Ph.D. (Center for Magnetic Resonance Research, University of Minnesota), Professor Aimo Rissanen, M.D. Ph.D. (Department of Neurology, Central Finland Central Hospital), Heidi Gröhn, Ph.D. and Pasi Tuunanen, M.Sc., for their invaluable contributions to this study. I especially wish to thank Jussi-Pekka Usenius, M.D. Ph.D. and his company (Keski-Suomen Magneettikuvaus Oy) for access to their clinical MRI scanner and for an exceptional working atmosphere.

I am also indebted to Docent Markku Penttonen, Ph.D. for introducing me to the exiting field of experimental neurosurgery and to Piia Valonen, M.Sc., Niina Kuhmonen and Maarit Pulkkinen for their skillful and expert technical assistance. I can not forget to thank Juhana Hakumäki, M.D. Ph.D., the present head of the Department of Biomedical NMR, as well as current and former members of the department for their support and friendship during my studies.

I am grateful to Kaija Pekkarinen, our departmental secretary, for countless times helping with administrative issues and an ever-cheerful smile on her face. My thanks also go to Docent Riita Keinänen, Ph.D., the coordinator of the Graduate School of the A.I. Virtanen Institute for her kind help over the years of my studies.

I wish to thank Jakub, Boryana, Šárka, Markko, Giedrius and Irina for great time spent together and to Ursula, exceptional and spontaneous Katarzyna, and Ferdinand, who was like a brother to me, for their support and warm friendship.

There is not enough thanks I can say to my dear parents Eduard and Jarmila for their love, sacrifices, perpetual and infinite support and encouragement, which I can never repay. To my brother Janko (and his family) for his faith in me, for all the skills he taught me and for every single discussion we had, I am truly grateful. I would also like to thank my great parents-in-law Ján and Katarína and my sister-in-law Kiťka and her (soon to be) husband Braňo for their love and support.

Over the years and particularly during this project, my dearest wife Mária has always stood beside me and shared my troubles and joys, highs and lows, excitement and frustration. Mária was always "the soldier in the front line" with me and if this work is finished it is thanks to her. I thank her for everything and anything from the

bottom of my heart.

Funding from the Academy of Finland, the Center for International Mobility (CIMO) and the Sigrid Juselius Foundation supported this research.

Kuopio, June 2004

Martin Kavec

Abbreviations

γ	gyromagnetic ratio
ω_0	Larmor frequency of a spin in a magnetic field
τ_{CP}	interpulse interval between consecutive refocusing pulses in Carr-Purcell spin echo type sequence
$\vec{B}_0$	main static magnetic field
$\vec{B}_1$	magnetic field component of a RF pulse
$\vec{M}_0$	equilibrium net magnetization
$\vec{M}_z$	longitudinal magnetization
$\vec{M}_{xy}$	transverse magnetization
b	coefficient of diffusion weighting
$C(t)$	contrast agent concentration at time t after injection
D_{av}	trace of diffusion tensor
$R_{1\rho}$	longitudinal relaxation rate in transverse plane; $R_{1\rho} = 1/T_{1\rho}$
R_2	apparent transverse relaxation rate; $R_2 = 1/T_2$
SI	MR image signal intensity
T_2^*	transverse relaxation time
T_1	longitudinal relaxation time
T_2	apparent transverse relaxation time
$T_{1\rho}$	longitudinal relaxation time in the rotating frame
$T_{2,\mathrm{diff}}$	proton diffusion component of transverse relaxation
$T_{2,\mathrm{exch}}$	proton exchange component of transverse relaxation
$T_{2,\mathrm{intr}}$	intrinsic transverse relaxation time

TE	echo time
TR	repetition time
AIF	arterial input function
ASL	arterial spin labelling
BAT	bolus arrival time
BOLD	blood oxygen level dependent
CBF	cerebral blood flow
CBV	cerebral blood volume
CCA	common carotid artery
$CMRO_2$	cerebral metabolic rate of oxygen
CPP	cerebral perfusion pressure
DSC MRI	dynamic susceptibility contrast MRI
DWI	diffusion weighted imaging
EPI	echo planar imaging
GM	grey matter
ICA	internal carotid artery
MCA	middle cerebral artery
MCAo	MCA occlusion
MPC	maximum peak concentration
MRI	magnetic resonance imaging
MTT	mean transit time
NMR	nuclear magnetic resonance
OER	oxygen extraction ratio
PET	positron emission tomography
PW	peak width
RF	radio-frequency
ROI	region of interest
SD	standard deviation
TTP	time to peak
VA	vertebral artery

List of original publications

This dissertation is based on the following publications referred to by their corresponding Roman numerals:

I Kavec, M., Gröhn, O. H. J., Kettunen, M. I., Silvennoinen, M. J., Penttonen, M., Kauppinen, R. A. (2001). Use of spin echo T_2 BOLD in assessment of cerebral misery perfusion at 1.5 T. MAGMA *12*(1), 32-9.

II Kavec, M., Usenius, J-P. , Tuunanen, P. I. , Rissanen, A., Kauppinen R. A. (2004). Assessment of cerebral haemodynamics and oxygen extraction using dynamic susceptibility contrast and spin echo blood oxygenation level dependent magnetic resonance imaging: applications to carotid stenosis patients. Neuroimage *22*(1), 258-67.

III Kavec, M., Gröhn, O. H. J., Kettunen, M. I., Silvennoinen, M. J., Garwood, M., Kauppinen, R. A. (2004). Acute cerebral ischaemia in rats studied by Carr-Purcell spin echo magnetic resonance imaging: assessment of blood oxygenation level dependent and tissue effects on transverse relaxation. Magnetic Resonance in Medicine. *51*(6), 1138-46.

IV Kavec, M., Gröhn, O. H. J., Garwood, M., Kauppinen, R. A. (2004). Dynamic dephasing changes in developing ischaemic cerebral infarction in rat studied by adiabatic Carr-Purcell T_2 MRI. *Submitted*.

Contents

Chapter 1

Introduction

The adult human brain represents approximately 2% of the total body mass, yet receives about 15% of resting cardiac output (Sokoloff, 1997). Under normal conditions, the brain is highly perfused and is very sensitive to any change or interruption of blood supply. Abruption of blood flow into the brain, i.e. caused by heart dysfunction or cerebrovascular disease, results in a loss of consciousness after a few seconds. Selective brain regions particularly sensitive to oxygen supply are permanently damaged after as early as 3-6 minutes and failing a restoration the blood flow beyond this time increases a risk of global brain damage.

Clinically, ischaemia is defined as a focal or global neurological impairment of sudden onset lasting for more than 24 hours. The main clinical indications of ischaemia are atherosclerotic occlusion of large vessels, embolic occlusion of distal vessels or arterial spasm following haemorrhage. The most common symptoms present in patients include numbness or weakness of face, arm or leg, which is often lateralised, confusion, difficulties in speaking or understanding speech, visual disturbances, mobility problems or severe headache. (Pettersson and Ringertz, 1998a)

Despite existence of vast body of preventive measures, ischaemic stroke was reported by World Health Organization (WHO) in 2002, as being the second leading cause of death in both the developing and developed countries. By the years to 2020, the number of people suffering from stroke will be substantially increasing annually worldwide.[1] Furthermore, cerebrovascular disease, as the most serious risk factor of cerebral ischaemia will be among the five most important causes of disability by 2020, and therefore will have a serious impact on societies and economics.[2]

It remains ironic that the ischaemic stroke is to a large extent preventable. Avoiding lifestyle habits such as cigarette smoking, improper diet, alcohol consumption and physical inactivity are known to significantly reduce the stroke risk. On the other hand, the clinical conditions such as hypertension, cardiac disease or dysfunction, atherosclerosis, diabetes, obesity and head and neck injuries are linked to accentuated risk of stroke. (Wolf, 1997)

Although the outcome of ischaemic events affecting the brain have been intensively studied for several decades, the factors determining the extent of final tissue

[1]Surveillance of Noncommunicable disease and Mental Health cluster, WHO, 2002.
[2]Lancet 1997; 349:1498-1504 & WHO, Evidence, Information and Policy, 2000

damage are not fully understood. However, both clinical and experimental evidence show that severity of blood supply reduction and the time, how long the brain tissue is exposed to low oxygen and nutrition supply, are the critical factors affecting ischaemia outcome. Consequently, only limited time window is available, in which to provide optimal diagnosis and treatment to a stroke victims. Furthermore, despite thorough clinical evaluation, neuroimaging with either computed tomography (CT), MRI or positron emission tomography (PET) is often needed for accurate diagnosis and choice of optimal patient treatment strategy, because these techniques allow for non-invasive visualization of the damaged brain.

The PET imaging has gained a unique place in neuroimaging of cerebrovascular diseases, providing quantitative data about cerebral haemodynamics, function and metabolism. PET, however, is not routinely employed in clinical setting due to high costs and few available equipments. Additionally, PET uses radiopharmaceutically labelled positron emitters as a primary source of information, thus imposing further possible health threats to a patient. Computed tomography remains the most commonly used modality for the initial evaluation of stroke due to higher availability of the CT scanners, lower cost of the examination and better access to critically ill patients. (Beauchamp and Bryan, 1997) Since only limited time window is available to improve the stroke outcome, usual clinical treatment of acute stroke involves a preliminary CT scan, to exclude the presence of a haemorrhage, followed by recombinant tissue plasminogen activator (rt-PA) treatment.[3] However, recent evidence established by clinical trials and experimental studies of cerebral ischaemia emphasises the advantages of MRI over the other neuroimaging modalities. Magnetic resonance imaging has superior sensitivity and specificity to acute stroke changes, has a potential to differentiate infarcted areas from those at risk of infarction and employing spectroscopic methods, it is able to estimate brain tissue metabolism. Recently applied magnetic resonance (MR) methods significantly contributed to the fact that MRI is becoming the method of choice in neuroimaging of ischaemic stroke.

[3] A blood clot dissolving drug; the only approved drug for clinical treatment of acute ischaemic stroke.

Chapter 2

Review of Literature

2.1 Cerebral circulation and cerebrovascular diseases

2.1.1 Cerebral circulation

The human brain and the brains of mammals in general are supplied by two pairs of main blood vessels (Fig. 2.1). Internal carotid arteries (ICA), branching from common carotid arteries form anterior circulation. Posterior circulation is formed by vertebral arteries (VA) joining to the basilary artery. Both right and left anterior and posterior vessels merge at the base of the brain and are interconnected by anterior and posterior communicating arteries to form a complete anastomotic[1] ring known as the circle of Willis[2]. Normally, blood from the ICA and VA does not mix much due to almost equal pressures in both arteries. However, the role of circle of Willis is crucial in cerebrovascular diseases (Hartkamp et al., 1999; Henderson et al., 2000; Hendrikse et al., 2001; Love et al., 1966; Perry et al., 1970; Roach et al., 1972). Focal obstruction of the feeding arteries, caused by stenosis or an embolism, may change the blood pressure balance and give rise to either anterior-posterior or side-to-side collateral flows, thus maintaining adequate cerebral blood flow (CBF). Three pairs of arteries that supply most of the brain tissues originate from the circle of Willis. These are the anterior, middle (MCA) and posterior cerebral arteries (Pettersson and Ringertz, 1998b; Mai et al., 1997). The arteries progressively divide to smaller blood vessels and form an anastomosing network of capillaries with mean diameter of 5 μm (Hudetz et al., 1993). Under normal physiological conditions, diffusive exchange of oxygen takes place in the capillaries and deoxygenated blood is drained to the venous network and takes out of the brain.

[1] Anastomosis - connection between tubular structures
[2] Thomas Willis; English anatomist and physician, 1621-1675

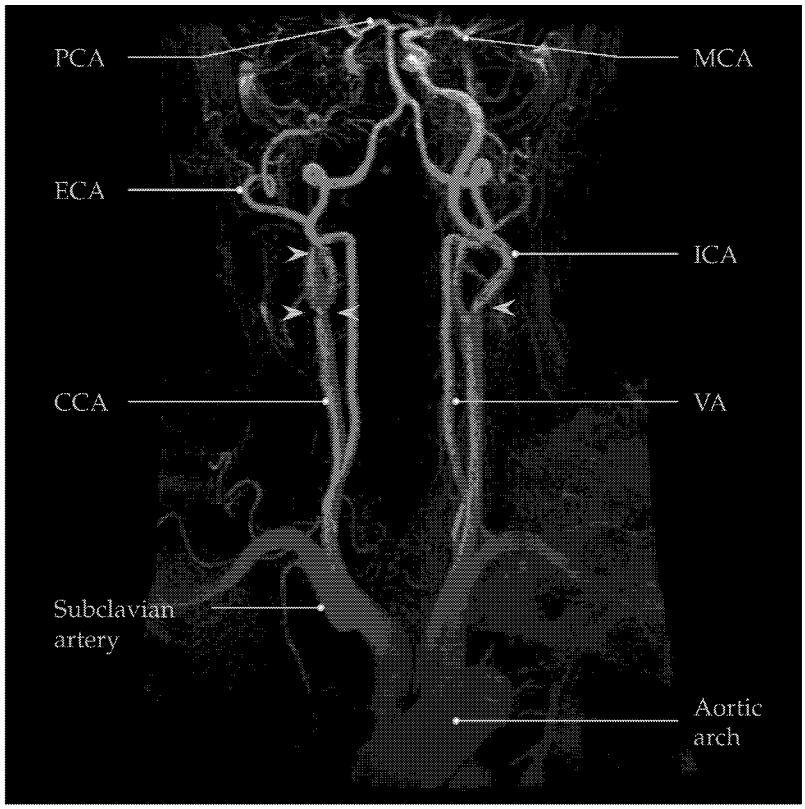

Figure 2.1: Arteriogram of human cerebral blood supply. CCA - common carotid artery, ECA - external carotid artery, ICA - internal carotid artery, MCA - middle cerebral artery, PCA - posterior cerebral artery, VA - vertebral artery. Note the stenoses of both CCA and occlusion of right ICA (arrowheads).[3]

2.1.2 Autoregulation of cerebral haemodynamics

Haemodynamic adaptations

Brain cells require a persistent and plentiful supply of oxygen and glucose from blood. The normal brain has several distinct mechanisms of haemodynamic autoregulation to maintain adequate cerebral perfusion pressure (CPP) over wide range of systemic blood pressure. Cerebral haemodynamic impairment often results from chronic hypotension or atherosclerotic disease. Severe stenosis of the carotid artery, VA or their intracranial branches may lead to reduced CPP in the peripheral microcirculation (Powers et al., 1987; White and Markus, 1997). It is well established that capillary dilatation reduces vascular resistance as a result of lowered CPP and thus prevents CBF decline (MacKenzie et al., 1979). This effect can be mathematically de-

[3]Subject with cerebrovascular disease. See page 59, subject 2, for more details.

scribed by Poiseuille's law[4]

$$\mathrm{CBF} = \frac{\pi\, r^4\, \Delta\mathrm{CPP}}{8\eta\, L} \tag{2.1}$$

where r, L and η are a vessel radius, length and blood viscosity, respectively.[5] Although a detailed discussion of the mechanisms that possibly mediate this vascular reflex is out of scope of this thesis, it is worth to mention that myogenic (smooth muscles relaxation), metabolic (concentration of O_2, CO_2, H^+, K^+, Ca^{2+} molecules and ions) and endothelial factors as well as neurotransmitters possibly affect this phenomenon (Chillon and Baumach, 1997). It is obvious that due to vasodilatation, more blood can be stored in a unit length of a microvessel, which results in an increase in cerebral blood volume (CBV). Indeed, experimental studies of cerebral hypoperfusion report a high microvascular CBV during haemodynamic challenge (Grubb et al., 1973; Grubb et al., 1975; Ferrari et al., 1992; Schumann et al., 1998; Zaharchuk et al., 1999).

When CPP begins to decline, the haemodynamic reserve of capillaries may become exhausted. In this situation, normal cerebral metabolism of oxygen ($\mathrm{CMRO_2}$) is preserved by augmentation of the oxygen extraction from capillaries. This physiochemical process depends on the oxygen tension gradient between the blood and tissues. A haemodynamic variable called the oxygen extraction ratio (OER) quantitatively expresses this process and is a measure of tissue oxygen metabolism and delivery:

$$\mathrm{OER} = \frac{\mathrm{CMRO_2}}{\mathrm{Hb}_{tot}\, \mathrm{CBF}\, Y_a} \tag{2.2}$$

where Hb_{tot} and Y_a are total haemoglobin and arterial oxygen saturation, respectively. PET studies of human subjects with severe haemodynamic impairment show elevated OER in vascular territories ipsilateral to arterial occlusive disease (Derdeyn et al., 1999b; Gibbs et al., 1984; Grubb, Jr et al., 1998; McHenry et al., 1961; Powers, 1991; Yamauchi et al., 1996).

Stages of cerebral haemodynamic impairment

Based on the adaptation processes to reduced CPP described above, Powers and colleagues proposed a two-stage sequential model of haemodynamic impairment in patients with atherosclerotic carotid artery disease (Powers et al., 1987). The first stage, known as autoregulatory vasodilatation, was identified as increased CBV or mean vascular time (the mathematical equivalent of CBV/CBF) with normal CBF, OER and $\mathrm{CMRO_2}$. Stage two, also called autoregulatory failure or misery perfusion (Baron et al., 1981), was characterized by reduced CBF and increased OER with normal oxygen metabolism. These stages were defined based on PET studies performed on patients with severe occlusive cerebrovascular disease and have been applied in classification of patients with carotid artery disease (Yamauchi et al., 1996) and animal models of graded reduction of CBF and acute ischaemia (Gröhn et al., 1998; Gröhn et al., 2000a).

[4] Jean Louis Poiseuille, French physician studying motion of liquids in the tubes with small diameter.

[5] Eq. 2.1 assumes constant velocity profile through the vessel diameter, instead of parabolic one, an implication of Newton's second law of motion.

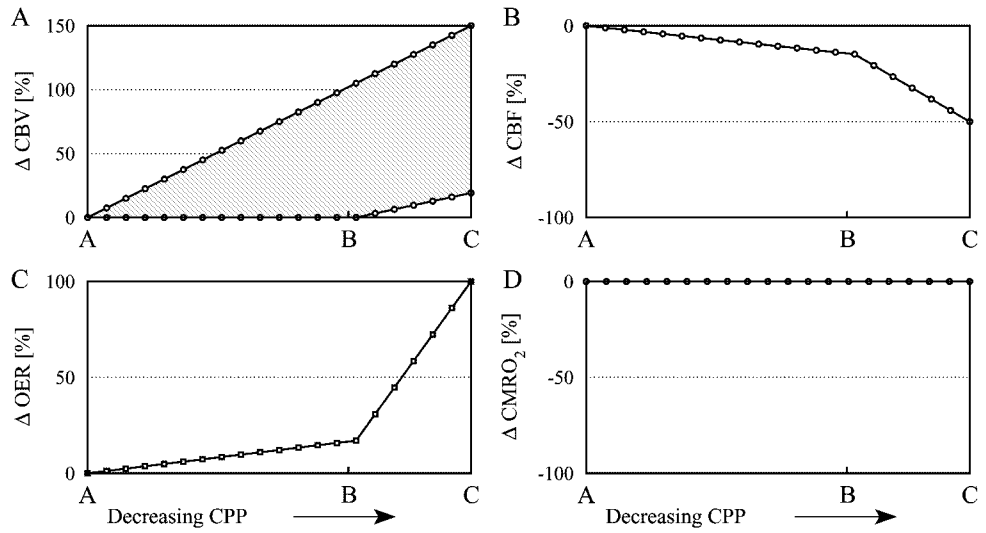

Figure 2.2: A model of haemodynamic and metabolic adaptations to a reduction in CPP. The distance between A and B point represents the autoregulatory range, and from B to C the exceeded autoregulatory range. Beyond point C, the compensatory mechanisms are exhausted and ischaemia onset follows. The shaded area (A) represents the interval of possible CBV values brain. (Derdeyn et al., 2002)

However, more recent experimental evidence has suggested that the sequential model is oversimplified by the assumption that OER would not increase, until the capacity of autoregulatory vasodilatation is exceeded. Therefore, the model has been revised by Derdeyn and colleagues in the following way (Fig. 2.2) (Derdeyn et al., 2002). As CPP decreases, CBF is reduced slightly in autoregulatory range (Dirnagl and Pulsinelli, 1990), and this leads to augmentation of OER prior to exhaustion of capillary vasodilatation (Fig. 2.2B, C). After this point, CBF decays as a function of pressure and OER may increase up to 100%. The studies of CBV upon reduced CPP report minimal or no increase in this parameter until autoregulatory capacity is exceeded (Schumann et al., 1998; Zaharchuk et al., 1999) and increased CBV within the range of autoregulation (Grubb et al., 1973; Grubb et al., 1975; Ferrari et al., 1992), respectively (Fig. 2.2A). Cerebral metabolism of oxygen remains unchanged within autoregulation, being maintained by a vasodilatation of the microcirculation and elevated OER (Fig. 2.2D) (McHenry et al., 1961; Grubb et al., 1975).

Clinically and diagnostically important observations emerge from the established model of compensatory mechanisms. High OER represents the state of exhausted cerebral haemodynamic autoregulation and is associated with high incidence of ischaemic stroke in patients with occlusive vascular disease (Grubb, Jr et al., 1998; Yamauchi et al., 1996). Recent revision of the two-stage adaptation model by Derdeyn et al. further refined the conclusion by claiming that augmentation of both CBV and OER represents a severe haemodynamic impairment, with high risk of subsequent stroke (Derdeyn et al., 2002).

2.1.3 Acute ischaemic stroke

Pathophysiology of acute ischaemia

Atherosclerotic vascular disease is among one of the most common indications in stroke patients.[6] Two basic mechanisms can explain the majority of the focal cerebral ischaemia in these cases: (a) thrombus fragmentation or vascular thrombosis that results in an embolic occlusion of a distal blood vessel and (b) limitation of the blood flow by narrowed vessel lumen, followed by haemodynamic stroke (Grubb, Jr et al., 1998). It is obvious that in the first case it is of crucial importance to identify the unstable lesion and by an appropriate treatment prevent the stroke. In the second case, because free arterial lumen is gradually reduced by growing atherosclerotic plaque, CPP decline in distal tissues is compensated by mechanisms described in Sec. 2.1.2. The onset of ischaemia is in this situation initiated by a reduction in microvascular blood flow below a threshold value. If the perfusion deficit persists, irreversible cellular damage follows quickly. The CBF threshold causing symptoms of ischaemia does not vary much among different mammals and its mean value was determined to be ~20 ml/100 g/min (Astrup et al., 1977; Gadian et al., 1987; Powers et al., 1987).

Under physiological conditions, energy-dependent electric potential gradient exists across cellular membranes.[7] By means of active transport, vital compounds including glucose, oxygen and water are transferred into the intracellular space, and products of cell metabolism are removed in the opposite direction. Experimental work on laboratory animals have demonstrated that a gradual reduction in CBF to ~22 ml/100 g/min causes a cessation in neuronal activity, while the cellular membrane potential is maintained (Astrup et al., 1977; Jones et al., 1981). Further studies revealed that the oxygen reserve is exhausted within seconds, while the energy is still available. At this point, cell metabolism becomes anaerobic, and is accompanied by lactate accumulation and acidosis (Hochachka and Mommsen, 1983; Katsura et al., 1991). When the energy supply runs out, ionic homeostasis is lost and anoxic depolarisation of the cellular membrane occures (Astrup et al., 1977; Nordström and Siesjö, 1978). Simultaneously, cytotoxic oedema, which is expressed as a shift of extracellular water into the cell body leads to cellular swelling (Crockard et al., 1980; Hossmann and Schuier, 1980). Since this happens in enclosed cranial space, cytotoxic oedema is usually associated with increased intracranial pressure that may be followed by displacement and compression of brain structures. It has been hypothesised that this process may further obstruct residual blood flow in capillaries and contribute to cell damage (Baethmann and Staub, 1997). Endothelial cells of capillaries and astrocytes are not spared from ischaemic injury. These cells constitute the so-called blood-brain barrier, a physiological interface between the blood and the brain parenchyma. Malfunction of blood-brain barrier renders leak of toxic compounds of plasma fluid into the extracellular space, causing irreversible cell damage (Garcia et al., 1977). Increased vascular permeability and influx of fluid containing plasma proteins into the extravascular space is a process termed vasogenic oedema and is clinically the most common type of brain oedema (Betz, 1997).

[6] The rest is attributed to systemic hypotension, cardiac disease, arterial dissection or unknown origin

[7] The gradient is a result of difference in extracellular and intracellular concentrations of K^+ and Na^+ ions and amounts between -60 and -90 mV.

Ischaemic penumbra

The idea of two CBF thresholds in the pathogenesis of cerebral infarction, functional one and morphological one, reported by Astrup and colleagues (Astrup et al., 1977) laid a basis for the concept of ischaemic penumbra. The penumbra was defined as the severely hypoperfused tissue surrounding ischaemic core with diminished electrical activity, but with residual CBF sufficient to maintain ionic cellular gradient (Astrup et al., 1981). It is believed that penumbra tissue is viable, but contributes to neurological deficit and is prone to death, unless the blood supply is restored. Because tolerance of a tissue to ischaemic damage is dependent on residual flow and the duration of flow disturbance (Heiss and Rosner, 1983), the ischaemic penumbra is a transient tissue condition. It exists for short period of time even in the ischaemic core, and may extend to increasing time periods in the more or less hypoperfused surrounding tissues (Heiss et al., 1994). The classical definition of penumbra with its attention focused on the cell, however, does not account for the temporal course of physiological perturbation. Therefore, penumbra is more appropriately characterized as the part of ischaemic tissue, which is potentially salvageable either by reperfusion or pharmacological intervention. It is a tissue in risk of irreversible ischaemia.

Over the past 25 years, ischaemic penumbra has been the target of intensive clinical and experimental research and many important diagnostic and therapeutic applications have emerged from these efforts. Experimental PET studies provided a unique insight into the metabolic and haemodynamic events, which characterize the evolution of an ischaemic core and penumbra, especially in relation to the function and viability (Heiss et al., 1994; Heiss et al., 1997; Pappata et al., 1993; Young et al., 1996). Despite the difficulties in obtaining PET data from hyperacute stroke patients, the concept of ischaemic penumbra was validated and resulted in several clinical studies.

2.2 Nuclear magnetic resonance

2.2.1 Concept of nuclear magnetic resonance

Spin and magnetism of nuclei

Historically, the basis of MR was laid down in 1920's, when during the development of quantum mechanical concepts of atomic structure, it became apparent that many of the atomic nuclei possess a property called spin angular momentum (Gerlach and Stern, 1924). Later, Rabi and coworkers (Rabi et al., 1938) explained the interaction of a proton with a magnetic field. These discoveries underpinned the research of Bloch (Bloch et al., 1946) and Purcell (Purcell et al., 1946), who successfully performed in 1946 the first nuclear magnetic resonance (NMR) experiments and introduced firm theoretical and experimental knowledge bases to this technique, for which they were awarded Nobel prize in physics in 1952. (Chen and Hoult, 1989; Haacke et al., 1999)

Magnetic resonance is a physical phenomenon of interaction of charged atomic particles that have non-zero intrinsic angular momentum (spin) with an external magnetic field. The intrinsic spin angular momentum $\vec{S}$ implies that spinning electric charge of a particle is associated with magnetic dipole moment $\vec{\mu}$. For a given particle, the exact relation between these quantities are:

$$\vec{\mu} = \gamma \vec{S} = \gamma m_s \hbar \qquad \text{and} \qquad \gamma \approx \frac{q}{2m} \tag{2.3}$$

where m_s, $\hbar$, q and m are the magnetic quantum number, the reduced Plank's constant and charge and the mass of a particle, respectively. In the Eq. 2.3, the proportionality constant γ, interrelating spin and magnetic property of a particle, is called the gyromagnetic ratio. For an unpaired electron, the intrinsic angular momentum $S = \pm 1/2$, resulting a non-zero magnetic dipole moment ($\gamma_e = 1.76\ 10^{11}$ rad/s/T). This, in principle, enables the observation of electron magnetic resonance.[8] The spin property of a proton is additionally affected by the presence of neutron. The spins of multiple nucleons in the heavier elements can compensate and in many cases result in a zero total angular momentum of a nucleus. Due to this fact, the magnetic moment of nucleus is commonly determined by measurement and is relatively smaller

Nucleus	Spin	γ [10^8 rad/s/T]	Concentration in human body
^{1}H	$\frac{1}{2}$	2.67	88 M
^{23}Na	$\frac{3}{2}$	0.78	80 mM
^{31}P	$\frac{1}{2}$	1.08	75 mM
^{17}O	$\frac{5}{2}$	-0.36	16 mM
^{19}F	$\frac{1}{2}$	2.51	4 μM

Table 2.1: Magnetic properties and concentrations in the human body of selected nuclei with non-zero spin angular momentum. (Haacke et al., 1999)

[8] The electron magnetic resonance techniques found the applications in anthropology, brewing industry, metalloenzyme biochemistry and the study of the electronic properties of molecules and atoms.

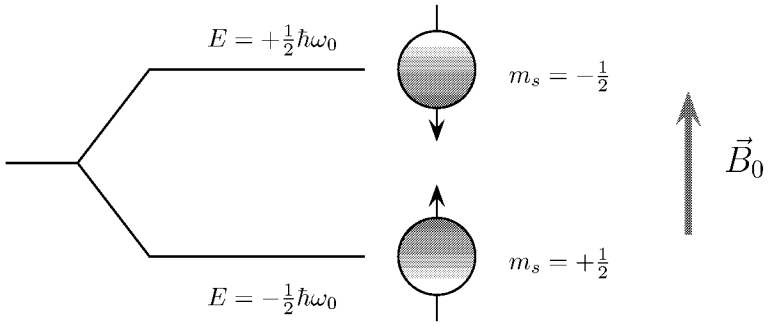

Figure 2.3: The Zeeman's energy levels with potential energies of $\pm\frac{1}{2}\hbar\omega_0$ for spins with $m_s = \mp 1/2$, such as ^{1}H.

than the magnetic moment of a single proton ($\gamma_p = 2.67\ 10^8$ rad/s/T). The nuclei listed in Table 2.1 all have non-zero spin, however, except for ^{1}H molecule, their low total magnetic moment and low concentration *in vivo* limit their biological NMR applications.

Interaction of spin and magnetic field

Brownian thermal motion of a molecule with magnetic spins is, under normal circumstances, responsible for the random orientation of nuclei and null net magnetic moment of a spin system. However, in the presence of applied external magnetic field $\vec{B}_0$, the spins are restricted to adopt either parallel or antiparallel orientations with respect to $\vec{B}_0$ (Fig. 2.3). Consequently, the spin populations N_p (parallel) and N_a (antiparallel) develop, with the energy status of N_a spins being higher than that of the N_p spins. The transition of the spin from higher to lower energy state is accompanied by the emission of an energy quantum (with frequency ω_0) equal to the potential energy difference between the levels:

$$\Delta E = E(N_a) - E(N_p) = [\mu(N_a) - \mu(N_p)]\, B_0 = \hbar\omega_0 = \gamma\hbar B_0 \tag{2.4}$$

One of the key conditions enabling the observation of NMR is the difference between the spin populations N_a and N_p. Since the spin system has a tendency to reach lower energy state, $N_p > N_a$, which yields an excess of spins aligned with external magnetic field $\vec{B}_0$.

The ratio of the spin populations is given by Boltzmann's probability distribution

$$\frac{N_a}{N_p} = e^{-\Delta E/kT} = e^{-\gamma\hbar B_0/kT} \tag{2.5}$$

where k and T are Boltzmann's constant and absolute temperature, respectively. At room temperature of $T = 300$ K and magnetic field $B_0 = 0.3$ T, there is probability that there is one spin out of million that is in a higher energy state and creating spin excess. Although, this number is very small, this is compensated by the very large

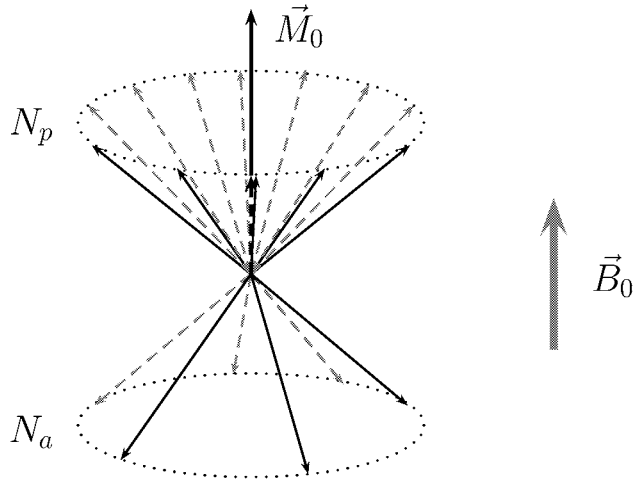

Figure 2.4: The difference in spin populations N_p and N_a in an external magnetic field $\vec{B}_0$ yields equilibrium magnetization $\vec{M}_0$.

numbers ($\sim 10^{23}$) of protons in a few grams of tissue. The combined signal from so many protons is sufficient to give a rise to a measurable equilibrium net magnetization $\vec{M}_0$, parallel to external magnetic field $\vec{B}_0$ (Fig. 2.4). Furthermore, Eq. 2.5 implies that the amplitude of the net magnetization $\vec{M}_0$ can be increased by either increasing amplitude of $\vec{B}_0$ or reducing the thermal motion of a spin system by decreasing its temperature.

The external magnetic field $\vec{B}_0$ applies an aligning force (torque) on rotating bulk spin system resulting a precession of the $\vec{M}_0$ around $\vec{B}_0$. The frequency of $\vec{M}_0$ precession is equal to a frequency of energy quantum, which is released during transition of a spin from high to low Zeeman's energy level.

$$\omega_0 = \gamma B_0 \tag{2.6}$$

Eq. 2.6 derives directly from Eq. 2.4, where ω_0 is so called Larmor frequency of proton spins in a magnetic field.[9] Eq. 2.6 is one of the key principles in NMR.

2.2.2 Proton spin excitation

In order to detect the NMR signal, the net magnetization $\vec{M}_0$ must be tilted from the direction of $\vec{B}_0$. This is accomplished by exposing the spin system to a radio-frequency (RF) pulse of the frequency satisfying resonance condition (rotation around $\vec{B}_0$ at frequency ω_0). Magnetization begin precession around the magnetic field component $\vec{B}_1$ of the RF pulse and is rotated from longitudinal direction towards the

[9]Sir Joseph Larmor; Irish physicist showed in 1897 that application of any aligning force to a spinning object results precession of the object.

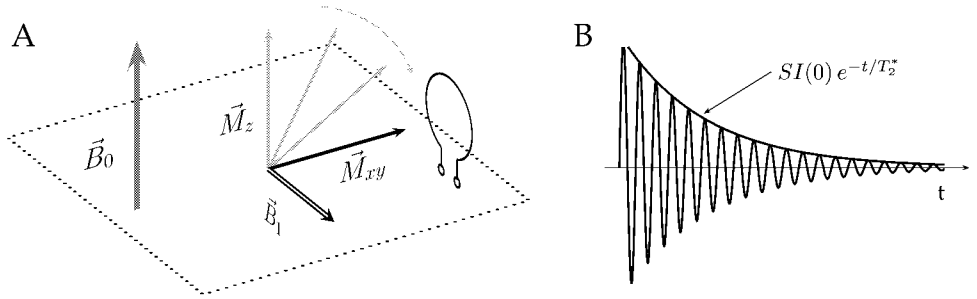

Figure 2.5: Longitudinal magnetization is rotated into the transverse plane by a 90° RF pulse $\vec{B}_1$ (A). Transverse magnetization $\vec{M}_{xy}$ induces alternating current in a receiver coil tuned to Larmor frequency (B).[10]

transverse plane (Fig. 2.5A). Projections of $\vec{M}_0$ into longitudinal direction and transverse plane are termed longitudinal ($\vec{M}_z$) and transverse ($\vec{M}_{xy}$) magnetizations, respectively. After the $\vec{B}_1$ is switched off, the $\vec{M}_z$ regains its amplitude and $\vec{M}_0$ returns to its equilibrium direction.

The flip angle of an on-resonance RF pulse is given by the amount of energy dissipated into the spin system during the RF transmittion ($t_0 - t_1$) (Eq. 2.7). The RF pulses, which rotate $\vec{M}_0$ by $\pi/2$ and π from its equilibrium direction are called 90° degree and inversion pulses, respectively.

$$\phi_1 = \gamma \int_{t_0}^{t_1} \vec{B}_1(t)dt \tag{2.7}$$

2.2.3 Return to equilibrium: T_1 relaxation

As described in the last section, irradiation of the spin system with an RF pulse at a Larmor frequency, the spins receive sufficient energy necessary to cross the barrier between the Zeeman's levels and this leads to a perturbation in the spin populations. This state is, however, unstable due to $\vec{B}_0$ favouring the parallel spin orientation. After the RF pulse is switched off, the spins begin to emit the excess energy into the surrounding lattice and return to the equilibrium state. The process of longitudinal magnetization $\vec{M}_z$ regrowth after a RF pulse irradiation is called spin-lattice or longitudinal relaxation.

The mechanisms of spin-lattice relaxation in the living systems are not fully understood. However, it is well established that the energy transmittion during spin-lattice relaxation is the most efficient, when the frequency of the processes receiving the energy is close to the Larmor frequency of the spins ω_0. The rotational and translational motion of molecules and chemical groups and spin exchange of bound and free water at macromolecule interfaces are known to enhance the longitudinal relaxation (Bottomley et al., 1984; Chen and Hoult, 1989).

[10]Fig. 2.5 takes place in so called rotating plane; the plane, which rotates around longitudinal direction at Larmor frequency.

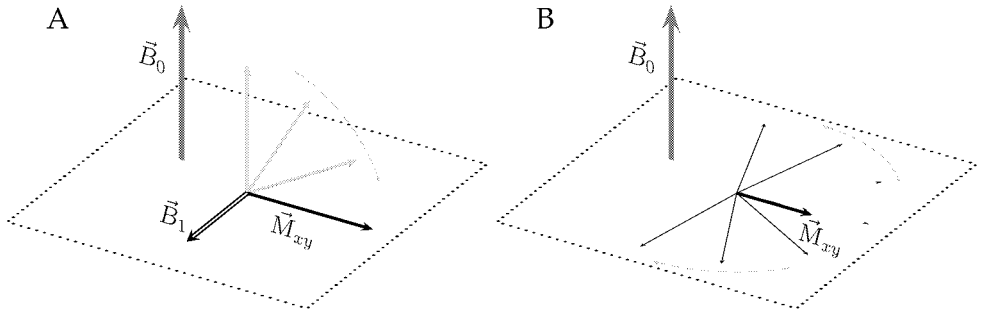

Figure 2.6: The spins in the transverse plane lose the phase coherence (B), resulting in decay of amplitude of the transverse magnetization M_{xy}.

The spin-lattice relaxation in NMR experiments is most commonly measured using the inversion recovery sequence of RF pulses.[11] Longitudinal magnetization $\vec{M}_z$ is initially inverted by a 180° RF pulse, followed by a delay period called the inversion time - TI. This delay is followed by 90° RF pulse and the immediate acquisition of MR signal. The amplitude of M_z is during TI delay determined by longitudinal relaxation and is given by Bloch equation (Bloch et al., 1946):

$$\frac{dM_z}{dt} = \frac{1}{T_1}(M_0 - M_z) \tag{2.8}$$

with a solution:

$$M_z(t) = M_z(0)(1 - 2e^{-t/T_1}) \qquad 0 < t < TI \tag{2.9}$$

In the Eqs. 2.8 and 2.9, T_1 is the constant characterizing a longitudinal relaxation in a measured sample.

2.2.4 Relaxation in the transverse plane

Spin-spin relaxation: transverse decay

The application of 90° pulse results in the precession of magnetization in the transverse plane and possible MR signal reception in a tuned receiver (Fig. 2.5). However, the signal reception would not last until the longitudinal magnetization $\vec{M}_z$ is fully relaxed, as could be deduced from previous section, but it decays rather fast. Immediately after 90° pulse is switched off, the spins begin to lose their phase coherence resulting in the fast decay of M_{xy} amplitude. This is termed as the transverse relaxation - T_2^* (Fig. 2.6). Generally, the inhomogeneities of the magnetic field $\Delta B_0(\vec{r}, t)$, which the spin system experiences, yield differences in Larmor frequency and leads to spin dephasing. In opposition to T_1, the temporal changes of the processes determining T_2^*, i.e. a frequency of $\Delta B_0(\vec{r}, t)$, must be slow in order to develop the phase

[11] Alternative is a saturation recovery, in which $\vec{M}_z$ is flipped into transverse plain by consecutive 90° RF pulse before $M_z(0)$ is recovered.

incoherence (Eq. 2.10).

$$\phi(\vec{r},t) = \gamma \int_{t_0}^{t_1} (B_0 + \Delta B_0(\vec{r},t))dt \tag{2.10}$$

One of the major factors determining the spin dephasing and T_2^* is inhomogeneity of the main magnetic field $\vec{B}_0$. The contribution of $\vec{B}_0$ inhomogeneities to T_2^* are accounted for in $T_2^{'}$ and determine the static dephasing regime:

$$\frac{1}{T_2^*} = \frac{1}{T_2^{'}} + \frac{1}{T_2} \tag{2.11}$$

Although, $\vec{B}_0$ inhomogeneities can be compensated for by applying local shimming fields, practical experience shows that only certain levels of $\vec{B}_0$ homogeneity are achievable, and it usually covers only small volume of a sample.

Another component of transverse dephasing is the apparent transverse relaxation T_2, which is determined by intrinsic transverse relaxation $T_{2,\text{intr}}$ and is governed by mechanisms including proton diffusion $T_{2,\text{diff}}$ and exchange $T_{2,\text{exch}}$. The diffusion and exchange specify dynamic dephasing and the Eqs. 2.13a and 2.13b quantitate the contributions of these to apparent transverse relaxation T_2:

$$\frac{1}{T_2} = \frac{1}{T_{2,\text{intr}}} + \frac{1}{T_{2,\text{diff}}} + \frac{1}{T_{2,\text{exch}}} \tag{2.12}$$

where

$$\frac{1}{T_{2,\text{diff}}} = \frac{1}{12} D(G\,\gamma\,\tau_{\text{CP}})^2 \tag{2.13a}$$

$$\frac{1}{T_{2,\text{exch}}} = \sum_i x_i\,\tau\,(\Delta\,\omega)^2 \left[1 - \frac{2\tau}{\tau_{\text{CP}}} \tanh \frac{\tau_{\text{CP}}}{2\tau}\right] \tag{2.13b}$$

In Eq. 2.13a, D, G and τ_{CP} are the spin diffusion coefficient, the background gradient amplitude and the parameter of measurement (which will be discussed later on), respectively (Hahn, 1950; Carr and Purcell, 1954). The inherent microscopic sample heterogeneity as well as the interfaces between sample compounds with different susceptibilities (for example different tissue types) generate background magnetic field gradients. Diffusion or exchange of the water molecules or spins through the susceptibility gradient further enhances T_2. Due to the facts that the trajectories of the spins and the time they spent in the gradient fluctuations are random, the spins gain random phase shifts (Eq. 2.10).

Under the condition of fast exchange time (τ) between the sites with different Larmor frequencies $\Delta\omega$, the $T_{2,\text{exch}}$ relaxation for a general multi-site system with a fraction of spins x_i occupying site i is given by Eq. 2.13b.

The intrinsic $T_{2,\text{intr}}$ relaxation is a physical property of a spin system driven by dipole-dipole interactions and energy exchange. As discussed in the Sec. 2.2.1, many atomic nuclei and electrons have spin properties and possess magnetic moments. These magnetic moments yield random local microscopic magnetic environments

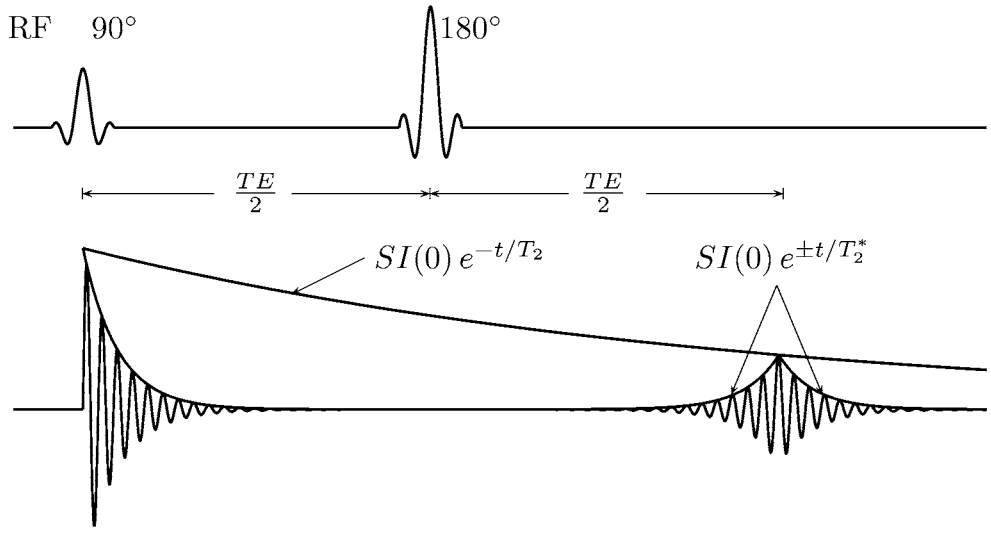

Figure 2.7: The Hahn echo experiment. Transverse magnetization is refocused by a 180° RF pulse at $TE/2$ time followed by spin echo signal acquisition at TE time.

observed by neighbouring spin, which vary rapidly and can be further affected by presence of paramagnetic compounds[12].

The apparent transverse relaxation is commonly measured using RF pulse sequences that produce spin echoes (Hahn, 1950; Carr and Purcell, 1954). Equilibrium magnetization $\vec{M}_0$ is initially rotated into the transverse plane by 90° RF pulse.The spins begin to dephase as a result of T_2^* effects and decaying $\vec{M}_{xy}$ induces a free induction decay (FID) signal in the tuned receiver (Fig. 2.7). At a time $TE/2$ the spins are refocused by a 180° pulse, which effectively inverts the phase of the spins in the transverse plane. At a time TE - echo time the spins are rephased (Fig. 2.7) and induce a spin echo signal in a proximal detector. Further echoes can be obtained with additional refocusing pulses, with the echo-to-echo amplitude decay driven by apparent T_2 relaxation. The dynamic dephasing contribution to the T_2 can be further minimized by the multiecho spin echo approach (Carr and Purcell, 1954). Carr and Purcell first observed the effect of increasing spin echo amplitude with increasing the number of the refocusing pulses. This was attributed to a partial recovery in spin phase coherence due to frequent application of the refocusing pulses with an interpulse interval τ_{CP}. This observation in the context of the Eqs. 2.13a and 2.13b implies that the transverse relaxation times measured with the multiecho spin echo approach ($\tau_{\mathrm{CP}} < TE$) are longer than with the single spin echo approach ($\tau_{\mathrm{CP}} = TE$).

Assuming spin-spin relaxation only, the amplitude of transverse magnetization

[12] A compound with a small but positive magnetic susceptibility, contains one or more unpaired electrons and may greatly reduce the relaxation times of water.

$\vec{M}_{xy}(t)$ at time t after a 90° RF pulse is given by a Bloch equation (Bloch et al., 1946):

$$\frac{dM_{xy}}{dt} = \frac{M_{xy}}{T_2} \tag{2.14}$$

with a solution:

$$M_{xy}(t) = M_{xy}(0)e^{-t/T_2} \qquad 0 < t \tag{2.15}$$

T_1 relaxation in rotating plane

The T_1 relaxation in the rotating plane is generally termed as $T_{1\rho}$ (Jones, 1966; Sepponen et al., 1985). Fig. 2.8 shows the experimental principle of $T_{1\rho}$ measurement. The net magnetization is initially tilted to the transverse plane by 90° RF pulse. This is then followed by a spin-lock RF pulse $\vec{B}_{1sl}$ applied in the direction of transverse magnetization. During the spin-lock time, $\vec{M}_{xy}$ precesses around the $\vec{B}_{1sl}$ with a resonance condition $\omega_{1sl} = \gamma B_{1sl}$. The discussion in Sec. 2.2.3 implies that the frequency of the processes contributing to $T_{1\rho}$ should be close to the resonance frequency and hence close to ω_{1sl}. This frequency is due to low B_{1sl} amplitude very low, leading to the high sensitivity of $T_{1\rho}$ to slow molecular motion of macromolecules and the interaction of water and protein molecules, respectively. A similar frequency range also affects transverse relaxation, and as $B_{1sl} \rightarrow 0$, $T_{1\rho}$ approaches T_2 relaxation.

The invaluable advantage of the spin-lock method is that it probes the relaxation at very low magnetic field strengths[13], yet it takes the advantage of spin polarization (Eq. 2.5) produced by several-folds higher B_0, which yields much higher signal.

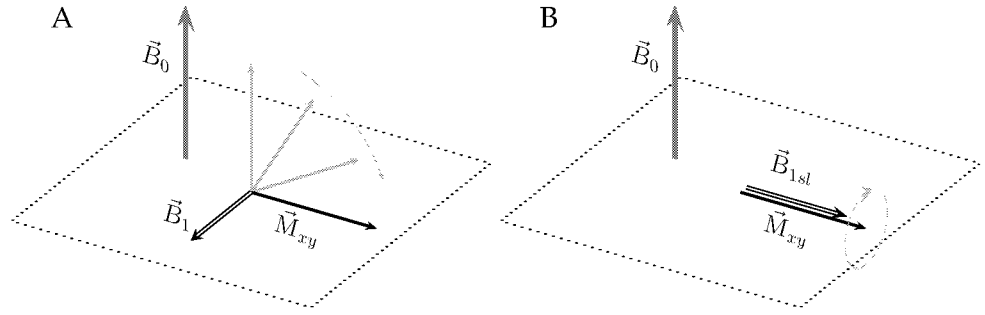

Figure 2.8: T_1 relaxation in the field of spin-lock RF pulse $\vec{B}_{1sl}$.

2.2.5 Magnetic resonance imaging: spatial encoding

Kudravcev and coworkers in National Institutes of Health in 1960 realized that field inhomogeneities could be used to encode the spatial information in a NMR experiment. In the following year, they successfully demonstrated this phenomenon using both static and alternating fields. However, at that time the potential of these

[13] B_{1sl} is of order of μT

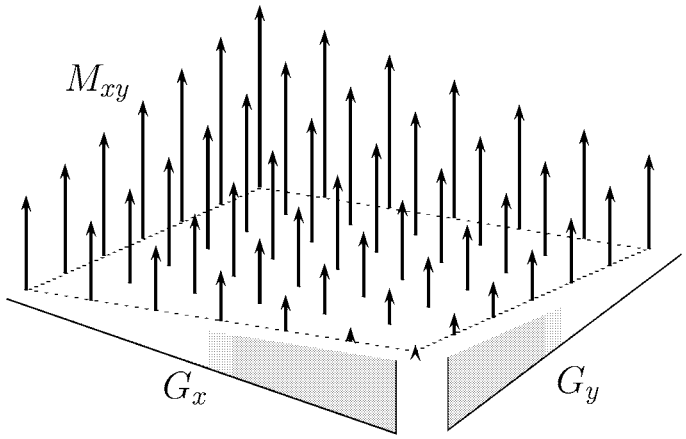

Figure 2.9: Encoding spatial information by means of magnetic field gradients. Larmor frequency of M_{xy} is proportional to the amplitude of field gradients at a particular spatial coordinate.

results was not recognized, and were never published. (Chen and Hoult, 1989) Substantial efforts were spent to further develop the spatial encoding and an efficient method of generating two-dimensional (2D) images was designed by Lauterbur and coworkers in early 70's (Lauterbur, 1973). This method relied on the relationship between spin resonance frequency and the linear gradient field and resulted for the first time 2D representation of the spin density and relaxation times. This invention increased the interest in the NMR methods for biological applications and resulted several innovations including: the idea of slice selection using frequency-selective RF pulses (Lauterbur et al., 1975), spin warp method (Edelstein et al., 1980), rotating frame imaging (Hoult, 1979), echo planar imaging (EPI) (Mansfield, 1977) and Fourier transformation imaging (Kumar et al., 1975).

The effect of field gradient on the Larmor frequency of the magnetization is essentially the same as the effect of generic field inhomogeneity given by Eq. 2.10. However, the controlled manner of varying magnetic field across a sample produces a signal with spatially varying frequency components:

$$\omega(\vec{r},t) = \omega_0 + \omega_G(\vec{r},t) = \omega_0 + \gamma\,\vec{r}\,G_{\vec{r}}(t) \tag{2.16}$$

where $\vec{r}$ and $G_{\vec{r}}(t)$ are a position vector and the magnetic field gradient, respectively. The frequency spectrum of the MR signal obtained from the sample is a composition of spin resonance frequencies linearly varying with the $\vec{r}$ (Eq. 2.16). The frequency domain to space domain transformation is accomplished by means of a Fourier transformation[14]. The expansion of the concept of the spatial encoding by applying the field gradients into two or three orthogonal directions yields after Fourier transformation 2D image or 3D representation of an object.

[14]Joseph Fourier (1768-1830), French mathematician and physicist

2.3 MRI of cerebrovascular disease and ischaemic stroke

2.3.1 Estimation of cerebrovascular reserve

Among the very first autoregulatory events in cerebrovascular disease is dilation of microvessels (Sec. 2.1.2). Measurement of vascular reactivity to vasodilatory stimuli can be utilized to identify the brain regions with abnormal or no reaction, which indicate the presence of maximally dilated vasculature. Mild hypercapnia, induced by i.e. CO_2 inhalation or breath-hold, or intravenous injection of acetazolamid are known to increase microvascular CBF in normally perfused tissue while metabolism remains unchanged. Haemodynamically challenged brain territories lack this signature.

In healthy subjects, blood oxygen level dependent (BOLD) MRI (Sec. 2.3.4) acquired during vasodilatory stimulus decreases concentration of paramagnetic deoxyhaemoglobin in the blood and results MR signal enhancement in T_2 and T_2^*-weighted images. This approach was used to assess cerebrovascular reserve in the patients with severe ICA occlusion and yielded attenuation of MR signal in the vascular territories of occluded arteries due to high concentration of deoxygenated haemoglobin (Kleinschmidt et al., 1995). Furthermore, Lythgoe and colleagues obtained significant correlation between vascular reactivity in MCA territory and blood velocity in MCA, determined by BOLD MRI and transcranial Doppler, respectively in the subjects with cerebrovascular disease with preserved vascular reflex (Lythgoe et al., 1999). By direct MRI measurement of CBF, acetazolamide stimulation revealed a decreased cerebrovascular reserve in the affected areas of the symptomatic hemisphere, indicating a severely compromised haemodynamics in cases with ICA stenosis or occlusion (Detre et al., 1999; Guckel et al., 1996; van Osch et al., 2002; Schreiber et al., 1998; Wiart et al., 2000).

2.3.2 Detection of oedema in acute ischaemia

With the advances in MR technology, particularly in gradient coil system design achieved during the last decade, new possibilities for acute stroke diagnosis have emerged. The ability of MR scanner gradient systems to produce high-amplitude and fast-switching gradient fields made it possible to study the diffusion of water molecules *in vivo* by means of diffusion-weighted imaging (DWI) (Moseley et al., 1990a; Moseley et al., 1990b; Stejskal and Tanner, 1965).

Diffusion sensitive sequences are usually designed by placing a pair of large-integral gradients on each side of refocusing RF pulse (Le Bihan et al., 1986). Because of Brownian motion of the water molecules in tissue, spins randomly change their position and orientation and thus gain random phase as they diffuse through field gradients (Eq. 2.10). The phase of the spins that moved during or after the first gradient is not rephased by the second one thereby the net transverse magnetization amplitude is a product of effective transverse relaxation and attenuation effect of the diffusion-sensitizing gradients:

$$M_{xy} = M_0\, e^{-\frac{t}{T_2}}\, e^{-b\cdot D} \qquad \text{where} \qquad b = (\gamma\, G\, \delta)^2(\Delta - \frac{\delta}{3}) \tag{2.17}$$

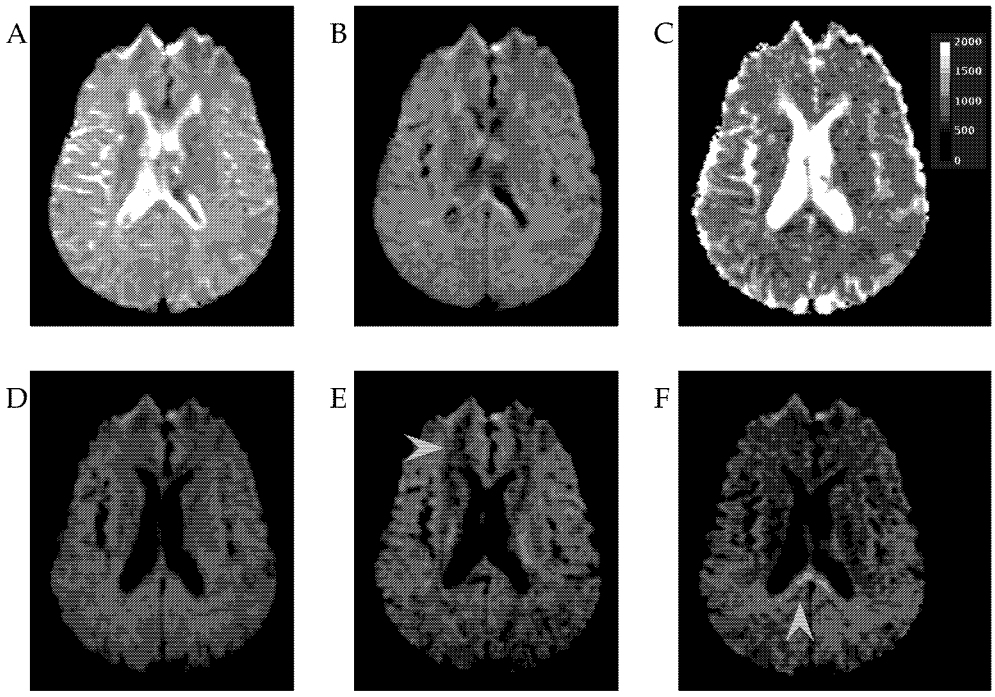

Figure 2.10: Diffusion-weighted images with b-value of 200 (A), 500 (B) and 1000 (D-F) s/mm^2 and corresponding map of D_{av} (mm^2/s) (C). Diffusion-weighted images (D-F) acquired with diffusion sensitizing gradients in different orthogonal directions, demonstrating orientation dependent contrast (arrowheads) due to anisotropy of water diffusion.[15]

where the coefficient of diffusion weighting b is a function of the gyromagnetic ratio (γ), the diffusion-sensitizing gradient amplitude (G), length (δ) and the time interval between onset of the gradient pair (Δ). It is clear from the Eq. 2.17 that when b and diffusion constant (D) are higher the signal attenuation becomes stronger (Fig. 2.10).

The degree of water molecule diffusion is expressed *in vivo* by apparent diffusion coefficient (ADC), which takes into account the effect of multiple environments (with different diffusion constants) that water molecule is exposed to during MR experiment. Additionally, water diffusion in living systems is restricted by neuronal fibres and cellular environment. This results in an orientation dependent contrast in DWI (Moseley et al., 1990a) (Fig. 2.10D-F). In this regard, water diffusion is described by tensor and an orientation independent estimate of diffusion constant that is given by the trace of the diffusion tensor (D_{av}). Practically, D_{av} is quantified either by averaging images obtained in three separate experiments, with diffusion gradients applied in three orthogonal directions (Basser et al., 1994; Pierpaoli et al., 1996) (Fig. 2.10C) or in single scan approach using bipolar diffusion gradients with cancelled off-diagonal tensor elements (Mori and van Zijl, 1995).

[15]Subject with cerebrovascular disease. See page 59, subject 2, for more details.

Applications of DWI MRI in ischaemia

As described in Sec. 2.1.3, cellular energy failure due to ischaemia results in the loss of ion homeostasis followed by water shifting into the intracellular environment (cytotoxic oedema). Intracellular water and metabolites diffusion becomes restricted by cell membrane and organelles and extracellular diffusion decreases due to cell swelling (de Crespigny et al., 1999; Decanniere et al., 1995; Hakumäki et al., 2000; van der Toorn et al., 1996a). Reduced diffusion in acute ischaemia yields less MR signal loss, hence can be identified as hyperintense areas in DWI MRI.

Moseley and colleagues reported that the signal intensity of ischaemic cat brain significantly increased in DWI 15 min after MCA occlusion, well before any changes in T_2-weighted images (Moseley et al., 1990a; Moseley et al., 1990b). Moseley et al. concluded that the early decrease of ADC is associated with cytotoxic oedema. Further evidence was provided by Busza et al., who determined that ADC drops at CBF of 20 ml/100 g/min (Busza et al., 1992), a value which is almost identical to threshold of anoxic depolarization in ischaemic monkeys (Astrup et al., 1977). Magnetic resonance spectroscopy studies of global ischaemia models combined with water diffusion measurement revealed agreement between the time course of ADC decrease and energy failure (Decanniere et al., 1995; Hossmann et al., 1994; van der Toorn et al., 1996b).

Depending on the severity of ischaemia, the diffusion coefficient can either stay low or even decrease further. Maximum decrease in ADC (down to 50-60% of control levels) was observed after 20 minutes of cardiac arrest or 24-48 hours after focal ischaemia in rats (Hoehn-Berlage et al., 1995; Knight et al., 1994). In the shorter ischaemia insult, the ADC is known to normalize; however, secondary ADC decline and delayed cell death may follow (Li et al., 1999). In the time scale of 24-48 hours, ADC begins to normalize and at later time points, ADC exceeding the normal values were measured in rats (Knight et al., 1991; Knight et al., 1994; Li et al., 1999; Verheul et al., 1992).

Due to inherent similarities in biophysical and anatomical properties of brain among mammalian species, most of the knowledge about experimental ischaemia is directly applicable to human patients. The introduction of DWI into the clinical environment was clearly a breakthrough in the diagnosis of acute stroke patients (Kohno et al., 1995; Moseley et al., 1995; Warach et al., 1992a; Warach et al., 1995). Diffusion MRI became a standard part of stroke neuroimaging protocols and opened up new prospects in the treatment and monitoring of acute and subacute stroke. The early reduction of ADC in human stroke was observed 1-2 hours after the symptom onset (Warach et al., 1992a), followed by pseudonormalization between 4-10 days and values higher than in normal tissue in the subacute phase (Lutsep et al., 1997; Schlaug et al., 1997; Sorensen et al., 1996; Warach et al., 1992a; Warach et al., 1995). Earlier normalization of ADC was observed in patients with restored perfusion (Schlaug et al., 1997; Kidwell et al., 2000), suggesting either a tissue recovery or an early infarction evolution. The study of 50 patients with symptoms of acute stroke demonstrated significant correlation between acute lesion volume determined by ADC decline and chronic lesion volumes (Lövblad et al., 1997). These results suggest that lesion volume determined by DWI in the acute phase of disease may predict clinical severity and the outcome of ischaemia.

2.3.3 MR methods for the assessment of cerebral haemodynamics

A knowledge of cerebral haemodynamics in occlusive cerebrovascular disease has increased greatly during last two decades and clinical trials stress the importance of this information in patient diagnosis (Grubb, Jr et al., 1998). Although, the methods to obtain this information have been developed (CT, PET, hydrogen clearance), the desirable criteria of total noninvasiveness, reproducibility, accuracy, high resolution, high availability and safety in single technique has not been attained.

The sensitivity of MR to large-scale motion of the spins was noted in the early stages, therefore not surprisingly, the methods to image perfusion were developed (Le Bihan et al., 1986). Over the last decade, two distinct MRI techniques have found applications in clinical settings and experimental studies. These are (1) Dynamic susceptibility contrast (DSC) MRI, also known as bolus tracking, which uses exogenous paramagnetic contrast agents and (2) Arterial spin labelling (ASL), employing the protons of water molecules in arterial blood as an endogenous contrast media (Calamante et al., 1999b; Detre et al., 1992; Thomas et al., 2000; Williams et al., 1992).

Bolus tracking perfusion imaging: DSC MRI

Bolus tracking perfusion-weighted imaging methods are not entirely noninvasive, since they require bolus injection of the contrast agent into a peripheral vein (typically 0.1-0.3 mmol/kg of body weight). The contrast agents used in DSC MRI contain paramagnetic compounds (most commonly gadolinium) that shorten the transverse relaxation. Contrast bolus passage through parenchyma is sampled by fast multislice MRI and leads to transient signal reduction in T_2 and T_2^*-weighted images (Fig. 2.11).Quantification of cerebral haemodynamics is based on the principle of kinetics of a nondiffusable tracers (Axel, 1980; Meier and Zierler, 1954; Zierler, 1965). The concentration of a contrast agent in a volume of interest is needed for this purpose. Since MRI is unable to directly measure the tracer concentration, its effect on signal intensity is employed. It has been shown, both empirically (Villringer et al., 1988; Rosen et al., 1990) and by Monte Carlo simulations (Boxerman et al., 1995; Weisskoff et al., 1994), that the tracer concentration can be estimated as follows:

$$C(t) = -\frac{k}{TE} \cdot ln\frac{SI(t)}{SI(0)} \tag{2.18}$$

,where $C(t)$ is a tissue tracer concentration at time t of bolus pass, $SI(t)$ and $SI(0)$ are the signal intensities at time t of bolus pass and intensity before contrast agent injection, respectively. The proportionality constant k depends on the sequence type, magnetic field strength, tissue type and contrast agent.

For absolute quantification, a tracer concentration in a feeding artery within a VOI is required (Axel, 1980; Meier and Zierler, 1954; Zierler, 1965). In DSC MRI arterial input function (AIF) is obtained by positioning the region of interest (ROI) on a feeding artery, i.e. MCA or ICA, and it was shown that this approach yields the concentration proportional to the values sampled from arterial blood (Rosen et al., 1991). The shape of AIF depends not only on the speed and amount of injected contrast agent, but also on cardiac output, vascular geometry and possible presence of vascular disease (Calamante et al., 2000; Lythgoe et al., 2000a; Perthen et al., 2002). Additionally, the

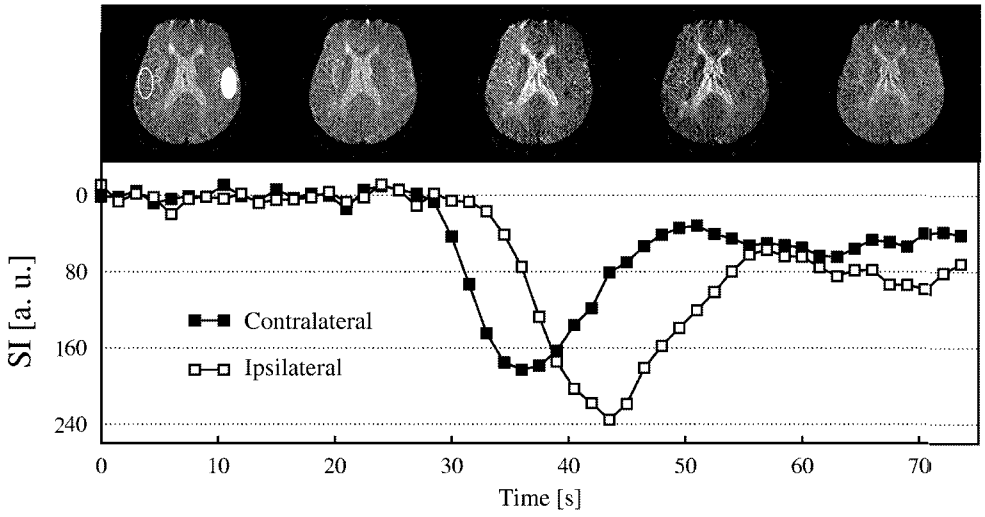

Figure 2.11: SE-EPI images and MR signal intensity in the regions of interest during contrast agent bolus passage. Note the significantly delayed bolus arrival and higher contrast agent concentration in the right hemisphere due to severe cerebrovascular disease (right ICA occlusion).[16]

AIF can be biased due to a partial volume effect with surrounding tissues. A method addressing this issue has been proposed by van Osch and colleagues (van Osch et al., 2001).

With knowledge of AIF, DSC MRI allows for the quantification of absolute CBF, CBV and mean transit time (MTT), as well as a qualitative estimation of cerebral haemodynamics by characterizing the bolus arrival time (BAT), time to peak (TTP), maximum peak concentration (MPC) and peak width (PW).

If a bolus of contrast agent injected into a peripheral vein is considered, the concentration of the tracer in a tissue as function of time is a convolution of arterial contrast media concentration $C_a(t)$ and a residue function $R_t(t)$[17].

$$C_t(t) = \frac{\rho}{k_h} \cdot \text{CBF} \cdot [C_a(t) \otimes R_t(t)] \tag{2.19}$$

Proportionality constants ρ and k_h take into account the density of a brain tissue and the hematocrit ratio in small and large vessels, respectively. To calculate CBF, the residue function ($R_t(t)$) must be deconvolved from Eq. 2.19. Østergaard and colleagues assessed performance of several deconvolution methods by both Monte Carlo simulations and human data (Østergaard et al., 1996a; Østergaard et al., 1996b). The results show that model-independent deconvolution by singular value decomposition (SVD) is the most robust, the least sensitive to noise and accurately estimates a wide range of CBF values. However, recently it has been shown that SVD is sensitive to bolus delay and dispersion and thus compromises the reliability of the CBF

[16]Subject with cerebrovascular disease. See page 59, subject 2, for more details.

[17]Fraction of tracer still present in tissue at time t, following an ideal bolus injection

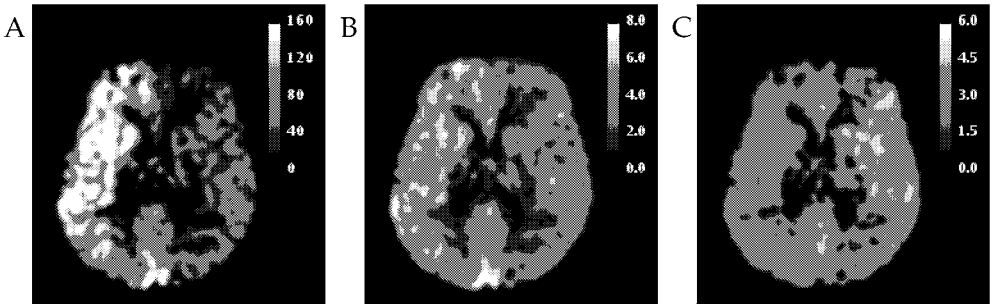

Figure 2.12: Maps of absolute CBF (ml/100 g/min) determined by SVD (A), CBV (ml/100 g) (B) and MTT (s) (C). Note the CBF overestimation, and therefore underestimation of MTT, in the right hemisphere due to delayed bolus arrival and dispersion (Fig. 2.11).[18]

values (Calamante et al., 2000). Bolus delay and dispersion are commonly observed in cerebrovascular disease (Calamante et al., 2001; Lythgoe et al., 2000a; Neumann-Haefelin et al., 2000c) and acute stroke, hence the use of SVD in these pathologies is seriously limitated. Recently, methods less sensitive to bolus dynamics (Østergaard et al., 1999) and employing fluid dynamics (Calamante et al., 2003) for correction of the bolus delay and dispersion were reported. However, the value of these methods in a clinical context has not been exploited yet.

Another important haemodynamic parameter, which can be derived from DSC MRI data is CBV. Quantification of CBV requires integration of the area under tissue and artery response to tracer media passage.

$$\mathrm{CBV} = \frac{k_h}{\rho} \cdot \frac{\int C_t(t)dt}{\int C_a(t)dt} \tag{2.20}$$

The integration is fairly simple to perform, yet CBV values can be severely biased due to contrast agent recirculation. To avoid this issue, concentration data are commonly fitted to a gamma-variate function (Thompson et al., 1964). For CBV quantification, $C_t(t)$ curves are usually integrated (a) after fitting to the gamma-variate function, (b) numerically integrated between thresholds, (c) numerically integrated from bolus arrival time until the end of the concentration time curve or (d) determined from residue function after SVD (Calamante et al., 1999b). The integration after SVD was shown to yield best CBV estimates (Perkiö et al., 2002), however, as mentioned earlier in the text, this method has limited applicability, unless bolus delay and dispersion are properly assessed.

The MTT is another physiological parameter often quantified from DSC MRI. By definition, MTT is the average time required by any tracer particle to pass through the tissue after an ideal bolus injection. Once CBF and CBV are known, the MTT can be calculated from the central volume theorem (Meier and Zierler, 1954):

$$\mathrm{MTT} = \frac{\mathrm{CBV}}{\mathrm{CBF}} \tag{2.21}$$

[18]Subject with cerebrovascular disease. See page 59, subject 2, for more details.

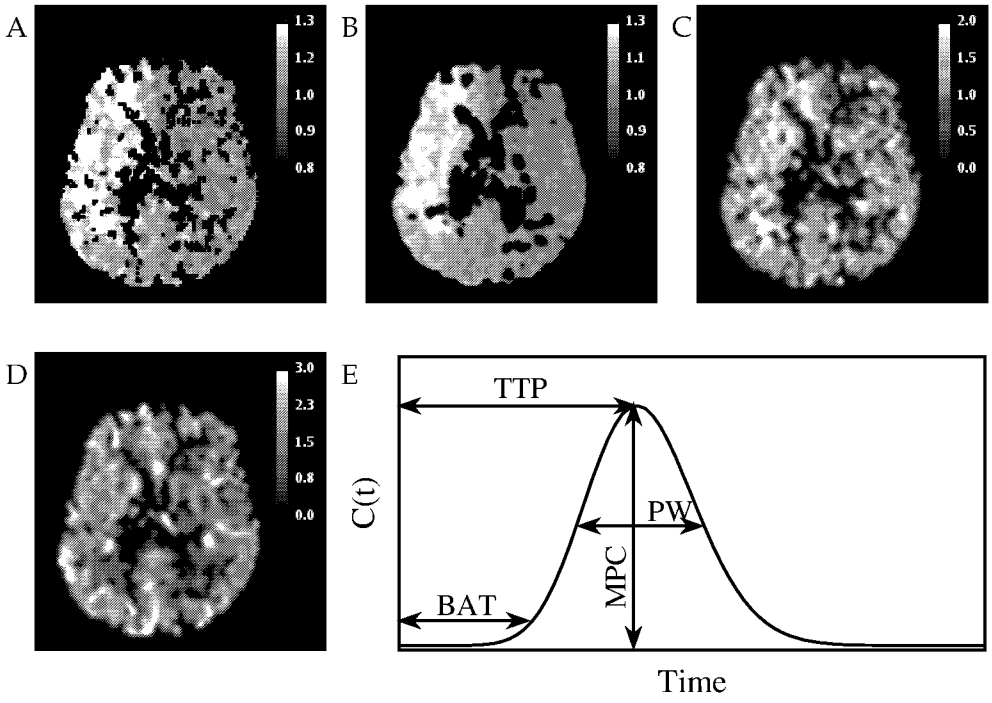

Figure 2.13: Relative maps (normalised to the mean value of the left hemisphere) of the summary parameters: BAT (A), TTP (B), PW (C) and MPC (D) and their illustration in (E). Delayed BAT and TTP are notable on the side of cerebrovascular disease.[19]

The summary parameters (TTP, BAT, MPC, PW) obtained directly from the $C_t(t)$ curve can be used for indirect estimation of cerebral perfusion (Fig. 2.13E). The summary parameters are frequently quoted both in animal (Gröhn et al., 1998; Kucharczyk et al., 1991; Kucharczyk et al., 1993; Li et al., 1999; Moseley et al., 1990a; Wendland et al., 1991) and clinical studies (Calamante et al., 2001; Maeda et al., 1999; Neumann-Haefelin et al., 1999; Nighoghossian et al., 1996; Schlaug et al., 1999) due to fast and straightforward analysis, which does not require AIF and deconvolution of residue function. However, Perthen and colleagues showed that the value of each summary parameter is highly dependent upon both the AIF and $R_t(t)$ and hence caution should be exercised in the interpretation of these parameters (Perthen et al., 2002).

As mentioned earlier, in principle, DSC MRI allows for the quantification of cerebral haemodynamics in absolute units. Here, either fixed values for relevant proportionality constants k_h and ρ (Eqs. 2.19 and 2.20) or calibration of DSC MRI derived values with PET, are used respectively. The studies employing the former approach have reported CBF and CBV values agreeing with PET in normal subjects and patients with cerebrovascular disease (Rempp et al., 1994; Guckel et al., 1996; Schreiber et al., 1998).

[19]Subject with cerebrovascular disease. See page 59, subject 2, for more details.

In the latter alternative, Østergaard and colleagues empirically determined the calibration factors in normal and hypercapnic pigs (Østergaard et al., 1998b) as well as in healthy human subjects (Østergaard et al., 1998a). Mukherjee and colleagues applied the latter method in patients with carotid stenosis and reported absolute CBF linearly correlated with the values measured by PET (Mukherjee et al., 2003). However, they concluded that DSC MRI was not accurate in the measurement of absolute CBF values.

Applications of DSC MRI

One of the first applications of DSC MRI were the studies of acute focal ischaemia in experimental animals. These pioneering studies revealed that DSC MRI is not only able to identify acute ischaemia within minutes of the onset, but also detect that the area of perfusion deficit is larger than the lesion depicted by DWI (Kucharczyk et al., 1991; Moseley et al., 1990a; Wendland et al., 1991; Warach et al., 1992b). In this context, the emphasis moved toward using DSC MRI as a complementary technique to DWI, with the ultimate aim to identify tissue at risk. The DSC summary parameters allowed in combination with high-speed ADC mapping a differentiation of mild and severe hypoperfusion and ischaemia (Gröhn et al., 1998), imaging of successful and failed reperfusion and delayed reperfusion injury (Kucharczyk et al., 1993; Li et al., 1999) as well as estimation of the effect of thrombolytic therapy using rt-PA after MCA occlusion in rats (Reith et al., 1996).

With the advent of thrombolytic therapy and the need for an early assessment of affected area, the emphasis on DSC studies has moved toward a diagnosis of hyperacute ischaemic patients, identification of a tissue at risk, and prediction of stroke outcome (Baird and Warach, 1998; Kidwell et al., 2003). A mismatch between perfusion and diffusion MRI lesion was reported by several clinical studies aimed at defining possibly salvageable tissue (Baird et al., 1997; Østergaard et al., 1996a; Schwamm et al., 1998; Sorensen et al., 1996). Using the combination of DSC and DWI MRI, four patterns of diffusion-perfusion abnormalities were identified: (a) perfusion volume $>$ DWI volume, (b) perfusion volume = DWI volume, (c) perfusion volume $<$ DWI volume, (d) normal perfusion and abnormal DWI (Baird et al., 1997). It was suggested that complete or partial reperfusion occurr in cases (c) and (d) while expansion of the ischaemic lesion takes place in (a) (Baird et al., 1997; Kidwell et al., 2003; Schwamm et al., 1998). Similarly, Sorensen and colleagues reason that the patients with matched diffusion-perfusion MRI may not benefit from thrombolytic therapy, since the regional injury had already reached its final size (Sorensen et al., 1996). These findings support the idea that lesion growth seems to be dependent on residual perfusion of the tissue. However, based on recent studies demonstrating partial or full normalization of diffusion within a lesion, Kidwell and colleagues (Kidwell et al., 2003) have suggested that even selected patients without a diffusion-perfusion mismatch may benefit from thrombolysis.

An alternative approach in classification of ischaemic damage involves the summary parameters (Calamante et al., 2001; Röther et al., 1996; Tsuchida et al., 1997). It was proposed that the complete loss of contrast agent bolus is associated with ischaemic core, while the delayed arrival, lower peak height and broaden width of the bolus identifies potentially salvageable tissue (Röther et al., 1996).

Perfusion imaging using arterial spin labelling

An alternative means to using DSC MRI in determining tissue perfusion by MRI is ASL. In contrast to DSC MRI, ASL employes electromagnetically labeled water protons of blood as an endogenous contrast agent. Assuming that blood water is a freely diffusible tracer, arterial blood flowing into the imaging slice completely exchanges with tissue water and thus influences the tissue MR signal. Perfusion-weighted MRI is commonly accomplished by subtracting an image with labeled inflowing blood spins from an image without spin labelling. Quantitative perfusion maps can be calculated if parameters such as tissue T_1, labeling efficacy and tissue-water ratio are known (Calamante et al., 1999b; Thomas et al., 2000). Under the general title of ASL, two distinct labeling methods are assumed: (a) continuous ASL (CASL) and (b) pulsed ASL (PASL).

In CASL methods, spin labelling is achieved either by spin saturation using a long train of RF pulses (Detre et al., 1992) or spin inversion by application of adiabatic RF pulses (Williams et al., 1992). However, two problems are associated with CASL. First, a transit time for spins to travel from labeling slice to different anatomical structures is different. During this period, T_1 relaxation takes place, hence the transit time dependent signal enhancement affects perfusion-weighted images. Secondly, the application of long off-resonance RF pulses causes saturation of macromolecular spins in imaging slices due to a magnetisation transfer (MT) effect, resulting in an attenuation of the free water signal. These problems determined that CASL methods could only be used to image single slices. An attempt to overcome transit time related issues was proposed by Alsop and colleagues, in which a delay greater than the arterial transit time was introduced into the pulse sequence (Alsop and Detre, 1996). Another simple and effective approach of avoiding MT effect in CASL useses a two-coil setup (Zhang et al., 1995). Here, a small labelling surface coil is placed on the artery supplying brain, while a separate coil is used for image acquisition. Alternatively, tailored pulses double-inverting (effectively leaving magnetization unchanged) arterial water magnetisation of control image were proposed, again, by Alsop and colleagues (Alsop and Detre, 1998).

In PASL methods, the sources of errors known in CASL are reduced by using short (typically 10 ms) RF pulses and by minimizing the distance between labelling and imaging regions. The most commonly used PASL sequence is flow-selective alternating inversion recovery (FAIR) (Kwong et al., 1992). In this sequence, labelling and control experiments are performed by slice selective inversion and non-slice selective (superimposed over imaging slice) experiments, respectively. Several modifications to FAIR sequence were recently designed and are aiming at minimizing MT effect (Edelman et al., 1994), radiation damping (Zhou et al., 1998) and vascular transit time (Golay et al., 1999).

In the applications of ASL to cerebral ischaemia, CASL was used to demonstrate redistribution of CBF through anastomoses after transient MCA occlusion in rat (Jiang et al., 1993), for monitoring the effect of experimental hypothermia on the recovery from transient MCA occlusion (Jiang et al., 1994) as well as to investigate perfusion levels in ischaemia followed by thrombolytic therapy (Jiang et al., 1998). In a clinical setting, Siewert and colleagues obtained CBF values in the stroke patients with single-slice ASL, which were comparable with those obtained by DSC MRI (Siewert

et al., 1997). Similar results were recently reported in patients with cerebrovascular disease (Detre et al., 1998) suggesting that ASL could be potentially useful in the clinical assessment of stroke pathophysiology.

2.3.4 Relaxation in transverse plane during cerebral ischaemia

Blood oxygenation level dependent MRI contrast

In the late 1970's, Brindle and colleagues realized that the transverse relaxation property of blood is related to the oxygenation level of haemoglobin molecules (Brindle et al., 1979). Iron atoms in the deoxygenated haemoglobin have four unpaired electrons and thus according to Eq. 2.3, possess magnetic dipole moments. Additionally, the interferences of the randomly fluctuating magnetic fields generated by the dipoles and main magnetic field $\vec{B}_0$ locally enhances transverse relaxation (Sec. 2.10). In oxygenated haemoglobin, on the other hand, the electron configuration becomes more complex and results a compensation of magnetic dipoles and longer local relaxation times. About a decade later, Ogawa and colleagues demonstrated that slight physiological alterations, such as neuronal activation, yield an interleaved cascade of changes in cerebral haemodynamics and this affects deoxyhaemoglobin concentration and results in blood oxygenation level dependent (BOLD) MR contrast (Ogawa et al., 1990a; Ogawa et al., 1990b). This observation initiated probably the most dynamically evolving branch of MRI applications during the last decade; functional MRI (fMRI) (Moonen et al., 1990; Belliveau et al., 1991).

In pathologies involving haemodynamic perturbations, such as cerebrovascular disease, ischaemia or highly perfused tumours, one would expect to observe local imbalances in deoxyhaemoglobin concentrations and hence BOLD related MR signal changes as well.

Intravascular BOLD *in vivo*

The following section describes the quantitative relation of parenchymal transverse relaxation T_2 and metabolic (OER, $CMRO_2$) and haemodynamic (CBV, CBF) status of brain parenchyma, based on the intravascular BOLD theory proposed by van Zijl and colleagues (van Zijl et al., 1998).

The theory models brain parenchyma as an uniform mixture of a tissue and randomly oriented microvasculature (i.e. arterioles, capillaries and venules). The MR voxel signal intensity (SI) measured with spin-echo sequence is a volume-weighted sum of tissue signal and the oxygenation-level-dependent signal of blood:

$$\frac{SI(t)}{SI(0)} = x_{\text{tissue}}\, e^{-t\, R_{2,\text{tissue}}} + \sum_i x_{\text{blood},i}\, e^{-t\, R_{2,\text{blood},i}} \tag{2.22}$$

$$x_{\text{tissue}} = 1 - \sum_i x_{\text{blood},i} = 1 - \sum_i \frac{\text{CBV}_i}{V_d + \text{CBV} - \text{CBV}_{norm}} \tag{2.23}$$

$i \in a, c, v$ (a - arterioles, c - capillaries, v - venules), where x_{tissue} and $x_{\text{blood},i}$ are relative tissue and microvascular blood volume fractions, respectively. Blood fractions in Eq. 2.23 are further expressed in terms of microvascular blood volume ratio (CBV_i), blood volume under normal CPP conditions ($\text{CBV}_{\text{norm}} = 4.7$ ml/100 g)

(Sandor et al., 1986; Leenders et al., 1990), total CBV and brain water distribution ($V_d = 82$ ml/100 g) (Schwab et al., 1997; Brooks et al., 1980). It should be noted that microvascular CBV_i can change in pathologic conditions, particularly hypoperfusion, which is associated with an autoregulatory vasodilatation (Sec. 2.1.2).

The relaxation rate of blood has been extensively studied *in vitro* and initially it was suggested that proton exchange between plasma and erythrocytes is the main relaxation mechanism in different vascular types (Bryant et al., 1990; van Zijl et al., 1998). However, recent studies indicate that water diffusion through susceptibility gradients generated by erythrocytes dominates in blood relaxation (Gillis et al., 1995; Jensen and Chandra, 2000). Yet, the equations for two-site exchange relaxation model are a good approximate of the magnitude of diffusion-based relaxation (Gillis et al., 1995; Jensen and Chandra, 2000). Thus, it is possible to obtain calibrating blood R_2 without having an exact knowledge of physical origin of the contributing mechanisms (Golay et al., 2001). This is represented by following equation:

$$R_{2,\mathrm{blood},i} = R_{2,\mathrm{plas}} + \mathrm{Hct_i}(R_{2,\mathrm{ery},i} - R_{2,\mathrm{plas}}) + R_{2,\mathrm{exch},i} \tag{2.24}$$

where $R_{2,\mathrm{plas}}$, $R_{2,\mathrm{ery},i}$ and Hct are the relaxation rates of plasma, erythrocytes and the cerebral hematocrit, respectively. Under physiological conditions the microvascular Hct is known to be approximately 85% of that in large vessels. However, both experimental (McHedlishvili et al., 1997) and clinical studies (Yamauchi et al., 1998) report locally decreased cerebral Hct in hypoperfused regions. This situation results elevated OER, which is due to a direct relation between these parameters (Ulatowski et al., 1996).

It is generally accepted that proton exchange between plasma and erythrocytes is fast (Herbst and Goldstein, 1989). Therefore, based on Eq. 2.13b, the contribution of microvascular exchange to blood relaxation ($R_{2,\mathrm{exch},i}$) can be written as (van Zijl et al., 1998)

$$R_{2,\mathrm{exch},i} = \tau_i \, \Delta\omega_i^2 \, \mathrm{Hct_i}(1 - \mathrm{Hct_i}) \left[1 - \frac{2\tau_i}{\tau_{\mathrm{CP}}} \cdot \tanh \frac{\tau_{\mathrm{CP}}}{2\tau_i}\right] \tag{2.25}$$

Eq. 2.25 simplifies the general multi-pool exchange model (Eq. 2.13b) proposed by Luz and Meiboom (Allerhand and Gutowsky, 1964; Luz and Meiboom, 1963) to two pools only, i.e. water exchange between plasma and erythrocytes. Than, τ_i is a water exchange lifetime between plasma and erythrocytes, τ_{CP} is an interval between refocusing pulses in Carr-Purcell multiecho pulse sequence and $\Delta\omega_i$ is the susceptibility difference between plasma and erythrocytes in the microvascular compartments. Eq. 2.25 and discussions in Sec. 2.2.4 imply that the total apparent relaxation rate of blood also depends on the type of spin-echo sequence. While in single Hahn echo sequence the sensitivity to BOLD is maximised ($\tau_{\mathrm{CP}} = \mathrm{TE}$), by shortening the interpulse interval between refocusing RF pulses in multiecho spin echo (Carr-Purcell) type sequence, the exchange contribution is reduced ($\lim_{\tau_{\mathrm{CP}} \to 0} (\tanh(\tau_{\mathrm{CP}}/2\tau_i)) = 0$) (Carr and Purcell, 1954; van Zijl et al., 1998). The magnitude of the susceptibility gradient between plasma and erythrocytes ($\Delta\omega_i(B_0)$) depends on the fraction of deoxygenated haemoglobin inside erythrocytes (x_{deoxy}), which is expressed in the microvessels as follows:

$$x_{\mathrm{deoxy},i} = 1 - Y_a + m_i \, \mathrm{OER} \, Y_a \tag{2.26}$$

where variable m_i reflects the deoxygenation process taking place in microvessels and equals 0, 0.5 and 1 in arterioles, capillaries and venules, respectively under normal physiological conditions (Filho et al., 1996). This figure, however, can change in hypoperfused parenchyma, where significant precapillary oxygen loss can take place (Popel and Gross, 1979; Intaglietta et al., 1996; Filho et al., 1996). Eq. 2.26 directly enters the calculations of blood transverse relaxation rate given by Eqs. 2.24 and 2.25 and thus completes the mathematical relationship between physiological and haemodynamic status of cerebral parenchyma and its apparent transverse relaxation rate.

Applications of intravascular BOLD *in vivo*

The minute BOLD related transverse relaxation changes of parenchyma at clinical 1.5 T field led to general acceptance of the fact that T_2 and T_2^* do not change during acute phase of ischaemia and hypoperfusion. The amplitude of the BOLD signal at 1.5 T is at the level of a few percent and its reliable detection in fMRI studies of brain activation is justified only by means of temporal correlation with patterns of activation stimulus.

The BOLD NMR experimental studies upon haemodynamic challenge commonly take the advantage of high B_0 fields, where T_2 and T_2^* scale down due to stronger transverse magnetization dephasing. In this regard, the T_2 or T_2^* BOLD effect was recently observed during acute experimental cerebral ischaemia, hypoxia and hypercapnia at 2.35 T (Roussel et al., 1995; Thomas et al., 2002), 4.7 T (Gröhn et al., 2000a; Kettunen et al., 2002b; Kettunen et al., 2002a), 8.5 T (Calamante et al., 1999a; Lythgoe et al., 2000b) and 9.4 T field strengths (Gröhn et al., 1998; Lei et al., 2003), respectively.

The intravascular BOLD theory (van Zijl et al., 1998), which quantitatively relates T_2, haemodynamics and the metabolism of cerebral parenchyma was described in the last section. Van Zijl and colleagues validated the approach *in vivo* and derived absolute CBV maps of hypercapnic cat, obtaining cortical and white matter CBV values that were in good agreement with PET values. The measurements of T_2 in studies of experimetal ischaemia at 4.7 T revealed areas of decreased transverse relaxation after 25 min of MCA, which were anatomically indistinguishable from the lesion of low D_{av} at more later time points post-ischaemia (Gröhn et al., 1998). The lesion corresponding to negative T_2 change can be explained in terms of intravascular BOLD as an area of high deoxyhaemoglobin concentration due to exhausted haemodynamic autoregulation and elevated OER (Derdeyn et al., 2002; Powers et al., 1987), which is at a later time point destined to be irreversibly damaged. The physiological effects of altered CPP on parenchymal T_2 were extensively analyzed and computer simulated by Gröhn and colleagues. This approaches yielded results with excellent correlation with *in vivo* experiments on the animal model of graded reduction of CBF (Gröhn et al., 2000a). The studies of transverse relaxation upon haemodynamic challenge including hypoxia, hypercapnia and global ischaemia conducted at 4.7 T by Kettunen and coworkers further established intravascular BOLD (Kettunen et al., 2002b; Kettunen et al., 2002a).

In human application at $B_0 = 1.5$ T, the intravascular BOLD was recently used to noninvasively estimate OER from venous blood draining out of the visual cortex during fMRI. The values obtained were of 0.18 ± 0.05 during visual stimulation and 0.38 ± 0.04 at rest conditions (Golay et al., 2001). These numbers are in very good

agreement with human PET studies.

$T_{1\rho}$ during acute ischaemia

As discussed earlier in the text (Sec. 2.2.4), altered water-macromolecule interactions, proton echange between various chemical groups (Mäkelä et al., 2001), classical dipole-dipole interactions and cross-relaxation are the major mechanisms affecting $T_{1\rho}$ relaxation *in vivo* (Mäkelä et al., 2004). There are several processes associated with acute ischaemia that cause the major on-resonance $T_{1\rho}$ increase within minutes after ischaemia onset (Gröhn et al., 1999; Kettunen et al., 2001). These include reduced pH as a result of anaerobic cell metabolism and lactic acid build up (Siesjö, 1992), vasogenic oedema and alterations in cellular cytoskeletons (Jenkins et al., 1979).

The recent MRI studies on rats revealed that $T_{1\rho}$ and dispersion of $T_{1\rho}$[20] are very sensitive markers of acute ischaemia (Gröhn et al., 1999; Gröhn et al., 2000b; Kettunen et al., 2001). Interestingly, Gröhn and coworkers reported higher correlation of $T_{1\rho}$ lesion with histologically determined neuronal damage than D_{av} MRI, beyond 2 hours of ischaemia (Gröhn et al., 1999). This is potentially important observation from point of view of a tissue viability and ischaemia outcome assessment. Both experimental (Hoehn-Berlage et al., 1995; Li et al., 1999; Neumann-Haefelin et al., 2000a) and clinical (Fiehler et al., 2002; Neumann-Haefelin et al., 2000b; Kidwell et al., 2000) evidence points to the fact that early restoration of blood flow results normalization of water diffusion in acute ischaemic tissue. Diffusion normalization is likely to be dependent on the duration and severity of ischaemia. Therefore in this regards, $T_{1\rho}$ MRI may provide higher specificity in delineating irreversible ischaemia.

[20] $T_{1\rho}$ as a function of amplitude of spin-lock field

Chapter 3

Aims of the Study

It is well established that occlusive cerebrovascular diseases trigger protective haemodynamic mechanisms to try to secure sufficient oxygen and glucose supply to the brain, resulting in increased CBV and OER (Derdeyn et al., 2002; Powers et al., 1987). In this regard, elevated OER is an indication of exhausted cerebral haemodynamic reserves and it is associated with a several-fold increase in the incidence of ischaemic stroke (Grubb, Jr et al., 1998). Recent animal studies have provided evidence that increased deoxyhaemoglobin concentration in blood, which is due to elevated OER, can be readily revealed by means of quantitative T_2 BOLD MRI at high magnetic fields (Gröhn et al., 1998; Gröhn et al., 2000a).

The present study was undertaken to investigate the value of T_2 BOLD in assessment of cerebrovascular insult at clinical field of 1.5 T and to examine effect of pathological processes associated with acute ischaemia on the transverse relaxation.

The aims of this study were as follows:

1. To theoretically estimate the magnitude of intravascular BOLD effect at 1.5 T using a model previously published and experimentally test the results with an animal model of cerebral hypoperfusion

2. To investigate T_2 BOLD MRI in carotid stenosis patients and to estimate tissue oxygen extraction.

3. To characterize contributions to the BOLD effect to the transverse relaxation in acute ischaemia, with particular reference to the contributions from intravascular and extravascular water pools.

4. To study *in vivo* dynamic dephasing contributions to transverse relaxation during evolution of ischaemia in rat brain.

Chapter 4

Materials and Methods

4.1 Experimental hypoperfusion and stroke (*I*, *III*, *IV*)

4.1.1 Animal preparation and monitoring

Animals

Male Wistar rats (National Laboratory Animal Centre, University of Kuopio) fed *ad libitum* and weighting 250-350g were used in the experiments. The experiments were approved by the Ethical Committee of the National Laboratory Animal Centre at the University of Kuopio.

The animals were anesthetized by inhalation of 0.8-1.5% of halothane in N_2O/O_2 (70%/30%). In the study of cerebral hypoperfusion (*I*), the animals were initially anesthetized with halothane for electro-coagulation of the vertebral artery. The animals were reanesthetized with an intra-peritoneal injection of Urethane (1.2-1.5 g/kg of body weight) two days later for MR measurement.

Physiologic monitoring

The body temperature was monitored and maintained close to 37° C either by a heating element during surgery or warm water circulated in a heating pad during MR experiments.

The physiological level of body fluids during experiments was complemented by intra-venous injection of saline, at a dose of 1 ml/kg/hour (*I*, *III*).

Arterial blood samples were analysed for pH, pO_2, pCO_2 (*I*, *III*) (ABL-5, Radiometer Inc., Copenhagen,Denmark; i-STAT, I-STAT Co, East Windsor, NJ) and blood pressure was measured invasively (Datex, Helsinki, Finland), via the cannulated femoral artery (*III*). The mixture of inhaled gases was monitored (*III*, *IV*) and in the hypercapnia study adjusted according to the experimental protocol (Capnomac II, Datex Helsinki, Finland).

CBF measurement (*I*)

CBF was determined using an invasive hydrogen-clearance method (Crockard et al., 1980) under Urethane anaesthesia. For this purpose, Pt-Ir electrodes (ϕ 100 μm) were implanted 1-1.5 mm into the both hemispheres of the cerebral cortex, 1.5 mm caudal to bregma and 3 mm lateral to midline. Ag-AgCl reference electrodes were inserted subcutaneously into the flank.

A hydrogen clearance curve was recorded and analysed using an initial slope approach (Olesen et al., 1971) after loading with mixture of $H_2/N_2O/O_2$ (10%/65%/25%).

4.1.2 Animal models

Hypoperfusion (*I*)

In a rat brain, a circle of Willis provides very efficient collateral flow paths between anterior and posterior and intra-hemispheric blood supply (Pulsinelli et al., 1982b). Therefore, to reduce cerebral blood flow close to ischaemia threshold, both the VA and ICA must be involved (Pulsinelli et al., 1982b).

Under halothane anesthesia, the right VA was permanently occluded by electrocoagulation. Following two days of post-operative recovery, the rats were reanesthetized with Urethane and both CCA were exposed through a middline cervical incision. Hypoperfusion in right cerebral cortex was induced by temporally occluding both CCAs using non-magnetic miniature aneurysm clips (Pulsinelli et al., 1982a).

Ischaemia (*III, IV*)

For the purpose of this study, three animal models of acute ischaemia were employed.

Global ischaemia was accomplished by cardiac arrest by intravenous injection of saturated KCl (0.5-0.7 ml) (*III*).

Focal cerebral ischaemia was induced using the intraluminal MCA occlusion (MCAo) model (Longa et al., 1989) (*III, IV*). Briefly, a bifurcation of CCA was exposed and a nylon thread (ϕ 220 μm) was inserted into the right CCA and advanced until it reached the M1 segment of MCA. The occlusion was maintained for either 30 (*III*) or 60 (*IV*) minutes followed by an in-bore retraction of the occluder and spontaneous reperfusion.

A modified model of MCAo described by Roussel and co-workers (Roussel et al., 1994) was employed, using a remote occluding device in order to study cerebral ischaemia shortly after its onset. In this approach, a driving tubing was inserted into the right CCA and the occluder thread was driven inside. Ninety minute occlusion was initiated by advancing the occluder in the magnet bore (*III*).

Hypercapnia (*III*)

In the hypercapnia study, the level of blood $PaCO_2$ was altered in spontaneously breathing animals by increasing the CO_2 content of the inhaled mixture in two steps. For the first 20 minutes the CO_2 concentration was 15-20%. This was followed by 30-40% CO_2 content in breathing mixture for a further 20 minutes. O_2 concentration was maintained at 30%, supplemented with N_2O up to 100%. After 40 minutes

hypercapnia, the animals were allowed to recover in a 0.8-1% halothane in N_2O/O_2 (70%/30%).

4.1.3 MRI methods

Hardware

The experimental cerebral hypoperfusion study (*I*) was conducted on a clinical 1.5 T whole body Magnetom Vision system (Siemens, AG, Erlangen, Germany) using a body coil as a transmitter and a 40 mm surface coil as a receiver. The studies of cerebral ischaemia (*III*/*IV*) were carried out on a 4.7 T horizontal magnet (Magnex Scientific Ltd, Abdington, UK) interfaced to an $^{\text{UNITY}}$*INOVA* console (Varian Inc, Palo Alto, California, USA) using a home-made surface coil in a transmit/receive mode.

Estimation of water diffusion

Diffusion-weighted images (*I*) were acquired using a Hahn echo sequence with diffusion sensitizing gradients along the y-axis ($TR/TE = 1500/100$ ms, $b = 900$ s/mm^2, resolution 0.3x0.6x2 mm^3).

The D_{av} was quantified (*III*, *IV*) using a Hahn echo sequence with four bipolar gradients along each gradient axis (Mori and van Zijl, 1995) with b values of 0, 330, 660 and 1000 s/mm^2 ($TR/TE = 1500/56$ ms). The data was acquired either as a line-scan profile (8 averages, 0.27x3x3 mm^3) (*III*) or a 2D images (2 averages, resolution 0.11x0.47x2 mm^3) (*IV*).

Quantification of T_2 and $T_{1\rho}$ relaxation

At 1.5 T magnetic field(*I*), maximum sensitivity to BOLD was achieved by acquiring a set of T_2-weighted MR images using Hahn echo sequence ($TR/TE = 1500/(35, 50, 75, 100)$ ms, resolution 0.3x0.6x2 mm^3).

As mentioned in the Sec. 2.3.4, the contribution of dynamic dephasing effects to transverse relaxation can be modulated by the length of inter-pulse interval (τ_{CP}) between refocusing RF pulses in a CP-type multiecho sequence. To address this issue during ischaemic stroke, CP-T_2 and $T_{1\rho}$ were measured using a LASER sequence (Garwood and DelaBarre, 2001) in line-scan (resolution 0.27x3x3 mm^3) and 2D imaging (resolution 0.27x0.54x2 mm^3) modes (*III*). For CP-T_2, different TEs were obtained either by increasing τ_{CP} ($\tau_{\text{CP}} = 6.1$-22.5 ms; referred to as long τ_{CP}; $TE = 42$-140 ms) or the number of refocusing pulses from 6 to 22 and keeping τ_{CP} constant ($\tau_{\text{CP}} = 6.1$ ms; referred to as short τ_{CP}; $TE = 42$-153 ms). $T_{1\rho}$ was quantified at B_{1sl} fields of 0.2 and 1 G by introducing adiabatic spin-lock pulses (length 10-70 ms) in front of the LASER sequence ($TE = 42$ ms).

The mechanisms of CP-T_2 relaxation were exploited by fully adiabatic multiecho spin echo sequence ($TR = 2500$ ms, resolution 0.11x0.31x2 mm^3, 2 averages) (*IV*). For spin excitation, a non-selective adiabatic half-passage pulse was used. Slice selection and magnetization refocusing were achieved by a pair of adiabatic hyperbolic secant (HS1) pulses. The CP pulse train consisted of 0, 16 or 32 HS1 pulses, phase cycled in MLEV pattern (Levitt and Freeman, 1981). Different TEs (15, 55, 95 ms) were obtained using the same approach as described above ($\tau_{\text{CP}} = 2.5$-20 ms; long τ_{CP} or

$\tau_{\mathrm{CP}} = 2.5$ ms; short τ_{CP}). Adiabatic pulses in the CP-train together with MLEV phase cycle have been shown to minimize signal loss due to pulse imperfections and surface coil B_1 filed inhomogeneity (Levitt and Freeman, 1981; Garwood and Ke, 1991).

4.1.4 Data analysis

The trace of diffusion tensor (D_{av}), T_2 and $T_{1\rho}$ were determined by fitting signal intensities (pixel values in 2D images; vector data in line-scan profiles) into a monoexponential function of a coefficient of diffusion weighting (Eq. 2.17), TE and length of spin-lock RF pulse, respectively. The contribution of dynamic dephasing effects to transverse relaxation was estimated by subtracting the pixel intensities of CP-T_2-weighted images acquired at TEs of 55 and 95 ms (Bartha et al., 2002; Michaeli et al., 2002) (*IV*).

$$\Delta = 100 \cdot \frac{SI\,(\text{short } \tau_{\mathrm{CP}}) - SI\,(\text{long } \tau_{\mathrm{CP}})}{SI\,(\text{long } \tau_{\mathrm{CP}})} \quad [\%] \tag{4.1}$$

The MR parameters were analysed from the ROIs covering the contralateral and ipsilateral parietal cortex (*I*, *III*), striatum (*III*, *IV*) and the cerebellum (*I*) (Paxinos and Watson, 1996). The data collected during brain insults were compared either to pre-insult (*I*, *III*, *IV*) or contralateral brain values (*III*). Wilcoxon's test (*I*) and Student's t-test (*III*, *IV*) were used for statistical analysis of the data.

4.2 MRI of symptomatic carotid stenosis patients (*II*)

4.2.1 Subject selection

Twenty two patients with cerebrovascular disease and 4 age-matched non-neurological reference subjects enrolled the study after signing informed written consent forms. Patients were selected from the database of the Department of Neurology of the Central Hospital of Central Finland in Jyväskylä after meeting following criteria: (a) previous evidence of transient ischaemic attacks, (b) more than 50% carotid stenosis determined by ultrasound or digital subtraction angiography or (c) other clinical signs of occlusive cerebrovascular disease.

4.2.2 MRI protocol

Hardware

The MR data were acquired on GE Signa CV/i clinical 1.5 T whole body imaging system (GE Medical Systems, Waukesha, WI, USA) using a quadrature birdcage coil as a transmitter/receiver.

Magnetic resonance angiography

Magnetic resonance angiography (MRA) of supra-aortic vessels up to the circle of Willis was obtained using a neck vascular array coil in both subject groups, in order to accurately determine the location and degree of vascular stenosis.

In reference subjects, 2D time-of-flight (TOF) MRA with magnetization transfer saturation (MTS) pulses was employed ($TR/TE = 16.9$ ms/4 ms, $\alpha = 50°$), coronal orientation, resolution 1.3x1.3x2 mm^3). TOF MRA contrast generation relies on a difference in the spin saturation of stationary tissue and blood flowing into the imaging slice (Gao et al., 1988; Haacke et al., 1990). Further contrast enhancement between tissue and blood signals can be achieved by using the tissue MTS effect (Edelman et al., 1992; Pike et al., 1992). However, the tendency to overestimate the degree of stenosis can be associated with TOF MRA due to intravoxel phase dispersion and signal loss (Haacke et al., 1999).

Vasculopathies in the patient group were assessed by contrast enhanced (CE) MRA. Here, 20 ml of Gd-DTPA (Dotarem; Guerbet, France) was administrated into antecubital vein by a MR compatible power injector (Medrad Inc.). Gd-DTPA reduces T_1 relaxation time of blood and results in an enhancement of signal from vascular structures in T_1-weighted MRI (Marchal et al., 1991; Lin et al., 1992). To achieve optimal artery/vein separations, a timing bolus technique (Rajagopalan and Prince, 2002) was used to synchronize contrast bolus injection and the acquisition of a 3D data MR set ($TR/TE/\alpha = 7.9$ ms/1.6 ms/30°, elliptical FOV, coronal orientation, resolution 0.6x1.2x1.6 mm^3). CE MRA is a promising method, providing high morphological details of a lesion, high signal-to-noise and contrast-to-noise ratios, good correlations with digital subtraction angiography, covers large area of interest and provides substantially shorter scan times (20x) than TOF MRA (Cloft et al., 1996; Kollias et al., 1999; Jager et al., 2000).

T_2 BOLD and perfusion MRI

Whole-head, high-resolution (0.9x1.2x1.3 mm^3) transverse T_1-weighted images ($TR/TE = 33$ ms/6 ms, $\alpha = 30°$), with good contrast between grey and white matter were acquired using a 3D SPGR sequence. These images were subsequently utilised as anatomical references in image post-processing.

Nine transverse slices (thickness 3 mm, spacing 2.5 mm) covering a large area of the ICA territory were placed according to pilot images and their position was kept constant in T_2 and perfusion MRI.

The parenchymal T_2 of grey matter (GM) was measured using a flow compensated spin echo EPI sequence. The k-space was covered in the phase-encoding direction by 16 segments. This was done in order to minimize additional magnetization dephasing due to long read-out interval ($TR/TE = 1500$ ms$/(30, 60, 90, 120)$ ms, 16 shots/k-space, read-out bandwidth 62.5 kHz, resolution 0.9x0.9x3 mm^3, 2 averages, transverse orientation). It was shown that this acquisition setup yields identical T_2 to the standard Hahn echo sequence. In another words, EPI read-out does not induce additional T_2^* effects (Oja et al., 1999).

Cerebral haemodynamics was assessed by means of DSC MRI. An additional slice was placed according to T_1-weighted 3D volume to cover the M1 segment of the MCA or a cavernous segment of the ICA. This enabled an estimation of AIF and the quantification of absolute CBV (Axel, 1980; Meier and Zierler, 1954; Zierler, 1965). A single shot spin echo EPI sequence was used ($TR/TE = 1500/75$ ms, resolution 1.9x1.9x3 mm^3). During a series of 60 consecutive scans (20 baseline scans), a bolus of 0.2 mmol/kg Gd-DTPA contrast agent (Omniscan; Nycomed Amersham) was injected into the antecubital vein (rate 5 ml/s) by a MR-compatible power injector, followed by saline flush.

4.2.3 Image processing

Fig. 4.1 shows a flowchart of the image processing carried out off-line using FMRIB software library (FSL, versions 2 and 3; Image Analysis Group, FMRIB, Oxford, UK). In order to reduce inherent noise in MR images without blurring, the entire image data set was initially filtered with a SUSAN nonlinear filter (3x3 kernel, SD = 0) (Smith and Brady, 1997). Since images from different MR scans were analysed in a pixel-by-pixel mode to avoid possible rigid body motions of the subject between the scans, the image alignment against T_1-weighted 3D volume was carried out (Jenkinson et al., 2002). The latter step preceded brain tissue extraction (Smith, 2002), thus increased alignment accuracy was achieved. Finally, automated segmentation (Zhang et al., 2001) was used to generate a GM mask from T_1-weighted volumes. The image registration ensured that all images were transformed into the same coordinate space origin and therefore the GM mask was applicable to the brain perfusion and T_2 maps generated.

Absolute CBV was quantified using Eq. 2.20, where proportionality constants $\rho = 1.04$ and $k_h = 0.85$ (Grubb et al., 1974; Leenders et al., 1990) were used. To avoid contrast recirculation, both $C_t(t)$ and $C_a(t)$ were numerically integrated between bolus arrival (a threshold of 7% of the bolus maximum) and recirculation (a threshold of 30% of the bolus maximum) for each pixel individually. Computer simulations as

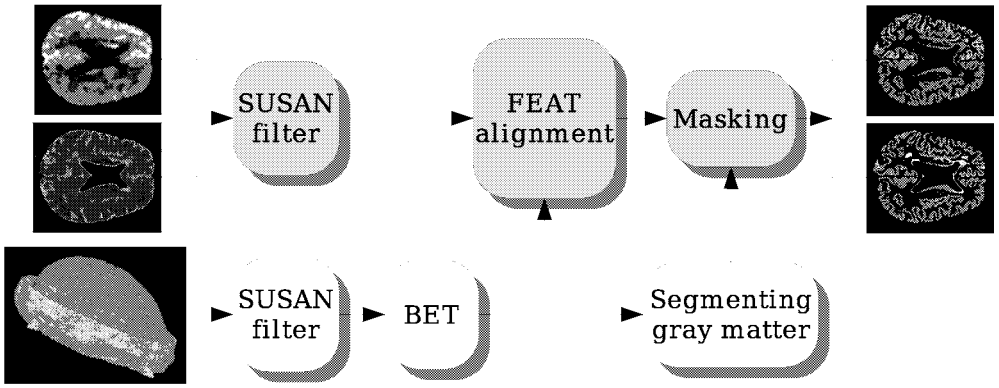

Figure 4.1: The image processing operations performed on spin echo BOLD and DSC MRI (grey boxes) and the reference high-resolution T_1-weighted 3D volume (white boxes).

well as clinical experiments have shown (Boxerman et al., 1997; Perkiö et al., 2002) that the above approach results in an accurate estimation of the absolute CBV.

The summary parameters (TTP, BAT, MPC, PW) were calculated from hemispheric GM $C_t(t)$, after fitting the curve to a gamma-variate function.

In order to indirectly estimate OER, the following analysis was performed. For each patient and control subject, GM CBV and GM T_2 maps were generated by multiplication of either T_2 or CBV map and the GM mask. From these, the dependence of parenchymal GM T_2 on GM CBV was constructed. Parenchymal pixels in GM CBV maps were grouped in 0.5 ml/100 g steps between 3 and 7.5 ml/100 g. Pixels above this range were excluded, since they were likely to have substantial large vessel contributions. The lower limit of 3 ml/100 g resulted from the strongly non-Gaussian distribution of the CBV histogram (An et al., 2001) and was chosen to avoid stroke tissue or white matter contamination. For each GM CBV pixel considered above, a pixel with the same coordinates in GM T_2 map was determined. Only T_2 below 100 ms was taken into account, in order to minimize partial volume effects arising from cerebrospinal fluid (CSF) and/or chronically ischaemic tissue. Using these criteria both substantial CSF (Zhou et al., 2001) and macrovascular contributions (Oja et al., 1999) were excluded. For each subject, GM T_2 as a function of GM CBV with OER as a parameter was simulated in 0.005 steps and a look-up-table (LUT) of OER as a function slope was created. The intersubject variability in macrovascular hematocrit may influence the accuracy of the present approach and therefore recent macrovascular hematocrit values determined from each subject's blood sample was used in the simulations. Ipsilateral and contralateral OERs were determined by matching the nearest slope of linearly fitted parenchymal GM T_2-CBV with the slope from the LUT.

4.2.4 Data analysis

Magnetic resonance angiography images were rendered by maximum intensity projection and examined from multiple angles by a trained radiologist without prior

knowledge of the patient status. A degree of stenosis of CCA, ICA and VA, respectively was calculated as a percent of narrowed arterial lumen. Patients were grouped based on the MRA finding as follows: (1) stenosis (20-69% stenosis), (2) severe stenosis (70-99% stenosis) and (3) occlusion (100% stenosis) in ICA.

Cerebral haemodynamic parameters including CBV, TTP, BAT, MPC, PW and OER were calculated from DSC MRI and T_2 maps in grey matter in cerebral hemispheres ipsi and contralateral to the dominant ICA stenosis and right and left cerebral hemispheres in patients and reference subjects, respectively. To avoid variability across the patient sample due to possible differences in contrast injection, ipsilateral-to-contralateral and right-to-left hemispheric ratios of summary parameters were calculated for both patients and controls.

Depending on the state of collateral flow, in cases such as those with severe bilateral ICA stenosis but without VA lesions, regional variations in haemodynamic parameters can be expected. To address this issue, regional haemodynamics was analysed in the vascular territories of the ICA in four patients with severe bilateral ICA stenoses without VA narrowing. The ROIs representing vascular territories were manually drawn on each GM mask according to the human brain atlas (Mai et al., 1997).

Absolute values and intrahemispheric ratios (ipsilateral/contralateral in patients and right/left in control subjects) of the above parameters were determined in each subject.

Chapter 5

Results

5.1 Misery perfusion in the rat brain studied by T_2 MRI at 1.5 T (*I*)

A detection of the mismatch between oxygen delivery and consumption in the haemodynamically compromised brain (such as in ischaemic penumbra or misery perfusion) would be of great clinical impact, since under these conditions, brain tissue is still metabolising oxygen and thus is considered to be potentially salvageable or at risk of permanent damage. Recent animal studies using high field MR scanners have indicated that misery perfusion can be detected as a negative BOLD effect (Gröhn et al., 1998; Gröhn et al., 2000a). Due to the magnetic field strength dependence of BOLD, it may well be that the amplitude of the BOLD effect may be too small to be detected at clinical field of 1.5 T, especially when spin echo MRI is used (Gröhn et al., 2000a). In the present work, the magnitude of the BOLD response associated with misery perfusion was both simulated using the intravascular BOLD model (van Zijl et al., 1998) and experimentally approached in a rat model by single echo T_2 MRI at 1.5 T.

The effect of cerebral hypoperfusion on parenchymal transverse relaxation was studied on an animal model of cerebral hypoperfusion. Permanent right VA and transient bilateral CCA occlusion reduced CBF in cerebral cortex ipsilateral to the permanently occluded VA to 17 ± 3 ml/100 g/min, while moderate CBF reduction was observed in the contralateral cortex (Fig. 5.1A). This figure is close to the energy failure threshold (Gadian et al., 1987; Kohno et al., 1995), but in this animal model, it did not induce cerebral ischaemia, because the DWI was unchanged. Yet, during transient bilateral CCA occlusion, a reduction in the absolute T_2 by 3%, i.e. negative BOLD effect, was observed (Fig. 5.1B). Interestingly, an overshoot followed by normalization of T_2 upon the removal of occluder clips was observed in the ipsilateral cortical ROI. This may be an indication of luxury perfusion due to hyperemia. It has been recently shown that in the post-ischaemic brain, prolonged T_2 is associated with elevated CBV due to luxury perfusion (Kettunen et al., 2002b). The absolute T_2 did not change significantly in the contralateral hemisphere during the observation period (Fig. 5.1B).

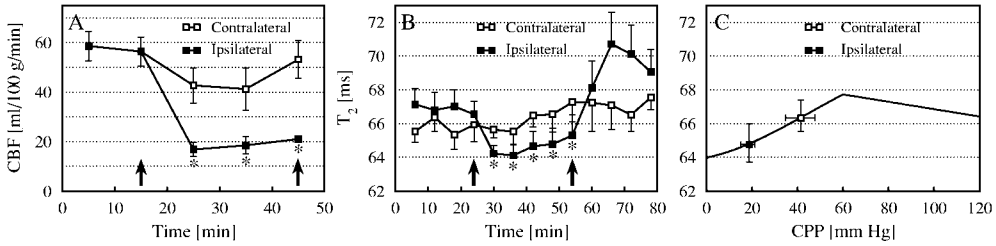

Figure 5.1: Absolute CBF (A) and parenchymal T_2 (B) during cortical misery perfusion (arrow heads), followed by reperfusion. Parenchymal T_2 as a function of CPP simulated using intravascular BOLD (C), with overlaid experimental T_2. The CPP values were determined from PET studies (Powers, 1991) and correspond to measured CBF.

In order to estimate the effect of the haemodynamic adaptation to compromised blood flow, parenchymal T_2 was simulated using intravascular BOLD theory (van Zijl et al., 1998) (Sec. 2.3.4). As expected, absolute T_2 initially prolongs as a result of microvessel dilatation and therefore elevates CBV (Fig. 5.1C). An elevated OER in a severely CBF compromised brain results in an accumulation of deoxyhaemoglobin, which balances the CBV effect on parenchymal T_2. This yields a shortening of the transverse relaxation time, or a negative BOLD, in the affected tissue. In this regards, it very interesting to note that the measured absolute T_2 values matched very well the simulated data (Fig. 5.1C).

5.2 MRI of haemodynamic and metabolic adaptation to carotid stenosis in man

It was very encouraging to note that single echo T_2 MRI was able to reveal mismatch in oxygen delivery and metabolism in misery perfusion in a rat at 1.5 T. This study provided a firm foundation to move towards clinical applications of this MR technique. Symptomatic carotid stenosis patients were chosen in this regard, because numerous PET studies indicate that haemodynamic alterations resembling misery perfusion occur in these patients (Derdeyn et al., 2002; Grubb, Jr et al., 1998; Powers et al., 1987; Powers, 1991).

The state of cerebral haemodynamics in carotid stenosis patients was assessed by means of DSC and absolute T_2 BOLD MRI, respectively (see Appendix A, page 59). The location and degree of vascular disease was explicitly determined by CE MRA (see Appendix A, page 59). Additionally, using the intravascular BOLD model of parenchymal transverse relaxation (van Zijl et al., 1998) and independently measured CBV, an indirect MRI method estimating hemispheric OER was proposed.

Parenchymal T_2 was simulated as a function of the CBV using the intravascular BOLD model in grey matter (Fig. 5.2). This interrelationship is influenced by both OER, microvascular Hct and $T_{2,\mathrm{tissue}}$. Furthermore, under normal physiological conditions, higher CBV is expected to prolong parenchymal T_2. It can be seen that a

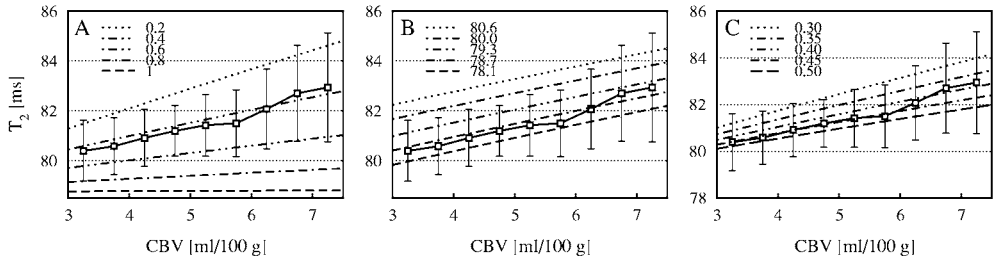

Figure 5.2: Computer simulated effect of OER (A), $T_{2,\mathrm{tissue}}$ [ms] (B) and microvascular hematocrit (C) on human parenchymal GM T_2 as a function of CBV at 1.5 T. For comparison, each set of graphs show the data from healthy volunteers, denoted by square symbols.

change in parenchymal GM T_2 in simulated CBV range is at 1.5 T strongly influenced by OER. Augmentation of OER flattens the slope and OER values greater than 0.85 would yield a negative slope in the simulated curve (Fig. 5.2A). The effect of OER on the slope is explained by an increase in deoxyhaemoglobin leading to T_2 shortening (van Zijl et al., 1998). Due to the intravascular origin of T_2 BOLD at 1.5 T, variations in $T_{2,\mathrm{tissue}}$ influences only the offset of the T_2 plots (Fig. 5.2B). The effect of a Hct change from 0.3 to 0.5 at OER = 0.4 is shown (Fig. 5.2C). An increase in Hct from 0.3 to 0.5 would decrease T_2 by 1.2 and 2 ms at CBV of 4 and 7 ml/100 g, respectively.

It is evident from the results of intravascular BOLD simulation discussed in the last paragraph that OER significantly influences parenchymal T_2 at 1.5 T. Additionally, provided CBV and microvascular Hct are known, OER estimates could be obtained from a T_2-CBV plot. For the control subjects GM T_2 as a function of CBV is shown in Fig. 5.2A. Interestingly, the data falls into the OER line of about 0.4, a value in excellent agreement of PET values for this parameter in healthy subjects (Leenders et al., 1990). Using the slopes from each individual, an average hemispheric GM OER of 0.40 ± 0.05 (range from 0.37 to 0.50) was obtained. Fig. 5.3 shows the average GM T_2 dependence on GM CBV in patients groups with occlusive vascular disease. Analysis of the slopes indicated normal GM OER in 13 cases. In three patients, this approach showed elevated ipsilateral OER (one group-2 case and two group-3 cases) and in six

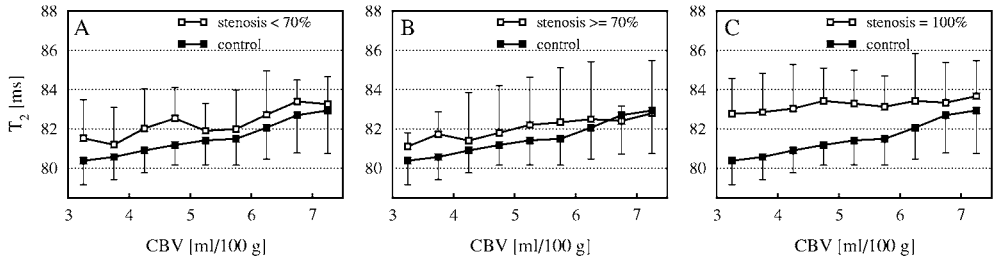

Figure 5.3: GM T_2 vs. GM CBV in three patients groups. For comparison, each plot includes data from control subjects.

Stenosis	$< 70\%$	$70 - 99\%$	100%	Controls
	$n = 8$	$n = 9$	$n = 5$	$n = 4$
$TTP_{I/C}$	1.002 ± 0.004	0.997 ± 0.009	1.039 ± 0.038	1.000 ± 0.004
$BAT_{I/C}$	1.003 ± 0.010	0.998 ± 0.013	1.044 ± 0.051	1.000 ± 0.006
$MPC_{I/C}$	0.978 ± 0.024	1.005 ± 0.032	1.003 ± 0.045	1.000 ± 0.016
$PW_{I/C}$	0.995 ± 0.032	1.001 ± 0.016	1.022 ± 0.043	0.993 ± 0.015
$CBV_{I/C}$	0.976 ± 0.044	0.991 ± 0.041	1.047 ± 0.109	0.998 ± 0.031
CBV_I	3.33 ± 0.55	3.73 ± 0.92	3.63 ± 0.79	3.49 ± 0.43
$OER_{I/C}$	1.084 ± 0.133	1.161 ± 0.179	1.254 ± 0.392	1.050 ± 0.15
OER_I	0.410 ± 0.115	0.517 ± 0.162	0.554 ± 0.214	0.396 ± 0.047

Table 5.1: Results of perfusion MRI in patients with occlusive cerebrovascular disease and control subjects. CBV_I is in ml/100 g. n - number of patients in the group, I - ipsilateral, C - contralateral. The data are $\text{mean} \pm \text{SEM}$.

cases bilaterally high OER (two group-1 cases, three group-2 cases and one group-3 case) (see Appendix A for individual values, page 59). However, statistical analysis did not reveal significant differences in OER between any of the stenosis and control groups, respectively (Table 5.1).

A summary of quantified haemodynamic parameters, including CBV, TTP, BAT, PW and MPC is presented in Table 5.1. The mean ipsilateral GM CBV values in the three stenosis groups were not significantly higher than in controls (Table 5.1). However, three subjects had CBV below normal (one case from each stenosis group) and four cases above (one group-1 case, two group-2 cases and one group-3 case) 2 SD of CBV from healthy controls (see Appendix A for individual values). The hemispheric ratios of GM CBV in the patient groups were not significantly different from those determined in control subjects (Table 5.1), however, asymmetry (beyond 2 SD of controls) was found in 4 cases. The ratio was increased in one case (a group-3 case) and decreased in three patients (two group-1 cases and one group-2 case) (see Appendix A for individual values, page 59).

The variations in haemodynamic parameters were analysed in vascular territories supplied by the anterior, medial and posterior cerebral arteries in four patients with severe bilateral ICA stenoses but without VA lesion. In three of these cases, both TTP and BAT hemispheric ratios were significantly above unity (see Appendix A for individual values), indicating delayed bolus arrival through collateral routes (Calamante et al., 2001). CBV and OER were not, however, different from hemispheric mean in the territories supplied by vascular territories, an observation agreeing with a recent PET study (Derdeyn et al., 1999a). A patient with an ICA occlusion and 30% contralateral ICA stenosis showed an OER of 0.86 in territories supplied by anterior and medial cerebral arteries ipsilateral to the ICA occlusion, but 0.55 in the posterior cerebral artery territory. This indicates insufficient collateral flow redistribution.

5.3 Carr-Purcell T_2 MRI of acute ischaemia in the rat (*III*)

A decrease in either T_2^* or single echo T_2 is a common observation in the early minutes of global (de Crespigny et al., 1992; Kettunen et al., 2002b) and focal ischaemia (Calamante et al., 1999a; Gröhn et al., 1998; Gröhn et al., 2000a; Grune et al., 1999) in the brain at high field MRI. These observations have been explained by increased deoxyhaemoglobin concentrations due to increased OER, which leads to negative a BOLD effect. Furthermore, recent modeling work has indicated that a large body of the Hahn echo T_2 change in acutely ischaemic brain can be explained by intravascular signal change due to deoxyhaemoglobin (Gröhn et al., 2000a; Kettunen et al., 2002b). Lei and coworkers have provided evidence from the rat ischaemia model arguing for a substantial extravascular contribution to the negative BOLD at 9.4 T (Lei et al., 2003). In order to estimate intra and extravascular contributions to the ischaemia induced BOLD, Carr-Purcell T_2 MRI was used in this study, together with modeling of intravascular BOLD using blood T_2 and tissue morphology information. By altering the τ_{CP}, it is possible to modulate the dynamic dephasing component of CP-T_2 and therefore to estimate the contribution of this effect on the transverse relaxation. Spin-lock MRI was employed to probe parenchymal responses to ischaemia, since $T_{1\rho}$ has evidently a much reduced inherent sensitivity to susceptibility effects, such as BOLD. Behaviour of MRI variables, including absolute CP-R_2, $R_{1\rho}$ and D_{av}, was studied in the group of animals exposed to cerebral ischaemia and hypercapnia.

The MR relaxation data from the hypercapnia experiments was used to estimate the value of $R_{2,\mathrm{tissue}}$, used in simulations of intravascular BOLD, for the sequences used in the *in vivo* experiments. Here, the level of blood $PaCO_2$ was altered in spontaneously breathing animals by increasing CO_2 content in the inhaled gas mixture. Hypercapnia caused an average decline in parenchymal CP-R_2 by 0.30 ± 0.09 and 0.50 ± 0.15 s^{-1} in the experiments acquired with short and long τ_{CP}, respectively. The latter figure is almost identical to that acquired with Hahn spin echo MRI at 4.7 T from rat brain exposed to comparable hypercapnia (Kettunen et al., 2002b). The effect of hypercapnia on transverse relaxation is firmly explained by the BOLD effect. This results from increased CBV and reduced OER (Kettunen et al., 2002b). Using the blood R_2 calibration values (Silvennoinen et al., 2002) and the physiological adaptations described above, $R_{2,\mathrm{tissue}}$ can be estimated from the hypercapnia experiment. This analysis gave values of 14.5 and 16.0 s^{-1} for short and long τ_{CP} CP-R_2, respectively and these values were used in subsequent simulations of parenchymal transverse relaxation in the ischaemic brain. Cerebral $R_{1\rho}$ decreased during hypercapnia, with the response being greater at a 1 G spin-lock field amplitude. The mean 2% decline in cerebral $R_{1\rho}$ at 0.2 G is consistent with a recent study, in which comparable hypercapnia levels (Kettunen et al., 2002b) were used and is chiefly explained by an increased CBV. However, a substantial tissue contribution to 1 G $R_{1\rho}$ can be expected due to hypercapnia induced tissue acidification (Kettunen et al., 2002b; Mäkelä et al., 2001).

As expected, global ischaemia caused a rapid decline in $R_{1\rho}$ at both B_{1sl} fields (Fig. 5.4B). However, the responses of CP-R_2 acquired with either short or long τ_{CP} were very different in the early minutes of global ischaemia (Fig. 5.4A). Short τ_{CP} CP-R_2 did not change during the first 6 minutes of ischaemia, while in long τ_{CP} CP-R_2 an increase by 0.70 ± 0.18 s^{-1} ($\sim$4%) was seen by 4 minutes, followed by

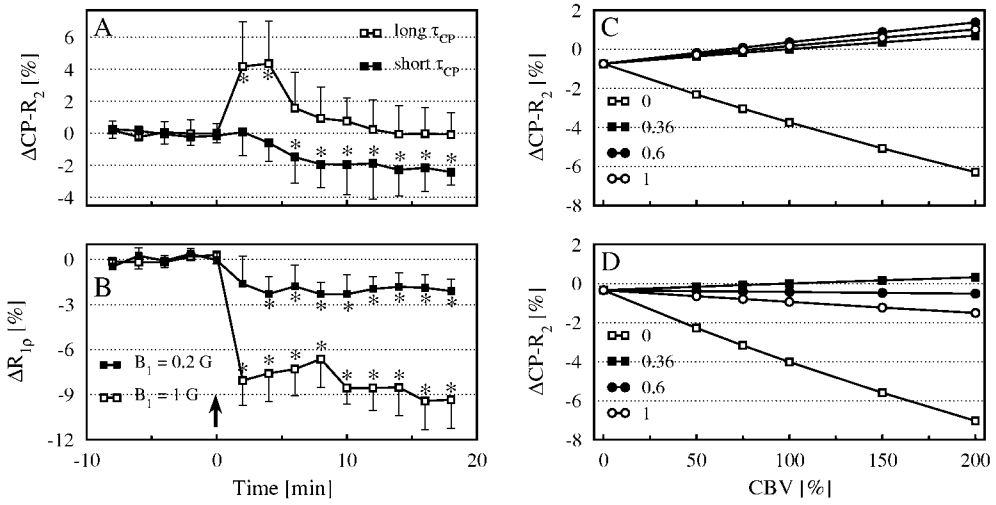

Figure 5.4: Relative changes of Carr-Purcell CP-R_2 (A), $R_{1\rho}$ (B) (relative to the respective preischaemia value) in a rat brain prior to and after induction of global ischaemia. Computer simulation of intravascular BOLD effect in a rat brain parenchyma at 4.7 T (C and D). An arrow indicates the time of KCl injection. * denotes P < 0.05, Student's paired t-test relative to preinjection value. The values are shown as mean±SD.

a downward drift towards the preischaemic value (Fig. 5.4A). Short τ_{CP} CP-R_2 has started to decline by 6 minutes after global ischaemia, showing a steady decay during the observation time (Fig. 5.4A). Additionally, it was interesting to note similarities in the time courses of short τ_{CP} CP-R_2 and $R_{1\rho}$ acquired at 0.2 G.

In 90 min ischaemic animals (*III*), diffusion MRI confirmed the presence of severe ischaemia upon in-bore MCA occlusion. Short τ_{CP} CP-R_2 did not change during the first 20 minutes of MCAo, but showed a time-dependent decline beyond that and also during reperfusion. An initial increase in long τ_{CP} CP-R_2 was evident upon MCA occlusion, followed by a downward trend after 10 minutes of ischaemia with a similar slope as for short τ_{CP} CP-R_2. Both $R_{1\rho}$ relaxation times had dropped by the first time point of MCA occlusion and continued to decrease after retraction of the the occluder.

Simulations of the intravascular BOLD contributions in short and long τ_{CP} CP-R_2 are shown in Fig. 5.4C and D. The relaxation rates were simulated for the experimental τ_{CP} values of 6.1 and 22.5 ms, respectively. For the control levels, physiological values for CBV (0.47 ml/100 g) and OER (0.36) were used. It is evident that in short τ_{CP} CP-R_2 either little or no increases should be observed upon ischaemia at high OER (Fig. 5.4C). On the other hand, long τ_{CP} CP-R_2 should be unaffected by intravascular BOLD effect during ischaemia (Fig. 5.4D). However, both these simulation results disagree with the experimental observations shown in Fig. 5.4A and B. This suggests that intravascular relaxation changes cannot explain enhanced parenchymal CP-R_2 detected by long τ_{CP} and may be alternatively explained by extravascular field gradients generated by intravascular deoxyhaemoglobin.

5.4 Relative dynamic dephasing contrast in infarcting rat brain (*IV*)

The ability of the CP-T_2 MRI to reveal dynamic dephasing contrast in the brain exposed to transient MCA occlusion was examined. It is well documented that in the early minutes of ischaemia both T_2^* and Hahn echo T_2 MRI reveal reduced relaxation times due to increased local deoxyhaemoglobin concentrations. The negative BOLD effect in the ischaemic brain is, however, only a short-lasting phenomenon due to collapsed collateral blood flow and oedema formation (Gröhn et al., 2000a).

In the MCA occlusion model, a decrease at the first time point was observed in long τ_{CP} CP-T_2 only. D_{av} had reduced from 0.69 ± 0.01 to 0.59 ± 0.02 10^{-3} mm^2/s, respectively by 3 minutes of MCA occlusion. Both short and long τ_{CP} CP-T_2 showed prolonged values in the striatum after 30 minutes of MCA occlusion. Estimates of relative dynamic dephasing computed from the short and long τ_{CP} images (Eq. 4.1) did not show changes, when either TE of 55 or 95 ms were used.

CP-T_2-weighted images (Fig. 5.5C) demonstrate striatal hyperintensity a day after MCA occlusion and this lasted for several days after ischaemia. Interestingly, the dynamic dephasing contrast shows reduced signal intensity in images and plots acquired with TE values of 55 and 95 ms (Fig. 5.5C). The relative dynamic dephasing images retained low contrast for several days after MCA occlusion and only returned

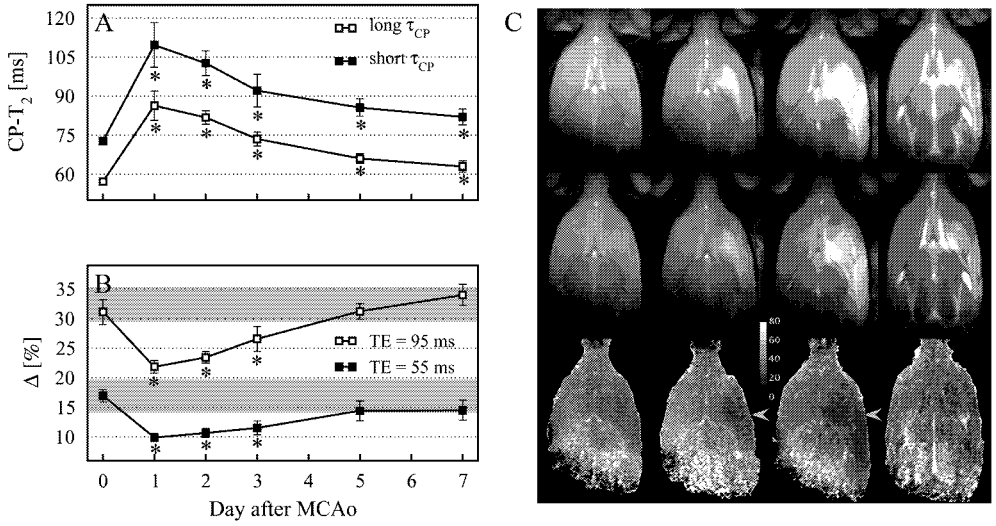

Figure 5.5: Absolute CP-T_2 (A) and relative dynamic dephasing (B) in ipsilateral striatum. (C) CP-T_2-weighted ($TE = 95$) short (upper row) and long (middle row) τ_{CP} images and relative dynamic dephasing images (bottom row) collected, from left to right, on a day 0, 1, 3 and 7 after MCAo. Note lower relative dynamic dephasing in ischaemic tissue (arrow heads), relative to normal brain. * denotes $P < 0.05$ relative to day 0 value. The shaded areas represent 95% confidence intervals of the respective value in non-ischaemic tissue.

to the control level by day 5. This change mirrored a decline in CP-T_2 values and normalisation of D_{av} in the infarcting striatum (*IV*).

Chapter 6

Discussion

Recent studies of experimental hypoperfusion and ischaemia have revealed that it is possibile to directly identify the mismatch between oxygen consumption and delivery by means of T_2 MRI (Gröhn et al., 1998; Gröhn et al., 2000a). This finding has indicated the potential usefulness of MRI in addressing the issue of tissue viability in a noninvasive manner. This information is expected to be of great clinical impact and may provide complementary information to that obtained from DWI and DSC MRI.

Reduction of the CPP in occlusive cerebrovascular disease is associated with haemodynamic compensatory mechanisms including microvascular dilatation and augmentation of oxygen extraction. Previously published PET studies of carotid artery stenosis patients stress the importance of cerebral haemodynamics in these cases (Grubb, Jr et al., 1998) and also linked elevated OER and CBV with a high risk of subsequent stroke (Derdeyn et al., 2002). The present work has added a great deal of mechanistic information about the BOLD effect associated with both misery perfusion and ischaemia in the brain. This information has proved to be useful in the interpretation of T_2 MRI in flow compromised brain as well as for the design of novel methods to quantify OER by MRI.

6.1 MRI of cerebral misery perfusion at 1.5 T

The present data demonstrates that the occlusion of three major arteries results in a significant reduction of the CBF in the rat. The measurement of absolute CBF in these experiments revealed severe hypoperfusion in the parietal cortex, ipsilateral to the permanent VA occlusion. However, it is important to note that this combination of vessel occlusions did not induced genuine ischaemia, since the signal enhancement in DWI associated with acute ischaemia (Moseley et al., 1990b) was not observed. The absolute CBF values obtained in this study by vessel occlusion are substantially lower than the CBF threshold of DWI enhancement in rat cerebral ischaemia reported by Kohno and coworkers (Kohno et al., 1995). This disagreement is likely to be caused by the different methods employed to measure of absolute CBF and an underestimation of the flow due to injurious placement of the hydrogen clearance electrode (Pell et al., 2003).

In the same tissue, the negative BOLD effect, as expressed by a reduction in absolute parenchymal T_2, was observed (Fig. 5.1B). The negative BOLD effect was recently observed by several studies upon reduction of CPP and was attributed to high concentrations of deoxyhaemoglobin, which was a result of elevated OER (Gröhn et al., 1998; Gröhn et al., 2000a; Kettunen et al., 2002b; Kettunen et al., 2002a). It is well established that increase in OER is a very sensitive compensatory mechanism upon reduction of cerebral perfusion and it has been shown to increase more than 2-fold in compromised CBF in man (Powers, 1991). The present data show that the magnitude of T_2 changes in perfused tissue upon compromised CBF can be explicitly deduced by the simulations of intravascular BOLD T_2 effects during known haemodynamic conditions (Fig. 5.1C). The good agreement between experimental T_2 data and the simulation of intravascular BOLD suggests that the changes contributing to negative BOLD at 1.5 T are of intravascular origin. Additionally, since preserved oxygen metabolism is mandatory to accumulate deoxyhaemoglobin, the negative BOLD effect and increased OER are only expressed in viable tissue (Gröhn et al., 1998; Gröhn et al., 2000a). The present data shows that the negative BOLD at 1.5 T field can serve as an index of cerebral misery perfusion and thus reveal viable tissue with an elevated OER.

The intravascular BOLD theory (van Zijl et al., 1998) together with CBV were exploited to quantify the OER in chronical carotid stenosis patients by MRI. It is well established that the adaptation of the cerebral haemodynamics in cerebrovascular disease is a very dynamic and complex process, which depends on a number of physiological and individual factors (Grubb, Jr et al., 1998; Derdeyn et al., 1999b; Derdeyn et al., 2002). Hence, the inherent variability of the obtained values compromised the statistical analysis of the results. However, the observations are in good agreements with several recent PET (Arakawa et al., 2003) and MRI (Maeda et al., 1999; Nighoghossian et al., 1996) studies matched patient populations. Additionally, the abnormal CBV values were observed with a comparable incidence as reported by either PET (Grubb, Jr et al., 1998; Derdeyn et al., 2002) or MRI (Lythgoe et al., 2000a; van Osch et al., 2002) studies of patients with symptomatic carotid stenosis.

The dynamics of contrast bolus passage in DCS MRI is expected to reveal indirectly the status of collateral flows in the presence of either stenosis or occlusion. A previous DSC MRI study of patients with Moyamoya disease has shown that TTP, BAT and PW values were greater in subjects with severe haemodynamic abnormalities compared to mild ones (Calamante et al., 2001). In the present patient group, eight cases were identified with TTP, BAT or PW intrahemispheric ratios significantly different from those observed in control subjects. Indeed, in 75% of these subjects, clinical data showed either watershed infarction or transient ischaemic attack, possibly suggesting that there is insufficient collateral function in these patients.

As discussed earlier in the text (Sec. 2.3.4), elevated OER yields a greater concentration of deoxyhaemoglobin in the microvasculature and thus enhances the parenchymal transverse relaxation. Depending upon the severity of a stenosis and the state of collateral flow, elevated OER can compensate the CBV effect on parenchymal T_2 which leads to the shallow or zero slope observed in the T_2-CBV curve. In the present study, hemispheric OER was derived from the T_2-CBV function by means of the intravascular BOLD effect (van Zijl et al., 1998). The slope of these fits yielded an estimate of OER of the 0.4 ± 0.05 for the control group of healthy subjects. This value

agrees well with those reported by PET (Derdeyn et al., 2002; Grubb, Jr et al., 1998; Leenders et al., 1990; Yamauchi et al., 1996) and MRI studies (An and Lin, 2002; Golay et al., 2001; Oja et al., 1999). This approach was applied together with the established DSC MRI to assess haemodynamic adaptation in carotid stenosis patients. In contrast to GM CBV, average GM OER in the ipsilateral hemisphere was clearly higher in the patient groups with severe ICA stenosis (0.52) and occlusion (0.55) than in control (0.40) and mild ICA stenosis (0.41) subjects, indicating compromised cerebral haemodynamics in the former group. It is worth noting that three of the patients with high GM OER also showed high GM CBV. This combination of haemodynamic adaptations due to vascular stenosis has recently been associated with a several-fold increased incidence of stroke (Derdeyn et al., 2002).

The present approach of OER quantification is an extension to the previously proposed MRI methods employing the intravascular BOLD, in which venous oxygen saturation and OER are determined from cerebral draining veins (Golay et al., 2001; Oja et al., 1999). The advantage of the present method is that it estimates parenchymal OER without requiring knowledge of tissue T_2. As shown in the Fig. 5.2C, altered microvascular Hct may potentially bias the estimation of OER, since it affects the slope of the T_2-CBV plot. It was estimated that a 10% change in the microvascular Hct would result appromaximately a 10% error in the OER estimate. However, the employment of recent macrovascular Hct values for each subject individually ensured accurate OER values.

The ultimate drawback of the presented OER quantification is the low dynamic range of the BOLD effect at 1.5 T field strength. Although, this limitation can be eliminated by the application of the method at higher magnetic field strength, the inevitable contribution of extravascular dephasing to the BOLD (Lei et al., 2003), as discussed in the following sections, would result in an overestimation of the parenchymal OER. A further handicap is posed by the assumption of a slow exchange regime in the intravascular BOLD model (van Zijl et al., 1998). This condition is likely to be violated in acute or chronic stroke implying that the approach can not be reliably applied to patients with acute ischaemic stroke.

An elevated $T_{2,\mathrm{tissue}}$ in the patient group with ICA occlusion (Fig. 5.3C) is not an unexpected observation, because previous clinical studies have shown that in severe carotid stenosis, cerebral metabolism becomes affected (van der Grond et al., 1995; Rutgers et al., 2000; Tsuchida et al., 2000). The NMR spectroscopy study has reported early signs of cell membrane damage in the brain regions displaying elevated OER (Tsuchida et al., 2000).

6.2 Effects of ischaemia on T_2 relaxation

The present data demonstrate that it is possible to modulate T_2 contrast in acute ischaemia by changing the interpulse interval τ_{CP} in the Carr-Purcell spin echo sequence. Long τ_{CP} CP-R_2 shows a positive change in the early phase of ischaemia (Fig. 5.4A), an observation which is consistent with data from Hahn echo R_2 MRI at 4.7 T (Gröhn et al., 2000a). In contrast, short τ_{CP} CP-R_2 does not indicate a relaxation change in hyperacute ischaemia, but rather a time-dependent decline in the ischaemic brain. Thus the latter MR relaxation parameter does not reveal the BOLD effect due

to ischaemia, but rather a complex pattern of changes indicated by long τ_{CP} CP-R_2 and $R_{1\rho}$.

The spin echo BOLD effect induced by hypoxia (van Zijl et al., 1998), hypercapnia (Ulatowski et al., 1999) and ischaemia (Gröhn et al., 2000a) has been modeled as an intravascular phenomenon at 4.7 T. All these studies have used Hahn spin echo MRI with maximal sensitivity to dynamic dephasing effects due to exchange and diffusion through susceptibility gradients. However, the simulations performed in the present study argue that the direct contribution of intravascular water to the BOLD effect is virtually zero during acute ischaemia at 4.7 T (Fig. 5.4C and D). Using an experimentally determined blood R_2, the simulations show unequivocally that $R_{2,\mathrm{blood}}$ is very short at OERs higher than 0.4. In other words, the large body of capillary and venous water spins dephase so rapidly that they do not contribute to the parenchymal R_2 at all. It is therefore likely that the observed BOLD contribution to the long τ_{CP} CP-R_2 is mainly caused by the extravascular water diffusing through the susceptibility gradients. Thus it appears that at high field, substantial extravascular contributions to the BOLD effect are inevitable in Hahn and long τ_{CP} CP-R_2 experiments and that these effects clearly outweigh those caused by direct tissue relaxation changes in the early phase of ischaemia. This conclusion is supported by the recent studies of metabolite relaxation times in the ischaemic brain (Lei et al., 2003).

The spin-lock MRI contrast, probed by $R_{1\rho}$ is inherently less sensitive to dynamic dephasing effects. This is quantitatively illustrated *in vivo* at 4.7 T MRI experiments with injected intravascular superparamagnetic iron oxide particle contrast agent (AMI-227) (Kettunen et al., 2002b). The concentration of AMI-227, which caused more than a 70% shortening of the cerebral Hahn echo R_2, results in only a 3% reduction in the $R_{1\rho}$ (Kettunen et al., 2002b). This data clearly shows that despite strong susceptibility gradients generated by AMI-227, $R_{1\rho}$ is only affected by the direct signal originating from the blood pool. Thus, it is likely that $R_{1\rho}$ MRI reveals exclusively tissue responses to ischaemia caused by factors such as pH change, altered macromolecular mobility and at later time points by magnetisation transfer (Kettunen et al., 2002b; Mäkelä et al., 2001; Mäkelä et al., 2002). In this regard, it is interesting to note that short τ_{CP} CP-R_2 behaves in a similar fashion to low B_{1sl} $R_{1\rho}$ (Fig. 5.4A and B) and thus showing reduced sensitivity to the dynamic dephasing effects with respect to the long τ_{CP} CP-R_2. As far as the absence of a change in short τ_{CP} CP-R_2 during the first minutes of ischaemia is concerned, it seems likely that the weak BOLD sensitivity of the method and tissue induced relaxation changes in the parenchyma are approximately equal, but of opposite signs and hence cancel out their effects on short τ_{CP} CP-R_2.

Recent studies indicate that the degree of irreversible neuronal damage can be predicted in the early moments of focal ischaemia with absolute $R_{1\rho}$ MRI, before any evidence of a change in R_2 (Gröhn et al., 1999; Gröhn et al., 2000b). The present results suggest that absolute CP-R_2, especially that acquired with short τ_{CP}, behaves in the irreversible ischaemia similarly as the $R_{1\rho}$ acquired with a B_{1sl} of 0.2 G. While spin-lock MRI acquired with high B_{1sl} may not be clinically feasible due to high RF energy deposition, CP-R_2 MRI can be used in clinical settings. Thus, it can be suggested that CP-R_2 contrast may have a potential in the assignment of ischaemic tissue in the early phase of pathology.

The CP-T_2 has been proposed to provide means of manipulating transverse re-

laxation MR contrast at high magnetic fields (Bartha et al., 2002). The present study provides evidence that supports this idea in regard to stroke imaging. The ability to modulate the T_2 contrast has been dealt with above and the dynamic dephasing signal changes in the infarcting brain have been demostrated. This is a very interesting observation, because it potentially adds a new dimension to stroke assessment by T_2 MRI. These changes in the infarcting brain may allow for the assessment of the age of ischaemia, which may not be possible from conventional T_2 MR images alone.

In the present model of MCAo, spin density in the infarcting tissue does not change within the first three hours after the insult suggesting that there is no net gain of water into the tissue (Mäkelä et al., 2002). In the tissue displaying low D_{av}, but no net water gain nor cell loss, CP-T_2 MRI does not show altered susceptibility contrast relative to the unexposed brain. Therefore, cytotoxic oedema, reduced extracellular volume, low bulk diffusion and intracellular acidosis as such, do not appear to influence the dynamic dephasing signal in the early phase of ischaemia. A day after MCAo, dynamic dephasing data indicate a decline in the infracting tissue. At these time points, processes including cell damage and severe cell loss substantially alter the microscopic structure of brain tissue, and therefore change the susceptibility gradients within the tissue.

The time course of D_{av} in the present MCA occlusion model bears interesting similarities with the dynamic dephasing contrast in the infracting brain. Both MR variables are low a day after the insult and returning to pre-ischaemic levels 5 days after the stroke. Hence, it would be tempting to hypothesize that low bulk diffusion could lead to a reduced dynamic dephasing contrast. However, the fact that D_{av} is severely attenuated in the early moments of ischaemia, when dynamic dephasing is still unchanged, argues against this hypothesis. On the other hand, it should be emphasised that water diffusion as measured by MRI is a weighted average of diffusion coefficients in several compartments. Consequently, the effect of altered diffusion in one or several of these pools on CP-T_2 can not be completely excluded.

Reduced concentrations of paramagnetic ferritin as a consequence of ischaemic cell loss could also decrease dynamic dephasing contrast. However, the most notable consequences of ischaemia include water accumulation and cell loss. Previous studies (Knight et al., 1994; Ordidge et al., 1991) show that the time course of net water gain into the infracting brain after MCAo closely follows that of the dynamic dephasing contrast reported here. Therefore, it is suggested that these two factors acting together could explain the present observation of declined dynamic dephasing contrast in the post-stroke brain.

Chapter 7

Summary and Conclusions

The present work has explored the physiological processes influencing transverse relaxation with respect to the perturbation of cerebral blood flow during cerebral ischaemia and hypoperfusion both in rats and carotid stenosis patients. Severe reduction of the CPP towards the ischaemia threshold is compensated by elevated CBV and OER that result in high concentrations of deoxyhaemoglobin and enhanced dynamic dephasing component of the transverse relaxation. This condition renders parenchymal T_2 relaxation sensitivity to a negative BOLD effect.

The magnitude of the dynamic dephasing component of T_2 can be modulated by an interpulse interval between consecutive refocusing pulses in a Carr-Purcell spin echo sequence. This provides novel MR contrast in the assessment of cerebral ischaemia.

The main observations are summarized as follows:

1. An acute drop in CBF causes a negative BOLD effect as manifested by a reduction in parenchymal T_2 relaxation time at 1.5 T and is a sign of insufficient perfusion which is haemodynamically compensated by an elevated OER. The magnitude of this effect can be accurately deduced by an intravascular BOLD model. Based on this observation, it is suggested that T_2 BOLD MRI may serve as an index of cerebral misery perfusion.

2. Severe carotid artery stenosis reduces the CPP in tissue distal to the vascular disease. In one class of carotid stenosis patients, the autoregulation of cerebral haemodynamics due to the reduced CPP results in an increase in the CBV, which can be revealed by DSC MRI. Elevated OER, as a sign of exhausted cerebral autoregulation in carotid stenosis patients, can be noninvasively assessed by means of intravascular T_2 BOLD and DSC MRI. The presented MRI approach for OER quantification can be potentially automated and extended to all types of brain tissues and therefore it may potentially find applications in the clinical environment in identification of patients with a high risk of ischaemic stroke.

3. At high magnetic fields (such as 4.7 T), the negative BOLD effect in acute ischaemia is not a consequence of a relaxation change in intravascular water, but

rather results from susceptibility gradients of deoxyhaemoglobin affecting extravascular water.

4. Short τ_{CP} CP-T_2 effectively reduces the negative BOLD effect in hyperacute cerebral ischaemia in rat at 4.7 T. The temporal evolution of short τ_{CP} CP-T_2 closely resembles low B_{1sl} $T_{1\rho}$ contrast in ischaemic tissue. Since $T_{1\rho}$ MRI may not be suitable in the clinical use due to high RF energy deposition, CP-T_2 may provide similar information about the tissue status avoiding this problem.

5. CP-T_2 MRI reveals dynamic dephasing signal changes in the developing infarction thet coincides with water accumulation and cell loss. The dynamic dephasing contrast may provide novel information in the assessment of the ischaemic brain in association with the T_2 MRI.

Appendix A

CE MRA and MRI of the patients with occlusive cerebrovascular disease

	Stenosis L/R [%]			CBV		OER		TTP	BAT	PW	MPC
	CCA	ICA	VA	I/C	I	I/C	I	I/C	I/C	I/C	I/C
1	55/25	50/100	40/60	1.001	3.57	1.000	0.63[a]	1.023[a]	1.020[a]	0.993	0.973
2	0/30	30/100		1.235[a]	4.70[a]	1.904[a]	0.89[a]	1.105[a]	1.133[a]	1.090[a]	1.079[a]
3	30/0	65/0		1.017	4.25	0.989	0.46	1.007	0.993	1.028[a]	1.006
4		40/50		0.931[a]	2.61[a]	0.931	0.27	0.999	1.003	0.981	0.964[a]
5		70/0		0.961	2.29[a]	0.943	0.41	1.005	1.015[a]	0.984	0.945[a]
6		100/75		0.992	3.72	1.343	0.45	1.024[a]	1.023[a]	1.041[a]	0.978
7		0/45		0.907[a]	2.76	1.151	0.30	1.008	1.220[a]	0.932[a]	0.942[a]
8	80/50	90/75		0.999	3.45	1.214	0.51[a]	0.980[a]	0.978[a]	1.003	1.032
9		70/0		1.015	4.97[a]	1.154	0.45	0.995	0.988	1.036[a]	1.021
10	0/40	0/40	0/70	0.942	2.99	1.357[a]	0.57[a]	0.999	1.005	0.978	0.949[a]
11	50/20	100/0	40/0	0.965	2.48[a]	0.973	0.36	1.009[a]	1.008	0.988	0.977
12		50/50		0.985	3.17	1.134	0.55[a]	0.999	0.999	1.013	0.984
13		70/40		0.996	4.89[a]	1.202	0.68[a]	0.995	0.996	0.996	1.028
14	30/0	50/50	0/100	0.995	4.65[a]	1.035	0.58[a]	0.990[a]	0.850[a]	1.002	1.021
15		70/20		0.961	2.93	1.333	0.40	0.997	1.001	0.987	1.004
16		0/45	30/0	1.003	3.38	1.054	0.29	1.004	1.004	0.998	1.002
17		50/85	0/100	1.041	3.39	1.500[a]	0.37	1.008	1.011	1.003	1.021
18		70/45		1.036	3.69	1.116	0.38	1.004	1.004	0.997	0.995
19		75/100		1.041	3.67	1.049	0.43	1.033[a]	1.036[a]	1.001	1.008
20		25/22		1.023	3.61	1.000	0.43	1.005	1.006	1.006	0.981
21		70/0		0.911[a]	3.34	0.955	0.85[a]	1.003	1.009	0.995	0.968
22		20/0		1.002	3.78	1.052	0.40	0.997	0.989	1.027[a]	0.993

L - left, R - right, I - ipsilateral, C - contralateral, [a] - values outside of 2·SD of control subjects. Ipsilateral CBV [ml/100 g].

References

Allerhand, A. and Gutowsky, H. S. (1964). Spin-echo NMR studies of chemical exchange. I. Some general aspects. *J Chem Phys*, 41:2115–2126.

Alsop, D. C. and Detre, J. A. (1996). Reduced transit-time sensitivity in noninvasive magnetic resonance imaging of human cerebral blood flow. *J Cereb Blood Flow Metab*, 16(6):1236–1249.

Alsop, D. C. and Detre, J. A. (1998). Multisection cerebral blood flow MR imaging with continuous arterial spin labeling. *Radiology*, 208(2):410–6.

An, H. and Lin, W. (2002). Cerebral oxygen extraction fraction and cerebral venous blood volume measurements using MRI: effects of magnetic field variation. *Magn Reson Med*, 47(5):958–66.

An, H., Lin, W., Celik, A., and Lee, Y. Z. (2001). Quantitative measurements of cerebral metabolic rate of oxygen utilization using MRI: a volunteer study. *NMR Biomed*, 14(7-8):441–7.

Arakawa, S., Minematsu, K., Hirano, T., Tanaka, Y., Hasegawa, Y., Hayashida, K., and Yamaguchi, T. (2003). Topographic distribution of misery perfusion in relation to internal and superficial borderzones. *AJNR Am J Neuroradiol*, 24(3):427–35.

Astrup, J., Siesjö, B. K., and Symon, L. (1981). Thresholds in cerebral ischemia - the ischemic penumbra. *Stroke*, 12(6):723–5.

Astrup, J., Symon, L., Branston, N. M., and Lassen, N. A. (1977). Cortical evoked potential and extracellular K^+ and H^+ at critical levels of brain ischemia. *Stroke*, 8(1):51–57.

Axel, L. (1980). Cerebral blood flow determination by rapid-sequence computed tomography: theoretical analysis. *Radiology*, 137(3):679–86.

Baethmann, A. and Staub, F. (1997). Cellular edema. In Welch, K., editor, *Primer on Cerebrovascular Diseases.*, pages 153–156. Academic Press, San Diego.

Baird, A., Benfield, A., Schlaug, G., Siewert, B., Lövblad, K., Edelman, R., and Warach, S. (1997). Enlargement of human cerebral ischemic lesion volumes measured by diffusion-weighted magnetic resonance imaging. *Ann Neurol*, 41(5):581–9.

Baird, A. E. and Warach, S. (1998). Magnetic resonance imaging of acute stroke. *J Cereb Blood Flow Metab*, 18(6):583–609.

Baron, J. C., Bousser, M. G., Rey, A., Guillard, A., Comar, D., and Castaigne, P. (1981). Reversal of focal "misery-perfusion syndrome" by extra-intracranial arterial bypass in hemodynamic cerebral ischemia. A case study with ^{15}O positron emission tomography. *Stroke*, 12:454–459.

Bartha, R., Michaeli, S., Merkle, H., Adriany, G., Andersen, P., Chen, W., Ugurbil, K., and Garwood, M. (2002). In vivo ^1H_2O $T_2^\dagger$ measurement in the human occipital lobe at 4 T

and 7 T by Carr-Purcell MRI: detection of microscopic susceptibility contrast. *Magn Reson Med*, 47(4):742–50.

Basser, P., Mattiello, J., and LeBihan, D. (1994). Estimation of the effective self-diffusion tensor from the NMR spin echo. *J Magn Reson B*, 103(3):247–54.

Beauchamp, N. J. and Bryan, R. N. (1997). Neuroimaging of stroke. In Welch, K., editor, *Primer on Cerebrovascular Diseases.*, pages 599–610. Academic Press, San Diego.

Belliveau, Kennedy, D. N., McKinstry, R. C., Buchbinder, B. R., Weisskoff, R. M., Cohen, M. S., Vevea, J. M., Brady, T. J., and Rosen, B. R. (1991). Functional mapping of human visual cortex by magnetic resonace imaging. *Science*, 254:716–719.

Betz, A. L. (1997). Vasogenic Brain Edema. In Welch, K., editor, *Primer on Cerebrovascular Diseases.*, pages 156–159. Academic Press, San Diego.

Bloch, F., Hansen, W. W., and Packard, M. E. (1946). Nuclear induction. *Phys. Rev.*, 69:127.

Bottomley, P. A., Foster, T. H., Argersinger, R. E., and Pfeifer, L. M. (1984). A review of normal tissue hydrogen NMR relaxation times and relaxation mechanisms from 1-100 MHz: dependence on tissue type, NMR frequency, temperature, species, excision, and age. *Med Phys*, 11:425–448.

Boxerman, J. L., Hamberg, L. M., Rosen, B. R., and Weisskoff, R. M. (1995). MR contrast due to intravascular magnetic susceptibility perturbations. *Magn Reson Med*, 34(4):555–66.

Boxerman, J. L., Rosen, B. R., and Weisskoff, R. M. (1997). Signal-to-noise analysis of cerebral blood volume maps from dynamic NMR imaging studies. *J Magn Reson Imaging*, 7(3):528–37.

Brindle, K. M., Brown, F. F., Cambell, I. D., Grathwohl, C., and Kuchel, P. W. (1979). Application of spin-echo nuclear magnetic resonance to whole-cell systems. *Biochem. J.*, 180:37–44.

Brooks, R. A., Chiro, G. D., and Keller, M. R. (1980). Explanation of cerebral white-gray contrast in computed tomography. *J Comput Assist Tomogr*, 4(4):489–491.

Bryant, R. G., Marill, K., Blackmore, C., and Francis, C. (1990). Magnetic relaxation in blood and blood clots. *Magn. Reson. Med.*, 13:133–144.

Busza, A. L., Allen, K. L., King, M. D., van Bruggen, N., Williams, S. R., and Gadian, D. G. (1992). Diffusion-weighted imaging studies of cerebral ischemia in gerbils. Potential relevance to energy failure. *Stroke*, 23:1602–1612.

Calamante, F., Gadian, D. G., and Connelly, A. (2000). Delay and dispersion effects in dynamic susceptibility contrast MRI: simulations using singular value decomposition. *Magn Reson Med*, 44(3):466–73.

Calamante, F., Ganesan, V., Kirkham, F. J., Jan, W., Chong, W. K., Gadian, D. G., and Connelly, A. (2001). MR perfusion imaging in Moyamoya Syndrome: potential implications for clinical evaluation of occlusive cerebrovascular disease. *Stroke*, 32(12):2810–6.

Calamante, F., Lythgoe, M. F., Pell, G. S., Thomas, D. L., King, M. D., Busza, A. L., Sotak, C. H., Williams, S. R., Ordidge, R. J., and Gadian, D. G. (1999a). Early changes in water diffusion, perfusion, T_1, and T_2 during focal cerebral ischemia in the rat studied at 8.5 T. *Magn Reson Med*, 41(3):479–85.

Calamante, F., Thomas, D. L., Pell, G. S., Wiersma, J., and Turner, R. (1999b). Measuring cerebral blood flow using magnetic resonance imaging techniques. *J Cereb Blood Flow Metab*, 19(7):701–35.

Calamante, F., Yim, P. J., and Cebral, J. R. (2003). Estimation of bolus dispersion effects in perfusion MRI using image-based computational fluid dynamics. *Neuroimage*, 19(2 Pt 1):341–53.

Carr, H. Y. and Purcell, E. M. (1954). Effects of diffusion on free precession in nuclear magnetic resonance experiments. *Physical Rev*, 94:630–638.

Chen, C. N. and Hoult, D. I. (1989). *Biomedical Magnetic Resonance Technology*. Institute of Physics, London, 3rd. edition.

Chillon, J.-M. and Baumach, G. L. (1997). Autoregulation of Cerebral Blood Flow. In Welch, K., editor, *Primer on Cerebrovascular Diseases.*, pages 751–56. Academic Press, San Diego.

Cloft, H. J., Murphy, K. J., Prince, M. R., and Brunberg, J. A. (1996). 3D gadolinium-enhanced MR angiography of the carotid arteries. *Magn Reson Imaging*, 14(6):593–600.

Crockard, A., Iannotti, F., Hunstock, A. T., Smith, R. D., Harris, R. J., and Symon, L. (1980). Cerebral blood flow and edema following carotid occlusion in the cerbil. *Stroke*, 11:494–498.

de Crespigny, A. J., Rother, J., Beaulieu, C., Moseley, M. E., and Hoehn, M. (1999). Rapid monitoring of diffusion, DC potential, and blood oxygenation changes during global ischemia. Effects of hypoglycemia, hyperglycemia, and TTX. *Stroke*, 30(10):2212–22.

de Crespigny, A. J., Wendland, M. F., Derugin, N., Kozniewska, E., and Moseley, M. E. (1992). Real time observation of transient focal ischemia and hyperemia in cat brain. *Magn Reson Med*, 27:391–397.

Decanniere, C., Eleff, S., Davis, D., and van Zijl, P. C. M. (1995). Correlation of rapid changes in the avarage water diffusion constant and the concentrations of lactate and ATP breakdown products during global ischemia in cat brain. *Magn. Reson. Med.*, 34:343–352.

Derdeyn, C. P., Shaibani, A., Moran, C. J., and Grubb, Jr, R. L., and Powers, W. J. (1999a). Lack of correlation between pattern of collateralization and misery perfusion in patients with carotid occlusion. *Stroke*, 30(5):1025–32.

Derdeyn, C. P., Videen, T. O., Fritsch, S. M., Carpenter, D. A., Grubb, Jr, R. L., and Powers, W. J. (1999b). Compensatory mechanisms for chronic cerebral hypoperfusion in patients with carotid occlusion. *Stroke*, 30(5):1019–24.

Derdeyn, C. P., Videen, T. O., Yundt, K. D., Fritsch, S. M., Carpenter, D. A., Grubb, R. L., and Powers, W. J. (2002). Variability of cerebral blood volume and oxygen extraction: stages of cerebral haemodynamic impairment revisited. *Brain*, 125(Pt 3):595–607.

Detre, J. A., Alsop, D. C., Vives, L. R., Maccotta, L., Teener, J. W., and Raps, E. C. (1998). Noninvasive MRI evaluation of cerebral blood flow in cerebrovascular disease. *Neurology*, 50(3):633–41.

Detre, J. A., Leigh, J. S., Williams, D. S., and Koretsky, A. P. (1992). Perfusion imaging. *Magn. Reson. Med.*, 23:37–45.

Detre, J. A., Samuels, O. B., Alsop, D. C., Gonzalez-At, J. B., Kasner, S. E., and Raps, E. C. (1999). Noninvasive magnetic resonance imaging evaluation of cerebral blood flow with acetazolamide challenge in patients with cerebrovascular stenosis. *J Magn Reson Imaging*, 10(5):870–5.

Dirnagl, U. and Pulsinelli, W. (1990). Autoregulation of cerebral blood flow in experimental focal brain ischemia. *J Cereb Blood Flow Metab*, 10(3):327–36.

Edelman, R., Ahn, S., Chien, D., Li, W., Goldmann, A., Mantello, M., Kramer, J., and Kleefield, J. (1992). Improved time-of-flight MR angiography of the brain with magnetization transfer contrast. *Radiology*, 184(2):395–9.

Edelman, R., Siewert, B., Darby, D., Thangaraj, V., Nobre, A., Mesulam, M., and Warach, S. (1994). Qualitative mapping of cerebral blood flow and functional localization with echo-planar MR imaging and signal targeting with alternating radio frequency. *Radiology*, 192(2):513–20.

Edelstein, W. A., Hutchinson, J. M. S., Johnson, G., and Redpath, T. W. (1980). Spin warp NMR imaging and applications to human whole-body imaging. *Phys Med Biol*, 25:751.

Ferrari, M., Wilson, D., Hanley, D., and Traystman, R. (1992). Effects of graded hypotension on cerebral blood flow, blood volume, and mean transit time in dogs. *Am J Physiol*, 262(6 Pt 2):H1908–14.

Fiehler, J., Foth, M., Kucinski, T., Knab, R., von Bezold, M., Weiller, C., Zeumer, H., and Rother, J. (2002). Severe ADC decreases do not predict irreversible tissue damage in humans. *Stroke*, 33(1):79–86.

Filho, I. P. T., Kerger, H., and Intaglietta, M. (1996). pO2 measurements in arteriolar networks. *Microvasc Res*, 51(2):202–12.

Gadian, D. G., Frackowiak, R. S. J., Crockard, H. A., Proctor, E., Allen, K., Williams, S. R., and Russell, R. W. R. (1987). Acute cerebral ischaemia: concurrent changes in cerebral blood flow, energy metabolites, pH, and lactate measured with hydrogen clearance and ^{31}P and ^{1}H nucler magnetic resonance spectroscopy. I. methology. *J Cereb Blood Flow Metab*, 7:199–206.

Gao, J., Holland, S., and Gore, J. (1988). Nuclear magnetic resonance signal from flowing nuclei in rapid imaging using gradient echoes. *Med Phys*, 15(6):809–14.

Garcia, J., Kalimo, H., Kamijyo, Y., and Trump, B. (1977). Cellular events during partial cerebral ischemia. I. Electron microscopy of feline cerebral cortex after middle-cerebral-artery occlusion. *Virchows Arch B Cell Pathol*, 25(3):191–206.

Garwood, M. and DelaBarre, L. (2001). The return of the frequency sweep: designing adiabatic pulses for contemporary NMR. *J Magn Reson*, 153(2):155–77.

Garwood, M. and Ke, Y. (1991). Symmetric pulses to induce arbitrary flip angles with compensation for RF inhomogeneity and resonance offsets. *J Magn Reson*, 94:511–525.

Gerlach, W. and Stern, O. (1924). Ueber die Richtungsquantelung im Magnetfeld. *Ann Phys*, 74:673.

Gibbs, J., Wise, R., Leenders, K., and Jones, T. (1984). Evaluation of cerebral perfusion reserve in patients with carotid-artery occlusion. *Lancet*, 1(8372):310–4.

Gillis, P., Peto, S., Moiny, F., Mispelter, J., and Cuenod, C. A. (1995). Proton transverse nuclear magnetic relaxation in oxidized blood: a numerical approach. *Magn Reson Med*, 33(1):93–100.

Golay, X., Silvennoinen, M. J., Zhou, J., Clingman, C. S., Kauppinen, R. A., Pekar, J. J., and van Zij, P. C. (2001). Measurement of tissue oxygen extraction ratios from venous blood T_2: increased precision and validation of principle. *Magn Reson Med*, 46(2):282–91.

Golay, X., Stuber, M., Pruessmann, K. P., Meier, D., and Boesiger, P. (1999). Transfer insensitive labeling technique (TILT): application to multislice functional perfusion imaging. *J Magn Reson Imaging*, 9(3):454–61.

Gröhn, O., Lukkarinen, J., Silvennoinen, M., Pitkänen, A., van Zijl, P., and Kauppinen, R. (1999). Quantitative magnetic resonance imaging assessment of cerebral ischemia in rat using on-resonance $T_{1\rho}$ in the rotating frame. *Magn Reson Med*, 42(2):268–76.

Gröhn, O. H., Kettunen, M. I., Penttonen, M., Oja, J. M., van Zijl, P. C., and Kauppinen, R. A. (2000a). Graded reduction of cerebral blood flow in rat as detected by the nuclear magnetic resonance relaxation time T_2: a theoretical and experimental approach. *J Cereb Blood Flow Metab*, 20(2):316–326.

Gröhn, O. H., Lukkarinen, J. A., Oja, J. M., van Zijl, P. C., Ulatowski, J. A., Traystman, R. J., and Kauppinen, R. A. (1998). Noninvasive detection of cerebral hypoperfusion and reversible ischemia from reductions in the magnetic resonance imaging relaxation time, T_2. *J Cereb Blood Flow Metab*, 18(8):911–20.

Gröhn, O. H. J., Kettunen, M. I., Mäkelä, H. I., Penttonen, M., Pitkänen, A., Lukkarinen, J. A., and Kauppinen, R. A. (2000b). Early detection of irreversible cerebral ischemia in the rat using dispersion of the magnetic resonance imaging relaxation time, $T_{1\rho}$. *J Cereb Blood Flow Metab*, 20(10):1457–66.

Grubb, R., Phelps, M., Raichle, M., and Ter-Pogossian, M. (1973). The effects of arterial blood pressure on the regional cerebral blood volume by X-ray fluorescence. *Stroke*, 4(3):390–9.

Grubb, R., Raichle, M., Eichling, J., and Ter-Pogossian, M. (1974). The effects of changes in $PaCO_2$ on cerebral blood volume, blood flow, and vascular mean transit time. *Stroke*, 5(5):630–9.

Grubb, R., Raichle, M., Phelps, M., and Ratcheson, R. (1975). Effects of increased intracranial pressure on cerebral blood volume, blood flow, and oxygen utilization in monkeys. *J Neurosurg*, 43(4):385–98.

Grubb, Jr, R. L., Derdeyn, C. P., Fritsch, S. M., Carpenter, D. A., Yundt, K. D., Videen, T. O., Spitznagel, E. L., and Powers, W. J. (1998). Importance of hemodynamic factors in the prognosis of symptomatic carotid occlusion. *JAMA*, 280(12):1055–60.

Grune, M., van Dorsten, F. A., Schwindt, W., Olah, L., and Hoehn, M. (1999). Quantitative T_2^* and $T_2^{'}$ maps during reversible focal cerebral ischemia in rats: separation of blood oxygenation from nonsusceptibility-based contributions. *Magn Reson Med*, 42(6):1027–32.

Guckel, F. J., Brix, G., Schmiedek, P., Piepgras, Z., Becker, G., Kopke, J., Gross, H., and Georgi, M. (1996). Cerebrovascular reserve capacity in patients with occlusive cerebrovascular disease: assessment with dynamic susceptibility contrast-enhanced MR imaging and the acetazolamide stimulation test. *Radiology*, 201(2):405–12.

Haacke, E., Masaryk, T., Wielopolski, P., Zypman, F., Tkach, J., Amartur, S., Mitchell, J., Clampitt, M., and Paschal, C. (1990). Optimizing blood vessel contrast in fast three-dimensional MRI. *Magn Reson Med*, 14(2):202–21.

Haacke, E. M., Brown, R. W., Thompson, M. R., and Venkatesan, R. (1999). *Magnetic Resonance Imaging: Physical principles and sequence design*. Wiley-Liss, Ney York.

Hahn, E. L. (1950). Spin echoes. *Physical Rev*, 80:580–594.

Hakumäki, J. M., Pirttilä, T.-R. M., and Kauppinen, R. A. (2000). Reduction in water and metabolite apparent diffusion coefficients during energy failure involves cation-dependent mechanisms. A nuclear magnetic resonance study of rat cortical brain slices. *J Cereb Blood Flow Metab*, 20:405–411.

Hartkamp, M. J., van Der Grond, J., van Everdingen, K. J., Hillen, B., and Mali, W. P. (1999). Circle of Willis collateral flow investigated by magnetic resonance angiography. *Stroke*, 30(12):2671–8.

Heiss, W., Graf, R., Löttgen, J., Ohta, K., Fujita, T., Wagner, R., Grond, M., and Weinhard, K. (1997). Repeat positron emission tomographic studies in transient middle cerebral artery occlusion in cats: residual perfusion and efficacy of postischemic reperfusion. *J Cereb Blood Flow Metab*, 17(4):388–400.

Heiss, W., Graf, R., Wienhard, K., Löttgen, J., Saito, R., Fujita, T., Rosner, G., and Wagner, R. (1994). Dynamic penumbra demonstrated by sequential multitracer PET after middle cerebral artery occlusion in cats. *J Cereb Blood Flow Metab*, 14(6):892–902.

Heiss, W. and Rosner, G. (1983). Functional recovery of cortical neurons as related to degree and duration of ischemia. *Ann Neurol*, 14(3):294–301.

Henderson, R. D., Eliasziw, M., Fox, A. J., Rothwell, P. M., and Barnett, H. J. (2000). Angiographically defined collateral circulation and risk of stroke in patients with severe carotid artery stenosis. North American Symptomatic Carotid Endarterectomy Trial (NASCET) group. *Stroke*, 31(1):128–32.

Hendrikse, J., Hartkamp, M. J., Hillen, B., Mali, W. P., and van der Grond, J. (2001). Collateral ability of the circle of Willis in patients with unilateral internal carotid artery occlusion: border zone infarcts and clinical symptoms. *Stroke*, 32(12):2768–73.

Herbst, M. D. and Goldstein, J. H. (1989). A review of water diffusion measurement by NMR in human red blood cells. *Am J Physiol*, 256:1097–1104.

Hochachka, P. and Mommsen, T. (1983). Protons and anaerobiosis. *Science*, 219(4591):1391–7.

Hoehn-Berlage, M., Norris, D. G., Kohno, K., Mies, G., Leibfritz, D., and Hossmann, K. A. (1995). Evolution of regional changes in apparent diffusion coefficient during focal ischemia of rat brain: the relationship of quantitative diffusion NMR imaging to reduction in cerebral blood flow and metabolic disturbances. *J. Cereb. Blood Flow Metab*, 15:1002–1011.

Hossmann, K. A., Fischer, M., Bockhorst, K., and Hoehn-Berlage, M. (1994). NMR imaging of the apparent diffusion coefficient (ADC) for the evaluation of metabolic suppression and recovery after prolonged cerebral ischemia. *J Cereb Blood Flow Metab*, 14(5):723–731.

Hossmann, K. A. and Schuier, F. J. (1980). Experimental brain infarcts in cats. I. Pathophysiological observations. *Stroke*, 11(6):583–92.

Hoult, D. I. (1979). Rotating frame zeugmatomography. *J Magn Reson*, 33:183–197.

Hudetz, A., Greene, A., Fehér, G., Knuese, D., and Cowley, A. (1993). Imaging system for three-dimensional mapping of cerebrocortical capillary networks *in vivo*. *Microvasc Res*, 46(3):293–309.

Intaglietta, M., Johnson, P. C., and Winslow, R. M. (1996). Microvascular and tissue oxygen distribution. *Cardiovasc Res*, 32(4):632–643.

Jager, H. R., Moore, E. A., Bynevelt, M., Coley, S., Mounfield, P., Kitchen, N., and Taylor, W. (2000). Contrast-enhanced MR angiography in patients with carotid artery stenosis: comparison of two different techniques with an unenhanced 2D time-of-flight sequence. *Neuroradiology*, 42(4):240–8.

Jenkins, L. W., Povlishock, J. T., Becker, D. P., Miller, J. D., and Sullivan, H. G. (1979). Complete cerebral ischemia. An ultrastructural study. *Acta Neuropathol (Berl)*, 48:113–125.

Jenkinson, M., Bannister, P., Brady, M., and Smith, S. (2002). Improved optimization for the robust and accurate linear registration and motion correction of brain images. *Neuroimage*, 17(2):825–41.

Jensen, J. and Chandra, R. (2000). NMR relaxation in tissues with weak magnetic inhomogeneities. *Magn Reson Med*, 44(1):144–56.

Jiang, Q., Chopp, M., Zhang, Z. G., Helpern, J. A., Ordidge, R. J., Ewing, J., Jiang, P., and Marchese, B. A. (1994). The effect of hypothermia on transient focal ischemia in rat brain evaluated by diffusion- and perfusion-weighted NMR imaging. *J Cereb Blood Flow Metab*, 14(5):732–741.

Jiang, Q., Zhang, R. L., Zhang, Z. G., Ewing, J. R., Divine, G. W., and Chopp, M. (1998). Diffusion-, T_2-, and perfusion-weighted nuclear magnetic resonance imaging of middle cerebral artery embolic stroke and recombinant tissue plasminogen activator intervention in the rat. *J Cereb Blood Flow Metab*, 18(7):758–767.

Jiang, Q., Zhang, Z., Chopp, M., Helpern, J., Ordidge, R., Garcia, J., Marchese, B., Qing, Z., and Knight, R. (1993). Temporal evolution and spatial distribution of the diffusion constant of water in rat brain after transient middle cerebral artery occlusion. *J Neurol Sci*, 120(2):123–30.

Jones, G. P. (1966). Spin-lattice relaxation in the rotating frame: weak-collision case. *Phys. Rev.*, 148:332–335.

Jones, T., Morawetz, R., Crowell, R., Marcoux, F., FitzGibbon, S., DeGirolami, U., and Ojemann, R. (1981). Thresholds of focal cerebral ischemia in awake monkeys. *J Neurosurg*, 54(6):773–82.

Katsura, K., Ekholm, A., Asplund, B., and Siesjö, B. (1991). Extracellular pH in the brain during ischemia: relationship to the severity of lactic acidosis. *J Cereb Blood Flow Metab*, 11(4):597–9.

Kettunen, M., Gröhn, O., Penttonen, M., and Kauppinen, R. (2001). Cerebral $T_{1\rho}$ relaxation time increases immediately upon global ischemia in the rat independently of blood glucose and anoxic depolarization. *Magn Reson Med*, 46(3):565–72.

Kettunen, M. I., Gröhn, O. H., Silvennoinen, M. J., Penttonen, M., and Kauppinen, R. A. (2002a). Effects of intracellular pH, blood, and tissue oxygen tension on $T_{1\rho}$ relaxation in rat brain. *Magn Reson Med*, 48(3):470–7.

Kettunen, M. I., Gröhn, O. H., Silvennoinen, M. J., Penttonen, M., and Kauppinen, R. A. (2002b). Quantitative assessment of the balance between oxygen delivery and consumption in the rat brain after transient ischemia with T_2-BOLD magnetic resonance imaging. *J Cereb Blood Flow Metab*, 22(3):262–70.

Kidwell, C. S., Alger, J. R., and Saver, J. L. (2003). Beyond mismatch: evolving paradigms in imaging the ischemic penumbra with multimodal magnetic resonance imaging. *Stroke*, 34(11):2729–35.

Kidwell, C. S., Saver, J. L., Mattiello, J., Starkman, S., Vinuela, F., Duckwiler, G., Gobin, Y. P., Jahan, R., Vespa, P., Kalafut, M., and Alger, J. R. (2000). Thrombolytic reversal of acute human cerebral ischemic injury shown by diffusion/perfusion magnetic resonance imaging. *Ann Neurol*, 47(4):462–9.

Kleinschmidt, A., Steinmetz, H., Sitzer, M., Merboldt, K. D., and Frahm, J. (1995). Magnetic resonance imaging of regional cerebral blood oxygenation changes under acetazolamide in carotid occlusive disease. *Stroke*, 26(1):106–10.

Knight, R. A., Dereski, M. O., Helpern, J. A., Ordidge, R. J., and Chopp, M. (1994). Magnetic resonance imaging assessment of evolving focal cerebral ischemia. Comparison with histopathology in rats. *Stroke*, 25(6):1252–1261.

Knight, R. A., Ordidge, R. J., Helpern, J. A., Chopp, M., Rodolosi, L. C., and Peck, D. (1991). Temporal evolution of ischemic damage in rat brain measured by proton nuclear magnetic resonance imaging. *Stroke*, 22(6):802–8.

Kohno, K., Hoehn-Berlage, M., Mies, G., Back, T., and Hossmann, K. A. (1995). Relationship between diffusion-weighted MR images, cerebral blood flow, and energy state in experimental brain infarction. *Magn Reson Imaging*, 13(1):73–80.

Kollias, S. S., Binkert, C. A., Ruesch, S., and Valavanis, A. (1999). Contrast-enhanced MR angiography of the supra-aortic vessels in 24 seconds: a feasibility study. *Neuroradiology*, 41(6):391–400.

Kucharczyk, J., Mintorovitch, J., Asgari, H., and Moseley, M. (1991). Diffusion/perfusion MR imaging of acute cerebral ischemia. *Magn Reson Med*, 19(2):311–5.

Kucharczyk, J., Vexler, Z. S., Roberts, T. P., Asgari, H. S., Mintorovitch, J., Derugin, N., Watson, A. D., and Moseley, M. E. (1993). Echo-planar perfusion-sensitive MR imaging of acute cerebral ischemia. *Radiology*, 188(3):711–717.

Kumar, I., Welti, D., and Ernst, R. R. (1975). NMR Fourier Zeugmatography. *J Magn Reson*, 18:69.

Kwong, K. K., Belliveau, J. W., Chesler, D. A., Goldberg, I. E., Weisskoff, R. M., Poncelet, B. P., Kennedy, D. N., Hoppel, B. E., Cohen, M. S., Turner, R., Cheng, H.-M., Brady, T. J., and Rosen, B. R. (1992). Dynamic magnetic resonance imaging of human brain activity during primary sensory stimulation. *Proc. Natl. Acad. Sci. USA*, 89:5675–5679.

Lauterbur, P. C. (1973). Image formation by induced local interaction: examples employing nuclear magnetic resonance. *Nature*, 242:190–191.

Lauterbur, P. C., Kramer, D., House, W. V., and Chen, C.-N. (1975). Chemical analysis by Magnetic Resonance Zeugmatomography. In *Proceedings*, volume 169, pages 54–54. American Chemical Society.

Le Bihan, D., Breton, E., Lallemand, D., Grenier, P., Cabanis, E., and Laval-Jeantet, M. (1986). MR imaging of intravoxel incoherent motions: application to diffusion and perfusion in neurologic disorders. *Radiology*, 161(2):401–407.

Leenders, K. L., Perani, D., Lammertsma, A. A., Heather, J. D., Buckingham, P., Healy, M. J. R., Gibbs, J. M., Wise, R. J. S., Hatazawa, J., Herold, S., Beaney, R. P., Brooks, D. J., Spinks, T., Rhodes, C., Frackowiak, R. S. J., and Jones, T. (1990). Cerebral blood flow, blood volume and oxygen utilization: normal values and effect of age. *Brain*, 113:27–47.

Lei, H., Zhang, Y., Zhu, X.-H., and Chen, W. (2003). Changes in the proton T_2 relaxation times of cerebral water and metabolites during forebrain ischemia in rat at 9.4 T. *Magn Reson Med*, 49(6):979–84.

Levitt, M. H. and Freeman, R. (1981). Compensation for pulse imperfections in NMR spin-echo experiments. *J Magn Reson*, 43:65–80.

Li, F., Han, S., Tatlisumak, T., Liu, K., Garcia, J., Sotak, C., and Fisher, M. (1999). Reversal of acute apparent diffusion coefficient abnormalities and delayed neuronal death following transient focal cerebral ischemia in rats. *Ann Neurol*, 46(3):333–42.

Lin, W., Haacke, E., Smith, A., and Clampitt, M. (1992). Gadolinium-enhanced high-resolution MR angiography with adaptive vessel tracking: preliminary results in the intracranial circulation. *J Magn Reson Imaging*, 2(3):277–84.

Longa, E. Z., Weinstein, P. R., Carlson, S., and Cummins, R. (1989). Reversible middle cerebral artery occlusion without craniectomy in rats. *Stroke*, 20(1):84–91.

Lövblad, K., Baird, A., Schlaug, G., Benfield, A., Siewert, B., Voetsch, B., Connor, A., Burzynski, C., Edelman, R., and Warach, S. (1997). Ischemic lesion volumes in acute stroke by diffusion-weighted magnetic resonance imaging correlate with clinical outcome. *Ann Neurol*, 42(2):164–70.

Love, L., Hill, B., Larson, S., Raimondi, A., and Lescher, A. (1966). Cranial collateral pathways in stroke syndrome. *Am J Roentgenol Radium Ther Nucl Med*, 98(3):637–47.

Lutsep, H. L., Albers, D. W., Crespigny, A. D., Kamat, G. N., Marks, M. P., and Moseley, M. E. (1997). Clinical utility of diffusion-weighted magnetic resonance imaging in the assessment of ischemic stroke. *Ann Neurol*, 41:574–580.

Luz, Z. and Meiboom, S. (1963). Nuclear Magnetic Resonance study of the protolysis of trimethylammonium ion in aqueous solution - Order of the reaction with respect to solvent. *J Chem Phys*, 39:366–370.

Lythgoe, D. J., Østergaard, L., William, S. C., Cluckie, A., Buxton-Thomas, M., Simmons, A., and Markus, H. S. (2000a). Quantitative perfusion imaging in carotid artery stenosis using dynamic susceptibility contrast-enhanced magnetic resonance imaging. *Magn Reson Imaging*, 18(1):1–11.

Lythgoe, D. J., Williams, S. C., Cullinane, M., and Markus, H. S. (1999). Mapping of cerebrovascular reactivity using BOLD magnetic resonance imaging. *Magn Reson Imaging*, 17(4):495–502.

Lythgoe, M., Thomas, D., Calamante, F., Pell, G., King, M., Busza, A., Sotak, C., Williams, S., Ordidge, R., and Gadian, D. (2000b). Acute changes in MRI diffusion, perfusion, T_1, and T_2 in a rat model of oligemia produced by partial occlusion of the middle cerebral artery. *Magn Reson Med*, 44(5):706–12.

MacKenzie, E., Farrar, J., Fitch, W., Graham, D., Gregory, P., and Harper, A. (1979). Effects of hemorrhagic hypotension on the cerebral circulation. I. Cerebral blood flow and pial arteriolar caliber. *Stroke*, 10(6):711–8.

Maeda, M., Yuh, W. T., Ueda, T., Maley, J. E., Crosby, D. L., Zhu, M. W., and Magnotta, V. A. (1999). Severe occlusive carotid artery disease: hemodynamic assessment by MR perfusion imaging in symptomatic patients. *AJNR Am J Neuroradiol*, 20(1):43–51.

Mai, J. K., Assheuer, J., and Paxinos, G. (1997). *Atlas of the Human Brain*. Academic Press, London.

Mäkelä, H., Gröhn, O., Kettunen, M., and Kauppinen, R. (2001). Proton exchange as a relaxation mechanism for T_1 in the rotating frame in native and immobilized protein solutions. *Biochem Biophys Res Commun*, 289(4):813–8.

Mäkelä, H. I., Kettunen, M. I., Gröhn, O. H. J., and Kauppinen, R. A. (2002). Quantitative $T_{1\rho}$ and magnetization transfer magnetic resonance imaging of acute cerebral ischemia in the rat. *J Cereb Blood Flow Metab*, 22(5):547–58.

Mäkelä, H. I., Vita, E. D., Gröhn, O. H. J., Kettunen, M. I., Kavec, M., Lythgoe, M., Garwood, M., Ordidge, R., and Kauppinen, R. A. (2004). B_0 dependence of the on-resonance longitudinal relaxation time in the rotating frame ($T_{1\rho}$) in protein phantoms and rat brain in vivo. *Magn Reson Med*, 51(1):4–8.

Mansfield, P. (1977). Multi-planar image formation using NMR spin echoes. *J Phys C*, 10:55–58.

Marchal, G., Bosmans, H., Hecke, P. V., Jiang, Y., Aerts, P., and Bauer, H. (1991). Experimental Gd-DTPA polylysine enhanced MR angiography: sequence optimization. *J Comput Assist Tomogr*, 15(4):711–5.

McHedlishvili, G., Varazashvili, M., Mamaladze, A., and Momtselidze, N. (1997). Blood flow structuring and its alterations in capillaries of the cerebral cortex. *Microvasc Res*, 53(3):201–210.

McHenry, L., Fazekas, J., and Sullivan, J. (1961). Cerebral hemodynamics of syncope. *Am J Med Sci*, 241:173–8.

Meier, P. and Zierler, K. (1954). On the theory of the indicator-dilution method for measurement of blood flow and volume. *J Appl Physiol*, 6(12):731–44.

Michaeli, S., Garwood, M., Zhu, X.-H., DelaBarre, L., Andersen, P., Adriany, G., Merkle, H., Ugurbil, K., and Chen, W. (2002). Proton T_2 relaxation study of water, N-acetylaspartate, and creatine in human brain using Hahn and Carr-Purcell spin echoes at 4 T and 7 T. *Magn Reson Med*, 47(4):629–33.

Moonen, C. T., van Zijl, P. C., Frank, J. A., Bihan, D. L., and Becker, E. D. (1990). Functional magnetic resonance imaging in medicine and physiology. *Science*, 250(4977):53–61.

Mori, S. and van Zijl, P. (1995). Diffusion weighting by the trace of the diffusion tensor within a single scan. *Magn Reson Med*, 33(1):41–52.

Moseley, M., Butts, K., Yenari, M., Marks, M., and de Crespigny, A. (1995). Clinical aspects of DWI. *NMR Biomed*, 8(7-8):387–96.

Moseley, M., Kucharczyk, J., Mintorovitch, J., Cohen, Y., Kurhanewicz, J., Derugin, N., Asgari, H., and Norman, D. (1990a). Diffusion-weighted MR imaging of acute stroke: correlation with T_2-weighted and magnetic susceptibility-enhanced MR imaging in cats. *AJNR Am J Neuroradiol*, 11(3):423–9.

Moseley, M. E., Cohen, Y., Mintorovitch, J., Chileuitt, L., Shimizu, H., Kucharczyk, J., Wendland, M. F., and Weinstein, P. R. (1990b). Early detection of regional cerebral ischemia in cats: comparison of diffusion- and T_2-weighted MRI and spectroscopy. *Magn Reson Med*, 14:330–346.

Mukherjee, P., Kang, H. C., Videen, T. O., McKinstry, R. C., Powers, W. J., and Derdeyn, C. P. (2003). Measurement of cerebral blood flow in chronic carotid occlusive disease: comparison of dynamic susceptibility contrast perfusion MR imaging with positron emission tomography. *AJNR Am J Neuroradiol*, 24(5):862–71.

Neumann-Haefelin, T., Kastrup, A., de Crespigny, A., Yenari, M., Ringer, T., Sun, G., and Moseley, M. (2000a). Serial MRI after transient focal cerebral ischemia in rats: dynamics of tissue injury, blood-brain barrier damage, and edema formation. *Stroke*, 31(8):1965–72.

Neumann-Haefelin, T., Wittsack, H., Wenserski, F., Li, T., Moseley, M., Siebler, M., and Freund, H. (2000b). Diffusion- and perfusion-weighted MRI in a patient with a prolonged reversible ischaemic neurological deficit. *Neuroradiology*, 42(6):444–7.

Neumann-Haefelin, T., Wittsack, H., Wenserski, F., Siebler, M., Seitz, R., Modder, U., and Freund, H. (1999). Diffusion- and perfusion-weighted MRI. The DWI/PWI mismatch region in acute stroke. *Stroke*, 30(8):1591–7.

Neumann-Haefelin, T., Wittsack, H. J., Fink, G. R., Wenserski, F., Li, T. Q., Seitz, R. J., Siebler, M., Modder, U., and Freund, H. J. (2000c). Diffusion- and perfusion-weighted MRI: influence of severe carotid artery stenosis on the DWI/PWI mismatch in acute stroke. *Stroke*, 31(6):1311–7.

Nighoghossian, N., Berthezene, Y., Philippon, B., Adeleine, P., Froment, J. C., and Trouillas, P. (1996). Hemodynamic parameter assessment with dynamic susceptibility contrast magnetic resonance imaging in unilateral symptomatic internal carotid artery occlusion. *Stroke*, 27(3):474–9.

Nordström, C. and Siesjö, B. (1978). Influence of phenobarbital on changes in the metabolites of the energy reserve of the cerebral cortex following complete ischemia. *Acta Physiol Scand*, 104(3):271–80.

Ogawa, S., Lee, T. M., Kay, A. R., and Tank, D. W. (1990a). Brain magnetic resonance imaging with contrast dependent on blood oxygenation. *Proc Natl Acad Sci USA*, 87:9868–9872.

Ogawa, S., Lee, T. M., Nayak, A. S., and Glynn, P. (1990b). Oxygenation-sensitive contrast in magnetic resonance image of rodent brain at high magnetic fields. *Magn Reson Med*, 14(1):68–78.

Oja, J. M., Gillen, J. S., Kauppinen, R. A., Kraut, M., and van Zijl, P. C. (1999). Determination of oxygen extraction ratios by magnetic resonance imaging. *J Cereb Blood Flow Metab*, 19(12):1289–1295.

Olesen, J., Paulson, O. B., and Lassen, N. A. (1971). Regional cerebral blood flow in man determined by the initial slope of the clearance of intra-arterially injected ^{133}Xe. *Stroke*, 2(6):519–540.

Ordidge, R., Helpern, J., Knight, R., Qing, Z., and Welch, K. (1991). Investigation of cerebral ischemia using magnetization transfer contrast (MTC) MR imaging. *Magn Reson Imaging*, 9(6):895–902.

Østergaard, L., Chesler, D. A., Weisskoff, R. M., Sorensen, A. G., and Rosen, B. R. (1999). Modeling cerebral blood flow and flow heterogeneity from magnetic resonance residue data. *J Cereb Blood Flow Metab*, 19(6):690–9.

Østergaard, L., Johannsen, P., Host-Poulsen, P., Vestergaard-Poulsen, P., Asboe, H., Gee, A. D., Hansen, S. B., Cold, G. E., Gjedde, A., and Gyldensted, C. (1998a). Cerebral blood flow measurements by magnetic resonance imaging bolus tracking: comparison with [^{15}O]H_2O positron emission tomography in humans. *J Cereb Blood Flow Metab*, 18(9):935–40.

Østergaard, L., Smith, D. F., Vestergaard-Poulsen, P., Hansen, S. B., Gee, A. D., Gjedde, A., and Gyldensted, C. (1998b). Absolute cerebral blood flow and blood volume measured by magnetic resonance imaging bolus tracking: comparison with positron emission tomography values. *J Cereb Blood Flow Metab*, 18(4):425–32.

Østergaard, L., Sorensen, A. G., Kwong, K. K., Weisskoff, R. M., Gyldensted, C., and Rosen, B. R. (1996a). High resolution measurement of cerebral blood flow using intravascular tracer bolus passages. part II: Experimental comparison and preliminary results. *Magn Reson Med*, 36(5):726–36.

Østergaard, L., Weisskoff, R. M., Chesler, D. A., Gyldensted, C., and Rosen, B. R. (1996b). High resolution measurement of cerebral blood flow using intravascular tracer bolus passages. part I: Mathematical approach and statistical analysis. *Magn Reson Med*, 36(5):715–25.

Pappata, S., Fiorelli, M., Rommel, T., Hartmann, A., Dettmers, C., Yamaguchi, T., Chabriat, H., Poline, J. B., Crouzel, C., L., and Giamberardino, D. (1993). PET study of changes in local brain hemodynamics and oxygen metabolism after unilateral middle cerebral artery occlusion in baboons. *J Cereb Blood Flow Metab*, 13(3):416–24.

Paxinos, G. T. and Watson, C. (1996). *The Rat Brain in Stereotaxic Coordinates*. Academic Press, London.

Pell, G. S., King, M. D., Proctor, E., Thomas, D. L., Lythgoe, M. F., Gadian, D. G., and Ordidge, R. J. (2003). Comparative study of the FAIR technique of perfusion quantification with the hydrogen clearance method. *J Cereb Blood Flow Metab*, 23(6):689–99.

Perkiö, J., Aronen, H. J., Kangasmäki, A., Liu, Y., Karonen, J., Savolainen, S., and Østergaard, L. (2002). Evaluation of four postprocessing methods for determination of cerebral blood volume and mean transit time by dynamic susceptibility contrast imaging. *Magn Reson Med*, 47(5):973–81.

Perry, M., Lee, J., and Horton, J. (1970). Maintenance of cerebral blood flow during carotid reconstruction. *Am J Surg*, 120(3):346–50.

Perthen, J. E., Calamante, F., Gadian, D. G., and Connelly, A. (2002). Is quantification of bolus tracking MRI reliable without deconvolution? *Magn Reson Med*, 47(1):61–7.

Pettersson, H. and Ringertz, H., editors (1998a). *The Encyclopaedia of Medical Imaging.*, volume VI. The NICER Institute, Lund.

Pettersson, H. and Ringertz, H., editors (1998b). *The Encyclopaedia of Medical Imaging.*, volume II. The NICER Institute, Lund.

Pierpaoli, C., Jezzard, P., Basser, P., Barnett, A., and Chiro, G. D. (1996). Diffusion tensor MR imaging of the human brain. *Radiology*, 201(3):637–48.

Pike, G., Hu, B., Glover, G., and Enzmann, D. (1992). Magnetization transfer time-of-flight magnetic resonance angiography. *Magn Reson Med*, 25(2):372–9.

Popel, A. S. and Gross, J. F. (1979). Analysis of oxygen diffusion from arteriolar networks. *Am J Physiol*, 237(6):681–689.

Powers, W., Press, G., Grubb, R., Gado, M., and Raichle, M. (1987). The effect of hemodynamically significant carotid artery disease on the hemodynamic status of the cerebral circulation. *Ann Intern Med*, 106(1):27–34.

Powers, W. J. (1991). Cerebral hemodynamics in ischemic cerebrovascular disease. *Ann. Neurol.*, 29:231–240.

Pulsinelli, W. A., Brierley, J. B., and Plum, F. (1982a). Temporal profile of neuronal damage in a model of transient forebrain ischemia. *Ann. Neurol.*, 11:491–498.

Pulsinelli, W. A., Levy, D. E., and Duffy, T. E. (1982b). Regional cerebral blood flow and glucose metabolism following transient forebrain ischemia. *Ann Neurol*, 11(5):499–502.

Purcell, E. M., Torrey, H. C., and Pound, R. V. (1946). Resonance absorption by nuclear magnetic moments in a solid. *Phys. Rev.*, 69:37–38.

Rabi, I. I., Millman, S., Kusch, P., and Zacharias, J. R. (1938). A new method for measuring nuclear magnetic moment. *Phys. Rev.*, 53:318.

Rajagopalan, S. and Prince, M. (2002). Magnetic resonance angiographic techniques for the diagnosis of arterial disease. *Cardiol Clin*, 20(4):501–12.

Reith, W., Dardzinski, B. J., Sotak, C. H., and Fisher, M. (1996). Monitoring of tissue plasminogen activator treatment with multi-slice diffusion mapping and perfusion imaging in a thromboembolic stroke model. *Int J Neuroradiol*, 2:397–407.

Rempp, K. A., Brix, G., Wenz, F., Becker, C. R., Guckel, F., and Lorenz, W. J. (1994). Quantification of regional cerebral blood flow and volume with dynamic susceptibility contrast-enhanced MR imaging. *Radiology*, 193(3):637–41.

Roach, M., Scott, S., and Ferguson, G. (1972). The hemodynamic importance of the geometry of bifurcations in the circle of Willis (glass model studies). *Stroke*, 3(3):255–67.

Rosen, B., Belliveau, J., Aronen, H., Kennedy, D., Buchbinder, B., Fischman, A., Gruber, M., Glas, J., Weisskoff, R., and Cohen, M. (1991). Susceptibility contrast imaging of cerebral blood volume: human experience. *Magn Reson Med*, 22(2):293–9.

Rosen, B., Belliveau, J., Vevea, J., and Brady, T. (1990). Perfusion imaging with NMR contrast agents. *Magn Reson Med*, 14(2):249–65.

Röther, J., Gückel, F., Neff, W., Schwartz, A., and Hennerici, M. (1996). Assessment of regional cerebral blood volume in acute human stroke by use of single-slice dynamic susceptibility contrast-enhanced magnetic resonance imaging. *Stroke*, 27(6):1088–1093.

Roussel, S. A., van Bruggen, N., King, M. D., and Gadian, D. G. (1995). Identification of collaterally perfused areas following focal ischemia in the rat by comparison of gradient echo and diffusion-weighted MRI. *J Cereb Blood Flow Metab*, 15:578–586.

Roussel, S. A., Vanbruggen, N., King, M. D., Houseman, J., Williams, S. R., and Gadian, D. G. (1994). Monitoring the initial expansion of focal ischaemic changes by diffusion-weighted MRI using a remote controlled method of occlusion. *NMR Biomed*, 7(1-2):21–28.

Rutgers, D. R., Klijn, C. J., Kappelle, L. J., and van der Grond, J. (2000). Cerebral metabolic changes in patients with a symptomatic occlusion of the internal carotid artery: a longitudinal ^{1}H magnetic resonance spectroscopy study. *J Magn Reson Imaging*, 11(3):279–86.

Sandor, P., van Put, J. C., de Jong, W., and de Wied, D. (1986). Continuous measurement of cerebral blood volume in rats with the photoelectric technique: effect of morphine and noloxone. *Life Sci*, 39:1657–1665.

Schlaug, G., Benfield, A., Baird, A., Siewert, B., Lövblad, K., Parker, R., Edelman, R., and Warach, S. (1999). The ischemic penumbra: operationally defined by diffusion and perfusion MRI. *Neurology*, 53(7):1528–37.

Schlaug, G., Siewert, B., Benfield, A., Edelman, R., and Warach, S. (1997). Time course of the apparent diffusion coefficient (ADC) abnormality in human stroke. *Neurology*, 49(1):113–9.

Schreiber, W. G., Guckel, F., Stritzke, P., Schmiedek, P., Schwartz, A., and Brix, G. (1998). Cerebral blood flow and cerebrovascular reserve capacity: estimation by dynamic magnetic resonance imaging. *J Cereb Blood Flow Metab*, 18(10):1143–56.

Schumann, P., Touzani, O., Young, A., Morello, R., Baron, J., and MacKenzie, E. (1998). Evaluation of the ratio of cerebral blood flow to cerebral blood volume as an index of local cerebral perfusion pressure. *Brain*, 121 (Pt 7):1369–79.

Schwab, M., Bauer, R., and Zwiener, U. (1997). The distribution of normal brain water content in wistar rats and its increase due to ischemia. *Brain Research*, 749:82–87.

Schwamm, L., Koroshetz, W., Sorensen, A., Wang, B., Copen, W., Budzik, R., Rordorf, G., Buonanno, F., Schaefer, P., and Gonzalez, R. (1998). Time course of lesion development in patients with acute stroke: serial diffusion- and hemodynamic-weighted magnetic resonance imaging. *Stroke*, 29(11):2268–76.

Sepponen, R. E., Pohjonen, J. A., Sipponen, J. T., and Tanttu, J. I. (1985). A method for $T_{1\rho}$ imaging. *J Comput Assist Tomogr*, 9:1007–1011.

Siesjö, B. K. (1992). Pathophysiology and treatment of focal cerebral ischemia. Part I: Pathophysiology. *J Neurosurg*, 77(2):169–184.

Siewert, B., Schlaug, G., Edelman, R., and Warach, S. (1997). Comparison of EPISTAR and T_2^*-weighted gadolinium-enhanced perfusion imaging in patients with acute cerebral ischemia. *Neurology*, 48(3):673–9.

Silvennoinen, M. J., Kettunen, M. I., Clingman, C. S., and Kauppinen, R. A. (2002). Blood NMR relaxation in the rotating frame: mechanistic implications. *Arch Biochem Biophys*, 405:78–86.

Smith, S. M. (2002). Fast robust automated brain extraction. *Hum Brain Mapp*, 17(3):143–55.

Smith, S. M. and Brady, M. J. (1997). SUSAN-a new approach to low level image processing. *International Journal of Computer Vision*, 23(1):45–78.

Sokoloff, L. (1997). Anatomy of Cerebral Circulation. In Welch, K., editor, *Primer on Cerebrovascular Diseases.*, pages 3–5. Academic Press, San Diego.

Sorensen, A. G., Buonanno, F. S., Gonzalez, R. G., Schwamm, L. H., Lev, M. H., Huang-Hellinger, F. R., Reese, T. G., Weisskoff, R. M., Davis, T. L., Suwanwela, N., Can, U., Moreira, J. A., Copen, W. A., Look, R. B., Finklestein, S. P., Rosen, B. R., and Koroshetz, W. J. (1996). Hyperacute stroke: evaluation with combined multisection diffusion-weighted and hemodynamic weighted echo-planar imaging. *Radiology*, 199:391–401.

Stejskal, E. O. and Tanner, J. E. (1965). Spin diffusion measurements: spin-echoes in the presence of a time-dependent field gradient. *J.Chem. Phys.*, 42:288–292.

Thomas, D. L., Lythgoe, M. F., Gadian, D. G., and Ordidge, R. J. (2002). Rapid simultaneous mapping of T_2 and T_2^* by multiple acquisition of spin and gradient echoes using interleaved echo planar imaging (MASAGE-IEPI). *Neuroimage*, 15(4):992–1002.

Thomas, D. L., Lythgoe, M. F., Pell, G. S., Calamante, F., and Ordidge, R. J. (2000). The measurement of diffusion and perfusion in biological systems using magnetic resonance imaging. *Phys Med Biol*, 45(8):97–138.

Thompson, H. K., Starmer, F., Whelen, R. H., and McIntosh, H. D. (1964). Indicator transit time considered as a gamma variate. *Circ. Res.*, 14:502–515.

Tsuchida, C., Kimura, H., Sadato, N., Tsuchida, T., Tokuriki, Y., and Yonekura, Y. (2000). Evaluation of brain metabolism in steno-occlusive carotid artery disease by proton MR spectroscopy: a correlative study with oxygen metabolism by PET. *J Nucl Med*, 41(8):1357–62.

Tsuchida, C., Yamada, H., Maeda, M., Sadato, N., Matsuda, T., Kawamura, Y., Hayashi, N., Yamamoto, K., Yonekura, Y., and Ishii, Y. (1997). Evaluation of peri-infacted hypoperfusion with T_2^*-weighted dynamic MRI. *J Magn Reson Imag*, 7:518–522.

Ulatowski, J. A., Bucci, E., Nishikawa, T., Razynska, A., Williams, M. A., Takeshima, R., Traystman, R. J., and Koehler, R. C. (1996). Cerebral O_2 transport with hematocrit reduced by cross-linked hemoglobin transfusion. *Am J Physiol*, 270:H466–H475.

Ulatowski, J. A., Oja, J. M., Suarez, J. I., Kauppinen, R. A., Traystman, R. J., and van Zijl, P. C. (1999). In vivo determination of absolute cerebral blood volume using hemoglobin as a natural contrast agent: an MRI study using altered arterial carbon dioxide tension. *J Cereb Blood Flow Metab*, 19(7):809–817.

van der Grond, J., Balm, R., Kappelle, L. J., Eikelboom, B. C., and Mali, W. P. (1995). Cerebral metabolism of patients with stenosis or occlusion of the internal carotid artery. A ^{1}H-MR spectroscopic imaging study. *Stroke*, 26(5):822–8.

van der Toorn, A., Dijkhuizen, R. M., Tulleken, C. A., and Nicolay, K. (1996a). Diffusion of metabolites in normal and ischemic rat brain measured by localized ^{1}H MRS. *Magn Reson Med*, 36(6):914–22.

van der Toorn, A., Sykova, E., Dijkhuizen, R. M., Vorisek, I., Vargova, L., Skobisova, E., van Lookeren Campagne, M., Reese, T., and Nicolay, K. (1996b). Dynamic changes in water ADC, energy metabolism, extracellular space volume, and tortuosity in neonatal rat brain during global ischemia. *Magn Reson Med*, 36(1):52–60.

van Osch, M. J., Rutgers, D. R., Vonken, E. P., van Huffelen, A. C., Klijn, C. J., Bakker, C. J., and van der Grond, J. (2002). Quantitative cerebral perfusion MRI and CO_2 reactivity measurements in patients with symptomatic internal carotid artery occlusion. *Neuroimage*, 17(1):469–78.

van Osch, M. J., Vonken, E. J., Bakker, C. J., and Viergever, M. A. (2001). Correcting partial volume artifacts of the arterial input function in quantitative cerebral perfusion MRI. *Magn Reson Med*, 45(3):477–85.

van Zijl, P. C., Eleff, S. M., Ulatowski, J. A., Oja, J. M., Ulug, A. M., Traystman, R. J., and Kauppinen, R. A. (1998). Quantitative assessment of blood flow, blood volume and blood oxygenation effects in functional magnetic resonance imaging. *Nat Med*, 4(2):159–167.

Verheul, H., van der Sprenkel, J. B., Tulleken, C., Tamminga, K., and Nicolay, K. (1992). Temporal evolution of focal cerebral ischemia in the rat assessed by T_2-weighted and diffusion-weighted magnetic resonance imaging. *Brain Topogr*, 5(2):171–6.

Villringer, A., Rosen, B., Belliveau, J., Ackerman, J., Lauffer, R., Buxton, R., Chao, Y., Wedeen, V., and Brady, T. (1988). Dynamic imaging with lanthanide chelates in normal brain: contrast due to magnetic susceptibility effects. *Magn Reson Med*, 6(2):164–74.

Warach, S., Chien, D., Li, W., Ronthal, M., and Edelman, R. R. (1992a). Fast magnetic resonance diffusion-weighted imaging of acute human stroke. *Neurology*, 42(9):1717–1723.

Warach, S., Gaa, J., Siewert, B., Wielopolski, P., and Edelman, R. (1995). Acute human stroke studied by whole brain echo planar diffusion-weighted magnetic resonance imaging. *Ann Neurol*, 37(2):231–41.

Warach, S., Li, W., Ronthal, M., and Edelman, R. (1992b). Acute cerebral ischemia: evaluation with dynamic contrast-enhanced MR imaging and MR angiography. *Radiology*, 182(1):41–7.

Weisskoff, R. M., Zuo, C. S., Boxerman, J. L., and Rosen, B. R. (1994). Microscopic susceptibility variation and transverse relaxation: theory and experiment. *Magn Reson Med*, 31(6):601–10.

Wendland, M., White, D., Aicher, K., Tzika, A., and Moseley, M. (1991). Detection with echo-planar MR imaging of transit of susceptibility contrast medium in a rat model of regional brain ischemia. *J Magn Reson Imaging*, 1(3):285–92.

White, R. P. and Markus, H. S. (1997). Impaired dynamic cerebral autoregulation in carotid artery stenosis. *Stroke*, 28(7):1340–1344.

Wiart, M., Berthezene, Y., Adeleine, P., Feugier, P., Trouillas, P., Froment, J. C., and Nighoghossian, N. (2000). Vasodilatory response of border zones to acetazolamide before and after endarterectomy : an echo planar imaging-dynamic susceptibility contrast-enhanced MRI study in patients with high-grade unilateral internal carotid artery stenosis. *Stroke*, 31(7):1561–5.

Williams, D. S., Detre, J. A., Leigh, J. S., and Kortesky, A. P. (1992). Magnetic resonance imaging of perfusion using spin inversion of arterial water. *Proc. Natl. Acad. Sci. USA*, 89:212–216.

Wolf, P. A. (1997). Epidemiology and Risk Factor Management. In Welch, K., editor, *Primer on Cerebrovascular Diseases.*, pages 751–56. Academic Press, San Diego.

Yamauchi, H., Fukuyama, H., Nagahama, Y., Katsumi, Y., and Okazawa, H. (1998). Cerebral hematocrit decreases with hemodynamic compromise in carotid artery occlusion: a PET study. *Stroke*, 29(1):98–103.

Yamauchi, H., Fukuyama, H., Nagahama, Y., Nabatame, H., Nakamura, K., Yamamoto, Y., Yonekura, Y., Konishi, J., and Kimura, J. (1996). Evidence of misery perfusion and risk for recurrent stroke in major cerebral arterial occlusive diseases from PET. *J Neurol Neurosurg Psychiatry*, 61(1):18–25.

Young, A. R., Sette, G., Touzani, O., Rioux, P., Derlon, J. M., MacKenzie, E. T., and Baron, J. C. (1996). Relationships between high oxygen extraction fraction in the acute stage and final infarction in reversible middle cerebral artery occlusion: an investigation in anesthetized baboons with positron emission tomography. *J Cereb Blood Flow Metab*, 16(6):1176–88.

Zaharchuk, G., Mandeville, J., Bogdanov, A., Weissleder, R., Rosen, B., and Marota, J. (1999). Cerebrovascular dynamics of autoregulation and hypoperfusion. An MRI study of CBF and changes in total and microvascular cerebral blood volume during hemorrhagic hypotension. *Stroke*, 30(10):2197–204.

Zhang, W., Silva, A. C., Williams, D. S., and Koretsky, A. P. (1995). NMR measurement of perfusion using arterial spin labeling without saturation of macromolecular spins. *Magn. Reson. Med.*, 33:370–376.

Zhang, Y., Brady, M., and Smith, S. (2001). Segmentation of brain MR images through a hidden markov random field model and the expectation-maximization algorithm. *IEEE Trans Med Imaging*, 20(1):45–57.

Zhou, J., Golay, X., van Zijl, P. C., Silvennoinen, M. J., Kauppinen, R., Pekar, J., and Kraut, M. (2001). Inverse T_2 contrast at 1.5 Tesla between gray matter and white matter in the occipital lobe of normal adult human brain. *Magn Reson Med*, 46(2):401–6.

Zhou, J., Mori, S., and van Zijl, P. C. M. (1998). FAIR excluding radiation damping (FAIRER). *Magnetic Resonance in Medicine*, 40:712–719.

Zierler, K. L. (1965). Theoretical basis of indicator-dilution methods for measuring flow and volume. *Circ Res*, 16:393–407.